Advanced Testing and Characterization of Iowa Soils and Geomaterials

Final Report
September 11th 2023- 1st Draft

Michigan State University
Department of Civil and Environmental Engineering

Technical Report Documentation Page

1. Report No. IHRB Project TR-780	2. Government Accession No.	3. Recipient's Catalog No.	
4. Title and Subtitle Advanced Testing and Characterization of Iowa Soils and Geomaterials		**5. Report Date**	
		6. Performing Organization Code	
7. Author(s) Ceren Aydin, Bora Cetin, Mustafa Hatipoglu and, Halil Ceylan		**8. Performing Organization Report No.**	
9. Performing Organization Name and Address Michigan State University 426 Auditorium Rd, East Lansing, MI 48824		**10. Work Unit No. (TRAIS)**	
		11. Contract or Grant No.	
12. Sponsoring Organization Name and Address Iowa Highway Research Board Iowa Department of Transportation 800 Lincoln Way Ames, IA 50010		**13. Type of Report and Period Covered** Final Report	
		14. Sponsoring Agency Code	

15. Supplementary Notes

16. Abstract

Accurate modeling of stress-strain characteristics of geomaterials plays a significant role in determining the achievable design life of roadways (e.g., granular roads and paved roads). Currently, the geomechanical characteristics of these materials are obtained from standard laboratory tests such as California Bearing Ratio (CBR) and standard resilient modulus (M_R). However, standard M_R tests commonly conducted in the laboratory do not always apply the most damaging field loading conditions for predicting M_R and permanent deformation (rutting) responses of granular roadways and pavement base/subbase/subgrade layers. This is the main problem that causes significant performance problems for roadways. The geomaterials used in granular road surfaces and pavement foundation layers exhibit cross-anisotropic behavior indicating that deformation characteristics of such materials depend on the direction of the applied loads. In the real field conditions, loads applied via moving wheels on the roadway systems are imposed to not only the vertical direction, but all three directions (both horizontal and vertical directions). Therefore, it is crucial for advanced material characterization test equipment to be built and used to determine the anisotropic (all directions) behavior of geomaterials. In addition, it's worth noting that the stiffness and plastic deformation of these geomaterials are also significantly affected by the freeze-thaw (F-T) cycles. This combination of directional dependency and sensitivity to F-T effects underscores the complex nature of their behavior under various conditions.

In this study, various geomaterials (granular aggregates and subgrade soils) collected from different regions of Iowa were tested in the laboratory through the advanced testing equipment (which was designed and built as part of this project) to determine and quantify the cross-anisotropic behavior of these materials in addition to the effect of F-T on the deformation characteristics. The findings revealed that the tested geomaterials exhibited cross-anisotropy regardless of factors like gradation, material origin, and applied stress levels. Notably, granular materials demonstrated higher cross-anisotropy, where the horizontal resilient modulus (M_R) was only a fraction of the vertical M_R, while fine-grained materials displayed the lowest cross-anisotropy; in certain cases, their horizontal stiffness even surpassed the vertical stiffness, depending on applied stress history. Anisotropy ratios (the ratio of horizontal M_R to vertical M_R) were calculated for all cross-anisotropic tests. Moreover, the M_R was observed to be influenced by stress history during simulated laboratory testing mimicking moving vehicle loads. For permanent deformation (PD), similar to stiffness behavior, all tested materials exhibited cross-anisotropy, with the highest deformations recorded horizontally for aggregate materials subgrade soils. Nevertheless, the discrepancy in deformation levels between different directions for the subgrade soil was relatively lower than that of the granular aggregate materials. Furthermore, investigations into F-T effects indicated that an increase in the fines content of granular materials, coupled with an escalation in applied F-T cycles, led to stiffness degradation and increased PDs.

17. Key Words M_R-PD-cross-anisotropy-anisotropy ratios-geomaterials-cyclic true triaxial-F-T		18. Distribution Statement No restrictions.	
19. Security Classification (of this report) Unclassified.	**20. Security Classification (of this page)** Unclassified.	**21. No. of Pages**	**22. Price** NA

Form DOT F 1700.7 (8-72)   **Reproduction of completed page authorized**

ADVANCED TESTING AND CHARACTERIZATION OF IOWA SOILS AND GEOMATERIALS

Final Report
September 4th 2023- 1st Draft

Principal Investigator
Bora Cetin, Associate Professor
Department of Civil and Environmental Engineering, Michigan State University

Co-Principal Investigator
Halil Ceylan, Director
Program for Sustainable Pavement Engineering & Research (PROSPER)
Institute for Transportation, Iowa State University

Research Assistant
Ceren Aydin

Authors
Ceren Aydin, Bora Cetin, Mustafa Hatipoglu and, Halil Ceylan

A report from
Michigan State University
426 Auditorium Rd,
East Lansing, MI 48824
Phone: +1 517-355-1855 / Fax: (517) 353-1647

TABLE OF CONTENTS

LIST OF TABLES

LIST OF FIGURES

Significant portions of this report were previously published as part of the following:

Aydin C., Hatipoglu M., Cetin B., Ceylan H., "*Preliminary Study on Directional and Stress Dependency of Stiffness Characteristics of Granular Roadway Materials*" 13th TRB International Conference on Low Volume Roads, Iowa, July 23-26, 2023. (Extended Abstract)

Aydin C., Coban H.S., Hatipoglu M., Cetin B., Ceylan H., "*Effect of Cyclic True-Triaxial Boundary Types on Stress-Strain Behavior of Unbound Material*" Geo Congress, Los Angeles, March 26-29, 2023. (Conference Paper)

Aydin C., Hatipoglu M., Cetin B., Ceylan H., "*A Cyclic True Triaxial with Rigid-Rigid-Flexible Boundary for Determination of Cross-Anisotropic Nature of Geomaterials*" Geotechnical Testing Journal, Volume 46, Issue 1, Oct. 2022. (Journal Paper)

Aydin C., Hatipoglu M., Cetin B., Ceylan H., "*The Determination of the MR for Anisotropic Stress Conditions*" IFCEE Dallas, Texas, May 10-14, 2021. (Conference Paper)

EXECUTIVE SUMMARY

The main goals of this study involved examining the cross-anisotropic properties of geomaterials employed in granular roadway surfaces and pavement foundation layers (base/subbase/subgrade) and investigating the impact of freeze-thaw (F-T) cycles on the elastic and plastic deformation characteristics of these geomaterials. This investigation was carried out using specialized, custom-designed cyclic triaxial equipment designed and built for advanced characterization of geomaterials.

A comprehensive review of existing literature was undertaken to summarize the cross-anisotropic resilient modulus (M_R) and permanent deformation (PD) behaviors of geomaterials. This encompassed an examination of pioneering cross-anisotropy studies conducted by various researchers, diverse methods involving cyclic true triaxial equipment for capturing M_R in both vertical and horizontal directions, and the rationale behind the significance of investigating these properties. Furthermore, the research investigated the influence of F-T cycles on the deformation characteristics of granular geomaterials. Through this literature survey, a notable gap was identified in the understanding of cross-anisotropic material attributes, specifically pertaining to M_R and PD.

The laboratory portion of this research involved the advanced characterization of the materials used as granular road surface and pavement foundation layers. Alongside evaluating M_R and PD characteristics in three directions, several additional investigations were undertaken to better understand into cross-anisotropy. These included exploring the influence of stress history, stress states, and how a moving wheel load affects the material`s geotechnical behavior. A standard characterization of the geomaterials was also studied within the scope of the laboratory efforts. Furthermore, F-T studies were conducted to analyze the impact of increased fines content on stiffness and PD, particularly when subjected to consecutive F-T cycles.

The geomaterials collected and tested in this phase of the study included six well-graded granular base and two poorly-graded granular subbase materials, and two subgrade soils: one predominantly consist of sand and the other of silt. These materials were collected from different regions of Iowa.

The findings obtained from the laboratory investigation indicate that geomaterials exhibit cross-anisotropic characteristics concerning both stiffness and PD, irrespective of factors such as gradation, material source, or applied stress levels. In addition, the study revealed that an increase in the fines content within granular base samples leads to heightened stiffness degradation and an increase in the extent of plastic deformation under the effect of F-T cycles.

By examining the cross-anisotropic properties of geomaterials and studying F-T effects, this research lays the groundwork for better analysis and development of durable roadways. Advanced cyclic true triaxial equipment enables a deeper understanding of pavement foundation materials. This work improves material selection, design, and construction, aiming for resilient and long-lasting transportation infrastructure. It is believed to be a step towards creating robust, sustainable roadway systems crucial for future transportation networks.

Overall observations, challenges, and recommendations are summarized based on the results of this project as follows:

- The main goal of this phase of the project is to design and build advanced equipment that can enable to determine the anisotropic characteristics of geomaterials and be able to apply consecutive free-thaw cycles and loads on them to better mimic the field conditions. While this goal is achieved, it is crucial to continue with testing a more comprehensive list of materials that are collected throughout Iowa to create a database that can be applied anywhere under any conditions considered in roadway design in Iowa.
- Changes in gradation and increases in fines contents had a significant impact on the performance of the materials, in particular, under freeze-thaw cycles. More comprehensive tests with a variety of gradations and materials need to be tested.
- Simulation of moving wheel loads was evaluated for selected samples. It is recommended to expand the list of materials and simulate this on a wide variety of geomaterials used in roadway systems.

CHAPTER 1 INTRODUCTION

1.1 Background

The structural performance of the roadway systems is strongly dependent on the foundation layers (i.e. base, subbase, and subgrade) and their properties. These layers serve as a support system to the overlaying asphalt or concrete layers that are constantly exposed to traffic loading so their properties play an important role to determine the longevity and overall performance of the pavement systems. Therefore, the characterization of the material properties which govern the response of the geomaterials to various loading and climatic conditions has become a necessity to ensure long-lasting and reliable pavement systems. Most pavement designs are typically based on the laboratory characterization material properties of the foundation layers. Thus, the accurate characterization of the material properties through laboratory tests contributes to the predictions and requirements regarding pavement performance and design life. However, considering the differences in the material behavior under the field and laboratory conditions where simplifications were done due to the capabilities of the laboratory equipment and time constraints, the predictions often do not align well with the actual performance of the pavement systems. Consequently, the behavior of the material might not accurately be characterized by the field conditions which causes predictions to be off from the actual response. Taking into account the role of the foundation layers in overall pavement integrity a need rises to employ advanced characterization of the material properties to evaluate how materials behave under realistic stress and climatic conditions.

The relationship between the geomaterials' stress-strain relationship and orientation has been widely acknowledged in the literature (Barden 1963, Graham and Houlsby 1983, Menkiti 1995, Lade and Abelev 2005, Gao et al. 2010, Melo and Cabral 2012, Lenart et al. 2014, Zapata-Medina et al. 2020, Aydin et al. 2021, Aydin et al. 2023). The studies have shown that the deformation characteristics of geomaterials are different in the vertical direction than the horizontal direction which is commonly referred to as a cross-anisotropic behavior which is a special type of anisotropy. The mechanical response of geomaterials to loading is influenced by their cross-anisotropic nature, which introduces the directional dependency of the stress-strain behavior of these materials. Thus, various researchers have been investigating the cross-anisotropic mechanical behavior of different geomaterials types. Barden (1963) conducted one of the earliest studies on the anisotropic nature of geomaterials by using linear elasticity solutions to show surface settlement. The author concluded that anisotropy contributes to an overestimation of the surface settlements. Later on, Graham and Houlsby (1983) investigated the anisotropy in lightly over-consolidated natural clays by using least squares solution and concluded that the clay is 1.8 times stiffer in the horizontal direction than the vertical direction. Menkiti 1995 performed hollow-cylinder tests to determine the anisotropy ratio (the ratio of horizontal stiffness to vertical stiffness) of clayey sands. The author reported the anisotropy ratio changing between 0.16 to 0.33. Another study done on the sandy soils reported the anisotropy ratio as 0.13 (Lade and Abelev 2005). Moreover, Lenart et al. 2014 studied the stress-strain characteristics of well-graded crushed stones for different directions and stated that the axial strains were almost two times less than the lateral strains. Zapata-Medina et al. 2019 investigated the stiffness anisotropy

of the clays at the Port of Alaska and reported the anisotropy ratios as 0.9 to 1.22 and 0.93 to 1.46 for lightly over-consolidated and over-consolidated conditions, respectively.

Despite the fact that researchers have been investigating the phenomenon of cross-anisotropy for over fifty years, it is only in recent times that studies have been conducted specifically focusing on the pavement foundation layers (Tutumluer and Seyhan 1999, Adu-Osei et al. 2001, Seyhan and Tutumluer 2002, Seyhan et al. 2005, Tutumluer 2009, Liu et al. 2014, Jing et al. 2017, Sidess et al. 2021). The cross-anisotropic nature of the geomaterials particularly becomes one of the most important factors affecting the mechanical response of foundation layers to continuous cyclic traffic loading. The nature of traffic loading induces complex stress states on geomaterials, characterized by the rotation of principal stresses where major principal stress is experienced not only in the vertical but horizontal direction (Figure 1, Lekarp et al. 2000). However, conventional testing systems are unable to accurately simulate these complex stress states, further highlighting the significance of the cross-anisotropic behavior of geomaterials in pavement foundation design.
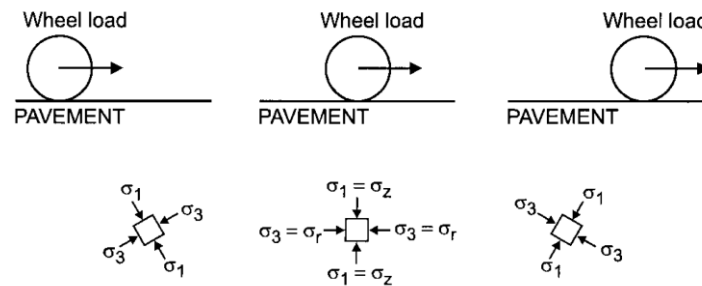
Figure 1. Principal stresses under continuous traffic loading (Lekarp et al. 2000)

The number of elastic material properties needed to characterize stress-strain behavior varies depending on the type of anisotropy present. Among different types of anisotropy, cross-anisotropic geomaterials require five independent elastic properties to solve the stress-strain problem. These properties consist of the elastic modulus in the vertical direction (E_v), elastic modulus in the horizontal direction (E_h), shear modulus in the vertical plane (G_{vh}), Poisson's ratio for the effect of vertical strain on horizontal strain (ν_{vh}), and Poisson's ratio for the effect of horizontal strain on horizontal strain at a right angle (ν_{hh}). However, in practice, geomaterials are often simplified and treated as isotropic materials, which only require two independent elastic components (E_v and ν_{vh}) to solve stress-strain problems. This simplification is primarily due to the limitations of conventional triaxial testing conducted in laboratories, which cannot accurately determine the remaining elastic components (E_h, G_{vh}, ν_{hh}). Additionally, these tests are unable to replicate realistic field stress states. The Mechanistic-Empirical Pavement Design Guide (MEPDG) (ARA 2004) utilizes a combination of mechanistic and empirical approaches for pavement system design and analysis. It considers various input parameters that impact pavement performance, including the material properties of pavement structures (e.g., stiffness characteristics of foundation layers), as well as traffic and climate conditions. M_R is commonly used to define the stiffness of geomaterials in pavement design and analysis under cyclic traffic loading. Therefore, M_R serves as a parameter corresponding to the elastic modulus of the elastic components used to solve the stress-strain problem for cross-anisotropic materials. Equations (1)

5

and (2) are used to calculate the direction-dependent M_R; vertical M_R (M^v_R) and horizontal M_R (M^h_R), respectively.

$$M^v_R = \frac{\Delta\sigma_x}{\varepsilon_x} \qquad (1)$$

$$M^h_R = \frac{\Delta\sigma_z}{\varepsilon_z} \qquad (2)$$

where $\Delta\sigma_x$ is the vertical cyclic stress, ε_x is the recoverable deformation in the x-axis, $\Delta\sigma_z$ is the horizontal cyclic stress, and ε_z is the recoverable deformation in the z-axis.

The initial studies on the cross-anisotropy of the pavement foundation layers of the M_R were performed by Tutumluer and Seyhan (1999). The authors utilized an advanced triaxial testing machine called the University of Illinois FastCell (UI-FC) to test cylindrical specimens. In the study, linear variable displacement transformers (LVDTs) were employed to measure deformations in the vertical and radial directions. The authors determined that M^h_R is lower than the M^v_R for granular materials except for the case of sandy gravel with high fines contents where M^h_R is higher than the M^v_R. Subsequently, Adu-Osei et al. (2001) conducted a study using a rapid triaxial testing (RaTT) cell to evaluate the cross-anisotropic characteristics of unbound granular materials in cylindrical specimens. The authors designed a testing program that involved recording deformations through LVDTs in both vertical and radial directions to determine M_R. In the study, the anisotropy ratio is stated as 0.5 for well-graded Texas limestone. Later on, Seyhan and Tutumluer (2002) reported anisotropy ratios for gravel and crushed stone aggregates as varying between 0.4 to 1.5. Kim et al. (2005) performed stiffness tests with RaTT on limestone, granite, and gravel and determined the anisotropy ratio as changing between 0.10 to 0.55. Melo and Cabral (2012) performed M_R tests on undisturbed subgrade material and showed that the soil has significant inherent anisotropy with a ratio varying between 0.7 to 1.0. Jing et al. (2017) investigated the cross-anisotropy of find sands used as subgrade through repeated load triaxial tests and determined that the anisotropy ratio varies between approximately 0.1 and 0.5 for different water contents and fines contents. Sidess et al. (2019) performed repeated load triaxial tests on the good-quality base material to investigate the stiffness cross-anisotropy and stated that the anisotropy ratio depends on both bulk and octahedral shear stress. Even though the researchers have been investigating the cross-anisotropy for pavement foundation layers for two decades, these studies were limited to cylindrical specimens, which do not allow direct measurement of lateral deformation corresponding to applied lateral stress. The volumetric strain under applied stresses could only be calculated using vertical and radial strains, rather than the more realistic approach of using principal strains (major = ε_1, intermediate = ε_2, and minor = ε_3), which would apply to a prismatic soil element. To address this limitation, advanced testing equipment such as cyclic true triaxial systems are required.

While the design of pavement systems relies on the use of M_R to assess the elastic response of foundation layers to traffic loading, it is important to acknowledge that these systems also experience plastic deformations due to continuous traffic load. The gradual accumulation of plastic deformation plays a significant role in the formation of wheel tracks and longitudinal surface depressions on the pavement. Moreover, it can serve as an indicator of pavement structure deterioration, which is a major concern. Although the amount of PD caused by each

load application is relatively small, these displacements are non-recoverable. When these loads are repeatedly applied over a high number of cycles, the cumulative effect of the unrecoverable deformations can become significant and lead to noticeable pavement distress. As a result, it becomes necessary to characterize and understand the PDs that occur in pavement systems for thorough characterization. To this end, researchers have performed repeated load triaxial tests to evaluate the plastic deformation properties of materials. Puppala et al. (1999) observed that the nature and magnitude of the plastic deformation of clayey soils are stress and moisture-depended. The authors also stated that sandy soils experience less plastic strain than clayey soils after performing repeated load triaxial tests. The definition of Shakedown, as provided by Werkmeister et al. (2001), refers to the point at which PD stabilizes, and the material begins to exhibit elastic behavior. In their study on granular materials subjected to PD tests at varying stress levels, the researchers classified the behavior into three distinct categories: A, B, and C. Category A represents a behavior characterized by the presence of Shakedown. In other words, the PD reaches a limit where it becomes stabilized, and the material exhibits elastic behavior beyond this point. Category B displays an intermediate behavior compared to the other categories. In this category, it is not possible to clearly identify the occurrence of Shakedown or the failure mechanism. The material's response falls within a transitional range, making it challenging to determine whether the PD is stabilizing or progressive failure is occurring. Category C pertains to the region where incremental failure takes place. In this category, the material experiences continuous and incremental deformation that eventually leads to failure. The PD does not reach a state of stabilization. These categories, as defined by Werkmeister et al. (2001) serve to classify the behavior of granular materials during PD tests under different stress levels. In Cerni et al. (2012), the authors focused on laboratory experiments aimed at examining the PD behavior of unbound granular materials used as a subbase. In the study, the authors incorporated the concept of shakedown and demonstrated its usefulness in comprehending the material's susceptibility to rutting. Many researchers have devoted their efforts to studying the PD behavior of pavement foundation layers (Puppala et al. 1999, Chai et al. 2002, Uzan 2004, Puppala et al. 2009, Saberian et al. 2018). However, it is worth noting that the existing literature lacks a comprehensive understanding of the cross-anisotropy of plastic deformations. This knowledge gap is primarily due to the scarcity of advanced testing equipment required for conducting such research, making it uncommon in the field.

True triaxial test setups have been developed as advanced systems for soil testing to overcome the limitations of conventional triaxial soil testing methods. While conventional triaxial testing can be useful in cases where loading and specimen geometry (cylindrical shape) are axisymmetric, it falls short when it comes to simulating complex stress conditions that are non-axisymmetric or generalized. To accurately replicate these complex stress conditions that are commonly encountered in the field, a true triaxial testing system becomes indispensable as it allows for testing geomaterials under three-dimensional (3D) stress states. Furthermore, the investigation of the soil element's behavior under the influence of three principal stresses can only be achieved through true triaxial tests, specifically by conducting stress path tests. Researchers such as Silvestri et al. (1988), Choi et al. (2007), Yin et al. (2010), Shao et al. (2017), and Aydin et al. (2021, 2023a,b) have emphasized the importance of true triaxial tests in studying the impact of these three principal stresses on soil behavior.

Based on the types of boundary conditions, researchers have categorized true triaxial test devices into three main groups: six rigid boundaries, six flexible boundaries, and a combination of rigid and flexible boundaries.

The initial development of a rigid-boundary apparatus by Kjellman (1936) allowed for the application of principal stress states to a cubical soil specimen using rigid end platens. This true triaxial device incorporated six rigid platens that were designed to slide relative to one another, enabling uniform deformation of the soil specimen while minimizing corner interference issues (Hambly 1969, Airey and Wood 1988, Ibsen and Prasstrup 2002). Furthermore, the use of rigid platens ensured that the soil specimen experienced variable principal stresses, with σ_3 potentially becoming intermediate or major principal stresses. However, it should be noted that the uniformity of stresses may not be as consistent as the deformations, and the preparation of the specimen using this apparatus could be challenging and time-consuming compared to other types of true triaxial testing techniques.

The utilization of six flexible boundaries involves subjecting cubical or prismatic samples to stress in all six directions using water-filled pressurized rubber cells. One of the early researchers to investigate the behavior of sand under general stress states using flexible boundaries was Bell (1965), who developed a 3D compression apparatus. Several other researchers have also contributed to the literature on true triaxial test devices with flexible boundaries, including Ko and Scott (1967), Sture and Desai (1979), Yamada and Ishihara (1979), Reddy et al. (1992), Mandeville and Penumadu (2004), Choi et al. (2008), and Voznesensky et al. (2013). While this type of true triaxial test device allows for achieving uniform stress states on each face of the specimen, it has a significant drawback. The potential occurrence of nonuniform large strains arises from the interference of deformations at the corners of the specimen in each direction.

The mixed-boundary true triaxial test devices encompass two main types: the one-direction rigid-boundary type and the two-direction flexible boundary type (rigid-flexible-flexible). This combination has been explored in studies conducted by Silvestri et al. (1988) and Shao et al. (2017). Additionally, there are mixed-boundary types involving two-direction rigid boundaries and one-direction flexible boundaries (rigid-rigid-flexible) as investigated by Green (1969), Lade and Duncan (1973), Shapiro and Yamamuro (2003), AnhDan and Koseki (2005), Yin et al. (2010), Ye et al. (2012), and Zheng et al. (2021). Green (1969) developed the first mixed-boundary true triaxial device for cubic specimens. In this device, both major and intermediate principal stresses were applied through rigid vertical and horizontal platens, respectively. The minor principal stress was exerted on the flexible boundary, which enclosed the soil with a rubber membrane, using cell pressure. The pressure cells in the device could be filled with either water or air. However, a concern with Green's design was the undersizing of the horizontal platens to prevent interference between the rigid platens. This undersizing could result in a nonuniform stress region on the rigid horizontal face of the specimen. Lade and Duncan (1973) made modifications to Green's design by introducing a special horizontal platen made of stainless steel and balsa wood. This modified platen had a low modulus in the vertical direction and a high modulus in the horizontal direction, aiming to eliminate the gap in the horizontal direction. Since then, researchers have developed various modifications and adaptations of mixed-boundary true triaxial apparatus based on the foundation laid by Green (1969) and Lade

and Duncan (1973). One of the main advantages of this type of true triaxial device is the achievement of uniform stress distribution at the flexible boundaries while preventing interferences at the edges of the specimen. This advantage helps reduce potential friction between the vertical and horizontal pistons. However, concerns regarding gaps at the corners of the specimen remain valid, especially if the specimen length exceeds the horizontal rigid plate. In such cases, nonuniform stresses and strains may occur in these regions, which can affect the overall deformation behavior of the specimen, leading to excessive deformation where the gaps exist. This phenomenon is referred to as soil squeezing (Xie et al. 2022). Researchers have made several attempts to address the issue of nonuniformity in the regions with gaps. One approach involves incorporating a trapezoidal joint in front of the rigid plates, as proposed by Li et al. (2016). This modification helps mitigate the nonuniformity in stress distribution. Another method, suggested by Yin et al. (2010), involves altering the movement mechanism of the rigid plates to create sliding rigid plates. This design is similar to the six rigid boundaries and aims to prevent the occurrence of nonuniform strains. However, it should be noted that even with sliding rigid plates, the stresses experienced on the specimen surface may still exhibit nonuniformity due to the frictional forces that can arise between the plates. Despite the limitations and drawbacks associated with various types of true triaxial apparatuses, these devices serve as highly valuable tools for independently controlling the three principal stresses. By enabling precise control over these stresses, true triaxial testing provides valuable insights into how changes in stress conditions affect both the principal strain values and the cross-anisotropic behavior of geomaterials.

M_R and PD play a crucial role as input parameters in pavement design. Consequently, researchers have extensively investigated the impact of environmental conditions, including freezing and thawing, on the stiffness characteristics and plastic deformation of pavement foundation layers. These studies have been conducted over the years by various researchers, particularly in cold regions like the majority of the states in the Midwest region to ensure long-term pavement performance (Simonsen et al. 2002, Konrad and Lemieux 2005, Qi et al. 2008, Li et al. 2011, Wang et al. 2018, Domitrović et al. 2019, Saberian and Li 2021, Liu et al. 2022).

One F-T cycle consists of a freezing phase and a thawing phase. During the freezing phase (typically occurring in winter), the M_R of geomaterials and pavement layers is expected to increase, as noted by Rosa et al. (2016). The water present in the material freezes and expands by approximately 10%, leading to an enlargement of pore sizes. Subsequently, in the thawing phase (usually in spring), the ice melts, resulting in a decrease in volume. This volume reduction, combined with the increased pore size from freezing, leads to an increase in the porous structure within the geomaterials. This increase in porosity, coupled with near-saturation conditions, generally compromises the integrity of the geomaterials and reduces the M_R, as highlighted by Rosa et al. in 2016. Simonsen et al. (2002) conducted M_R tests on silty sands and sands to emphasize the significance of a complete F-T cycle on the M_R of soils. The researchers observed a decrease of approximately 20-60% in M_R values after a single F-T cycle. Similar findings were reported by Li et al. (2011) for Alaska granular base materials. Li et al. (2011) also investigated the impact of gradation on M_R degradation. The study revealed that an increase in fines content made the base materials more susceptible to F-T effects when exceeding the optimum fines content. This led to issues with strength and stability due to reduced bonding between the coarser

particles, which in turn diminished the beneficial effects of angularity and interlocking mechanisms (Mishra et al. 2010). Ultimately, these factors contributed to lower M_R values. Furthermore, during the freezing phase, the internal pressure within the soil or aggregate matrix increases as a result of the volume expansion during water freezing. This rise in internal pressure can lead to the deterioration of particles within the matrix. Such particle deterioration contributes to an increase in the fines content of the material, ultimately reducing its M_R and increasing its susceptibility to frost, as discussed by Konrad and Lemieux (2005). However, it is worth noting that an increase in fines content within a soil or aggregate matrix can also have the potential to enhance the M_R of the material to some extent. Each material typically has an optimum fines content at which it exhibits the highest stiffness properties. An increase in fines content, caused by the F-T action, can help the material reach its optimal fines content and more effectively fill the voids within the matrix. However, as multiple F-T cycles occur consecutively, the M_R properties of geomaterials are expected to decrease due to excessive fines content, as highlighted by Wang et al. (2018). Therefore, while fines content can have both positive and negative effects on the M_R properties of materials, prolonged exposure to F-T cycles may lead to a reduction in M_R properties due to the accumulation of excessive fines content.

F-T cycles have a similar impact on the PD characteristics of materials as they do on the M_R. Bilodeau et al. (2012) conducted PD tests to examine the influence of F-T cycles on unbound granular materials. The study revealed that the effect of F-T cycles is more significant than the gradation of the materials in terms of altering the PD behavior. Li et al. 2019 studied the PD characteristics of Alaskan granular base course materials. The authors observed that the PD values of the materials increased after the F-T cycle also depending on the systems' accessibility to a water source. In their study, Akbas et al. (2021) investigated how F-T cycles affected the plastic strain of subbase and base materials. The authors found that the plastic deformation increased as the number of F-T cycles increased for the subbase. However, it was concluded that the plastic deformation of base materials did not exhibit significant changes after undergoing F-T cycles.

The existing literature lacks studies that accurately replicate realistic F-T cycle conditions experienced by pavement foundation layers in the field. In the field, geomaterials undergo F-T cycles while being subjected to specific surcharge loading and horizontal confinement. However, most laboratory experiments typically involve subjecting geomaterials to F-T cycles in freezer units and subsequently transferring them to testing equipment. This discrepancy between laboratory testing conditions and field conditions introduces limitations in the research findings. The handling and transportation of specimens from the freezer units to the testing equipment can lead to disturbances in the specimens, potentially resulting in reductions in the measured M_R and an increase in PD values. These factors contribute to a lack of studies that accurately capture the true impact of realistic F-T cycles on pavement foundation layers.

1.2 Problem Statement

Most pavement designs and road infrastructure performance predictions are made based on the laboratory characterization of the materials that are used during pavement construction.

However, these designs made with material properties tested with standard test methodologies do not typically fulfill their predicted service life and often require early and more frequent maintenance practices. Moreover, field and laboratory performance of pavement materials do not usually agree well with each other which adds more complexity to the pavement designs. The main reason for these problems is the standard test methods used to characterize the strength and stiffness of materials used in pavement designs. Standard testing methods do not incorporate the cross-anisotropic behavior and stress dependency of materials and do not simulate climate conditions (cold and hot temperatures) on materials. These parameters become more critical, especially with geomaterial characterization when used in pavement foundation systems. The geomechanical properties of pavement foundation materials (geomaterials) used in mechanistic pavement design are the level one input. These geomaterials include both fine-grained and coarse-grained soils and aggregate materials. Currently, the geomechanical characteristics of these materials are obtained from standard laboratory tests such as California Bearing Ratio (CBR) and standard M_R. Nevertheless, standard M_R tests commonly conducted in the laboratory do not always apply the most damaging field loading conditions for predicting M_R and PD responses of pavement base/subbase/subgrade layers due to moving wheels. This is the main problem that causes significant pavement performance problems. These problems are causing pumping and erosion failures for rigid pavements and rutting and corrugation for flexible pavements. In addition, potholes, wash-boarding, and rutting occurrences on unpaved roads become more frequent due to a lack of understanding of the geomaterials/soils characterization.

In a typical standard M_R test, test samples are prepared in cylindrical shapes and compacted in the vertical direction (z-axis). Then, the dynamic load is applied in the same direction as the material gets more compacted (z-axis). Thus, the M_R and PD of the geomaterials tested become the least conservative values. In the real field conditions, loads applied via moving wheel on the pavement foundations systems are imposed to not only the z-axis but all three directions (x-, y-, z-axes)

Previous research has shown that the continuous rotation of principal stresses due to the rolling nature of moving wheel loads would lead to lower M_R and higher accumulated PDs (Brown 1996). Unfortunately, standard tests commonly performed in the laboratory do not consider such effects of moving wheel loads and directional (x-, y-, z-axes) dependency (which is called anisotropy) of material properties (AASHTO T307 2017).

The United States has 6 different climatic regions for pavement design. Iowa is in climatic region 3, which experiences wet-hard freeze-spring thaw. With high availability of moisture and the large number of freezing and thawing cycles, proper testing and advanced characterization of Iowa soils and geomaterials is essential to achieve good, long-term performance of Iowa transportation infrastructure systems. Since F-T has a significant impact on geomaterials performance, it is very important to be able to test the behavior of soils in the laboratory under circumstances that represent the actual field conditions. Unfortunately, current standard methods are not able to test the geomaterials' behavior under these actual field conditions. Currently, laboratory specimens are tested at ambient room temperature and room humidity. However, in the field, geomaterials are subjected to wheel loads under different temperature and humidity

conditions and continuous F-T cycles. These conditions will result in different pavement performance than those measured from the current laboratory test methodologies.

The present study evaluates, the anisotropic behavior of geomaterials in three directions and under different climatic conditions through an advanced testing system. Laboratory tests were conducted on 10 different geomaterials collected from a variety of sources in Iowa. These geomaterials included well-graded and poorly-graded aggregates, silty sand, and low-plasticity silt. The geomaterials were exposed to varying stress states concerning all three directions to have a deeper understanding of the cross-anisotropy concept for both M_R and PD. Anisotropy ratios (ratio of M^h_R to M^v_R) were determined for the geomaterials to quantify the anisotropy. These data will serve as geomaterials performance indicators for determining the quality, stiffness, and strength properties of geomaterials under various field-loading conditions and climatic conditions. In addition to cross-anisotropic testing, M_R and PD characteristics of granular geomaterials with an increase in fines content were evaluated through F-T testing.

1.3 Objectives

The objectives of the research are to:

- **Evaluating the Anisotropic Behavior of Geomaterials**

This objective was achieved by constructing a series of laboratory tests on geomaterials samples collected from Iowa. The total number of different materials that were tested is 10, including coarse-grained and fine-grained soils. M_R and PD were determined for all three directions. The anisotropy ratios were calculated for the geomaterials tested.

- **Determining the Performance of Geomaterials under Different Climatic Conditions**

Specimens were tested under different temperature conditions with the help of an environmental chamber to determine the actual field performance of materials in the laboratory test. Granular specimens with varying fines contents were subjected to a certain number of F-T cycles and tested for M_R and PD.

1.4 Research Plan

The proposed research consisted of seven tasks, described in detail below:

Task 1: Meet with the Project's Technical Advisory Committee (TAC) to Review the Project Scope and Work Plan
Task 2: Literature Review
Task 3: Collection of Materials and Development of a Laboratory Test Matrix
Task 4: Laboratory Testing
Task 5: Advance Characterization of Geomaterials
Task 6: Evaluation of Actual F-T Performance of Geomaterials

Task 7: Preparation of Draft Final Report

1.5 Research Benefits

The results of this study are expected to improve the performance, economics, and service lifespans of both paved and granular roads in Iowa. The results and recommendations of this project provide a foundation for further development of decision-making tools to evaluate the relative paved and unpaved road performances for Iowa. The benefits of this research are summarized below:

- Results obtained from this equipment will estimate the field performance of granular road surface and pavement foundation materials better since it will take into account field conditions during testing such as temperature and soil behavior and response in x, y, and z axes (cross-anisotropy).
- Designs made based on the data obtained from this equipment will be the most representative of complex field loadings and will provide more reliable performance predictions. The actual F-T performance of geomaterials is also simulated with this equipment due to the advanced features.
- Data obtained from these tests result in an improved understanding of granular road surface and pavement foundation system behavior and thus will increase the performance of the Iowa transportation infrastructure system.

CHAPTER 2 PHYSICAL CHARACTERIZATION OF MATERIALS

Ten distinct materials sourced from various regions of Iowa were gathered to assess the properties of the Iowa base, subbase, and subgrades (Figure 2). Among these materials, six were designated as base materials [Ames Mine, Bethany Falls Limestone, Crocker Pit, Oneota Formation Dolomite, Plano Quarry, and Weber Quarry) Figure 2a-f], while two were categorized as subbase materials (Shambaugh Quarry and Stone City Quarry, Figure 2g-h), and the remaining two were identified as subgrade materials [Pottawattamie County CBIS (Council Bluffs Interstate System 'CBIS' and Plymouth County (95) 'Plymouth County', Figure 2i-j].
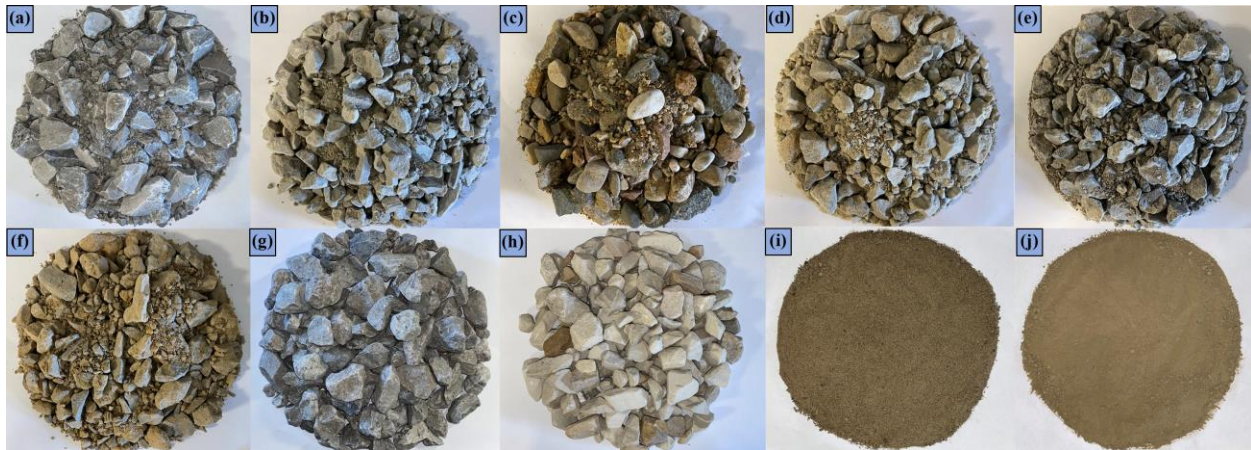
Figure 2. Materials used in the study: (a) Ames Mine, (b) Bethany Falls Limestone, (c) Crocker Pit, (d) Oneota Formation Dolomite, (e) Plano Quarry, (f) Weber Quarry, (g) Shambaugh Quarry, (h) Stone City, (i) Pottawattamie County CBIS (Council Bluffs Interstate System), (j) Plymouth County (95)

2.1 Classification of Materials

To identify the characteristics of the materials, a series of index tests have been conducted within the scope of the report.

The material classification was determined through various tests. Sieve analysis (ASTM D6913/D6913M-17) was employed to assess the gradation of the materials, while Atterberg limits and their liquid and plastic limits were determined using ASTM D4318-17e1. Additionally, hydrometer analysis (ASTM D7928-21e1) was conducted to determine the silt and clay content of the two subgrade materials. To ensure consistency in behavior concerning gradation, a designated gradation was applied to the base materials following the ASTM D1241 – 15 while the remaining materials were used in their original, as-received gradation. The results of the abovementioned tests (sieve and Atterberg limits) were used to determine the soil classification according to the Unified Soil Classification System (USCS) (ASTM D2487) and the American Association of State Highway and Transportation Officials (AASHTO) soil

classification system (AASHTO M 145). Table 1 shows the percentages of the gravel, sand, fine-grained, and Atterberg limits along with the soil classification.

Table 1. Index properties of materials

Material	Layer	Gravel (%)	Sand (%)	Fines (%)	LL	PI	USCS	AASHTO
Ames Mine	Base	64	31	5	NP	NP	GW	A-1-a
Bethany Falls Limestone	Base	64	31	5	NP	NP	GW	A-1-a
Crocker Pit	Base	64	31	5	NP	NP	GW	A-1-a
Oneota Formation Dolomite	Base	64	31	5	NP	NP	GW	A-1-a
Plano Quarry	Base	64	31	5	NP	NP	GW	A-1-a
Weber Quarry	Base	64	31	5	NP	NP	GW	A-1-a
Shambaugh Quarry	Subbase	99	1	0	NP	NP	GP	A-1-a
Stone City Quarry	Subbase	99	1	0	NP	NP	GP	A-1-a
Pottawattamie County CBIS (Council Bluffs Interstate System)	Subgrade	0	84	16*	NP	NP	SM	A-2-4
Plymouth County (95)	Subgrade	1	4	95**	36	25	ML	A-6

Fines = silt and clay
LL = liquid limit
PI = plasticity index;
USCS = Unified Soil Classification System
AASHTO = American Association of State Highway and Transportation Officials
NP = non-plastic
*Hydrometer analysis showed that fines contain 38% silt and 62% clay
**Hydrometer analysis showed that fines contain 74% silt and 26% clay

All six base materials were classified as well-graded (GW) and A-1-a, according to the USCS and AASHTO, respectively. The two subbase layers were classified as poorly graded (GP) and A-1-a, according to the USCS and AASHTO, respectively. CBIS, the subgrade, was classified as silty sand (SM) and A-2-4, according to the USCS and AASHTO, respectively. Meanwhile, Plymouth, the subgrade, was classified as low plasticity silt (ML) and A-6, according to the USCS and AASHTO, respectively.

2.2 Specific Gravity (G_s) and Absorption

After conducting particle gradation analysis, specific gravity (G_s) tests were performed on the materials. The base and subbase materials were subjected to ASTM C127 and C128, while ASTM D854 was utilized for the subgrade materials. Additionally, the absorption capacity of the base and subbase materials was determined following the ASTM C127 and C128. The G_s and

absorption of each material (excluding the subgrade materials) were calculated by taking the weighted average of the coarse fraction (> No. 4 sieve) and fine fraction (< No. 4 sieve) of the material, following the prescribed calculation outlined in ASTM C127 and C128. Table 2 presents the oven-dry (OD), saturated-surface-dry (SSD), and apparent G_s, as well as the absorption capacity of base and subbase materials. It should be noted that for the subgrade, only the G_s value was reported, as ASTM D854 does not include the measurement of absorption.

Table 2. Specific gravity (G_s) and absorption of materials

Material	Oven-Dry (OD) G_s	Saturated - Surface-Dry (SSD) G_s	Apparent G_s	Absorption (%)
Ames Mine	2.61	2.65	2.72	1.03
Bethany Falls Limestone	2.57	2.63	2.72	2.10
Crocker Pit	2.60	2.65	2.73	1.73
Oneota Formation Dolomite	2.66	2.69	2.75	1.21
Plano Quarry	2.66	2.69	2.75	1.21
Weber Quarry	2.64	2.68	2.75	1.07
Shambaugh Quarry	2.51	2.58	2.69	2.78
Stone City Quarry	2.28	2.44	2.71	6.93
Pottawattamie County CBIS (Council Bluffs Interstate System)	NA	NA	2.62	NA
Plymouth County (95)	NA	NA	2.67	NA

G_s = specific gravity

NA = not available

For the base materials, namely Ames Mine, Bethany Falls Limestone, Crocker Pit, Oneota Formation Dolomite, Plano Quarry, and Weber Quarry, the G_s values varied between 2.57 and 2.66 for the oven-dry (OD) condition, between 2.63 and 2.69 for the saturated surface-dry (SSD) condition, and between 2.72 and 2.75 for the apparent condition. Additionally, the absorption values for these materials ranged from 1.03 to 2.10%. Regarding the subbase materials, Shambaugh Quarry and Stone City Quarry, the G_s values ranged from 2.28 to 2.51 for OD, from 2.44 to 2.58 for SSD, and from 2.69 to 2.71 for apparent conditions. Moreover, the absorption capacity for these subbase materials was relatively higher, with values ranging from 2.78% to 6.96%. For the subgrade materials, CBIS and Plymouth County, only the apparent G_s values showed variation, ranging from 2.62 to 2.67. The other properties were not applicable to these subgrade materials. Overall, as anticipated, the highest G_s value was observed for the apparent condition across all types of materials.

2.3 Proctor Compaction

The maximum dry unit weight (MDU) and optimum moisture content (OMC) values for the base and subgrade materials were determined according to the ASTM D698-12. However, for the

subbase materials, which possess an open-graded gradation, the MDU was determined using the vibratory hammer following the ASTM D7382-20 standard. In the case of the base materials that contained oversize particles, corrections were made following the guidelines of ASTM D4718. These corrections were applied to calculate the corrected MDU and OMC values for the base materials, taking into account the presence of these oversize particles. Table 3 presents a summary of both the Proctor compaction test results (conducted as per ASTM D698-12) and the corresponding corrected unit weight and moisture content values (determined following ASTM D4718) for base and subgrade materials. For the base materials, the report utilizes the corrected values for all subsequent analyses and discussions.

Table 3. Uncorrected (actual) and corrected Proctor compaction test results

Material	Proctor Compaction Results		Corrected Proctor Compaction Results	
	MDU (pcf)	OMC %	MDU (pcf)	OMC %
Ames Mine	131	6.5	146	3.5
Bethany Falls Limestone	143	7.3	150	4.8
Crocker Pit	146	8.4	153	5.0
Oneota Formation Dolomite	132	8.8	146	4.9
Plano Quarry	130	8.6	145	4.6
Weber Quarry	130	7.2	143	4.4
Pottawattamie County CBIS (Council Bluffs Interstate System)	109	15.0	NA	NA
Plymouth County (95)	110	16.3	NA	NA

MDU = maximum dry unit weight
OMC = optimum moisture content
NA = not available

The results indicated that after applying the oversize correction, the MDU of the base materials increased, while the OMC decreased. This can be attributed to the presence of coarse aggregates and their low absorption capacity. The low absorption capacity of these aggregates leads to a reduced OMC, as they do not retain as much moisture. Following corrections, MDU and OMC of Ames Mine were determined as 146 pcf and 3.5%, respectively. Bethany Falls Limestone had MDU and OMC as 150 pcf and 4.8%, respectively. Crocker Pit yielded the highest MDU with 153 pcf corresponding to 5.0% OMC. Oneota Formation Dolomite had MDU and OMC as 146 pcf and 4.9%. MDU and OMC were determined as 145 pcf and 4.6% for Plano Quarry. Weber Quarry had the minimum MDU of 146 pcf and OMC of 4.4%. As expected subgrade materials yielded lower MDU and higher OMC due to their finer gradation. CBIS had MDU as 109 pcf and 15% of OMC while Plymouth County had MDU and OMC as 110 pcf and 16.3%, respectively.

2.4 Vibratory Hammer

For the subbase materials MDU obtained following the ASTM D7382-20 is presented in Table 4. Due to the open-graded nature of the subbase materials, no water was utilized during the test, resulting in the absence of an OMC value.

Table 4. Maximum dry density (MDU) of subbase materials

Material	MDU (pcf)
Shambaugh Quarry	101
Stone City Quarry	100

MDU = maximum dry unit weight

The compressibility of the subbase materials exhibited a high level of similarity, with an MDU of 101 pcf for Shambaugh Quarry and 100 pcf for Stone City Quarry. As expected, the open-graded subbase materials, characterized by the absence of fine aggregate and fine-grained materials in their particle size distribution, yielded lower MDU values overall.

CHAPTER 3 STANDARD MECHANICAL CHARACTERIZATION OF GEOMATERIALS

The structural capacity of the pavement systems, regardless of the type i.e. flexible, rigid, or composite, depends on all the components that make up the system. Inadequate design or construction of any of these components frequently results in diminished functionality or deterioration of the system which causes distress and reduced serviceability. Therefore characterizing the mechanical properties of these components is of utmost importance to ensure reliable pavement service analysis.

3.1 Resilient Modulus of Unbound Layers

Although most of the performance criteria for pavements are focused on surface conditions, it should be noted that a significant portion of surface distresses can be attributed to the underlying unbound layers, commonly referred to as pavement foundation layers. Therefore, understanding the mechanical behavior i.e. stress-strain characteristics of these layers contributes highly to maximizing pavement performance. In a study conducted by Christopher et al. in 2006, the researchers provided a summary of the geotechnical factors that contribute to distress in flexible pavements, rigid pavements, and composite pavements. The composite pavement configuration considered in the study assumed an asphalt concrete (AC) overlay placed on top of a Portland cement concrete (PCC) rigid pavement. A modified version of the distress summary is presented in Table 5.

As can be seen from Table 5, the authors concluded that among the other geotechnical factors, stiffness and strength of the pavement foundation layers are dominantly affecting the many pavement distresses when it is considered both moisture/drainage problems and freeze/thaw directly affecting those factors. Due to the nature of the traffic loading, pavement systems are designed not to experience any stress levels that could cause strength failure in pavement foundation layers. Therefore, conventional strength parameters such as cohesion and friction angle are not needed for the structural capacity of the unbound layers. To this end stiffness property referred to as M_R is highly used for pavement analysis.

The stiffness of unbound materials plays a crucial role as the most significant mechanical characteristic in pavements. It determines how stresses and strains are distributed within the pavement system, as the relative stiffnesses of different layers dictate this distribution. It is widely acknowledged that the stiffness of unbound layers has a direct impact on the tensile strain experienced at the bottom of the asphalt layer and the compressive vertical strain observed at the top of the subgrade (Christopher et al. 2006).

Laboratory characterization of the M_R is one of the most commonly used methods to determine the stiffness characteristics of the unbound layers. M_R is a parameter that defines the ratio between the cyclic stress ($\Delta\sigma$) applied to a material and the corresponding recoverable (elastic) strain after undergoing multiple cycles of repeated loading which represents the traffic loading.

19

As such, the M_R serves as a direct measure of the stiffness of unbound materials within pavement systems.

Table 5. Geotechnical factors influencing pavement distresses

	Pavement distress	Inefficient base stiffness/strength	Inefficient subgrade stiffness/strength	Moisture/Drainage Problems	Freeze/Thaw	Swelling	Contamination	Erosion	Spatial Variability
Flexible pavement	Fatigue Cracking	X	X	X	X		X		
	Rutting	X	X	X	X		X		
	Corrugations	X							
	Bumps				X	X			X
	Depressions	X		X	X		X		X
	Potholes			X	X				X
	Roughness	X	X	X	X	X	X		X
Rigid pavement	Fatigue Cracking	X	X	X	X		X	X	
	Punchouts (CRCP)	X	X	X	X		X	X	
	Pumping			X				X	
	Faulting	X		X	X		X	X	
	Roughness	X		X	X		X	X	X
Composite pavement	Reflection Cracking	X		X				X	
	Roughness	X		X	X	X		X	X

CRCP = continuously reinforced concrete pavement
Source = modified from Christopher et al. (2006)

M_R of unbound layers is primarily investigated using conventional triaxial cells that have the capability of applying cyclic loads. This method is the preferred choice among various laboratory tests due to several reasons. Firstly, these triaxial cells are readily available and accessible in many laboratories, making them widely used. Secondly, they allow for controlled drainage during testing, which is crucial for accurately simulating field conditions. Lastly, over the years, standardized testing protocols for M_R determination in unbound materials have been developed and continuously improved, further enhancing the reliability and consistency of the results obtained from triaxial cell testing. However, one disadvantage of conventional triaxial systems for investigating the M_R of unbound layers is their limited ability to simulate the stress states that occur in the field due to the moving nature of traffic loads. To address this limitation, true triaxial equipment can be used. True triaxial systems provide more realistic stress conditions by allowing for the application of multidirectional stresses, better representing the complex loading states experienced by pavements under traffic. This enhanced simulation capability offers a more

accurate representation of field conditions, leading to an improved understanding and characterization of the behavior of unbound materials in pavement systems. Chapter 4 of this report will provide a more comprehensive exploration of the true behavior of unbound layers under realistic field loading conditions. M_R of unbound materials is simply calculated as the ratio of applied $\Delta\sigma$ to the corresponding elastic strain (ε_a) as shown in Equation (1) (Chapter 1).

3.2 Methods/Test Procedure

This report utilizes cyclic true triaxial equipment that has the capability to conduct both conventional tests with cylindrical specimens and advanced true triaxial testing with prismatic specimens. The equipment was utilized to determine the stiffness characteristics of base, subbase, and subgrade materials collected from different locations within Iowa. For this chapter, cyclic true triaxial equipment was used in its conventional testing configuration. This approach allows for the accurate evaluation of the stiffness properties of the mentioned pavement layers, providing valuable insights into their behavior under cyclic loading conditions for conventional testing methods.

A custom-designed Soil Poly-Axial Test System, SPAX-3000, consists of five main parts: (a) a desktop computer, (b) a digital servo controller and data acquisition system (SCON-3000), (c) a pressure control panel and volume changing device (PCP-200), (d) a hydraulic power supply (HPS), and (e) a cyclic true triaxial unit as shown in Figure 3. Figure 3 shows the components of the true triaxial regarding only the cylindrical specimen. The advanced features (horizontal load actuators and deformation measurements) of the SPAX-3000 will be shared in more detail in Chapter 4.

The desktop computer is equipped with the software referred to as CATS Software provided by the manufacturer to control and send commands to SCON-3000. The desktop computer with the software plays a crucial role in operating the entire system effectively.

SPAX-3000 uses SCON-3000 to control displacements, loads, and temperatures. SCON-3000 includes a complete and self-contained digital signal conditioning system with a wireless control unit that employs a built-in function generator, data acquisition, and digital input/output (I/O) units shown in Figure 3, front and rear, respectively.

The confining pressure applied to the specimen is provided to the true triaxial cell by PCP-200. PCP-200 also has a feature to control top and bottom pore pressure which is not used for M_R testing. In addition, PCP-200 enables to apply vacuum to the specimen with the built-in vacuum when it is needed (during compaction or the assembly of the specimen pre-confining pressure).

HPS supplies hydraulic pressure to all the hydraulic testing systems. Load actuators, which apply forces to the test specimens in both vertical and horizontal directions, are connected to the HPS via hydraulic hoses.

Lastly, the cyclic true triaxial unit, the main component of the SPAX-3000, is a stress-controlled rigid-rigid-rigid boundary type of loading device with the ability to run tests with various boundary conditions (rigid-rigid-flexible, rigid-flexible-flexible) and also cylindrical standard M_R testing with specimen dimensions of 6 inches by 12 inches (diameter by height). For the standard testing, only the vertical actuator equipped with the dynamic load cell (capacity of 25,000 lbf) was used along with the external LVDTs with a capacity of ± 1.0 inches. In addition, the internal LVDTs with a capacity of measuring ± 0.25 inches were used to measure the deformations following the AASHTO T307 (2017).
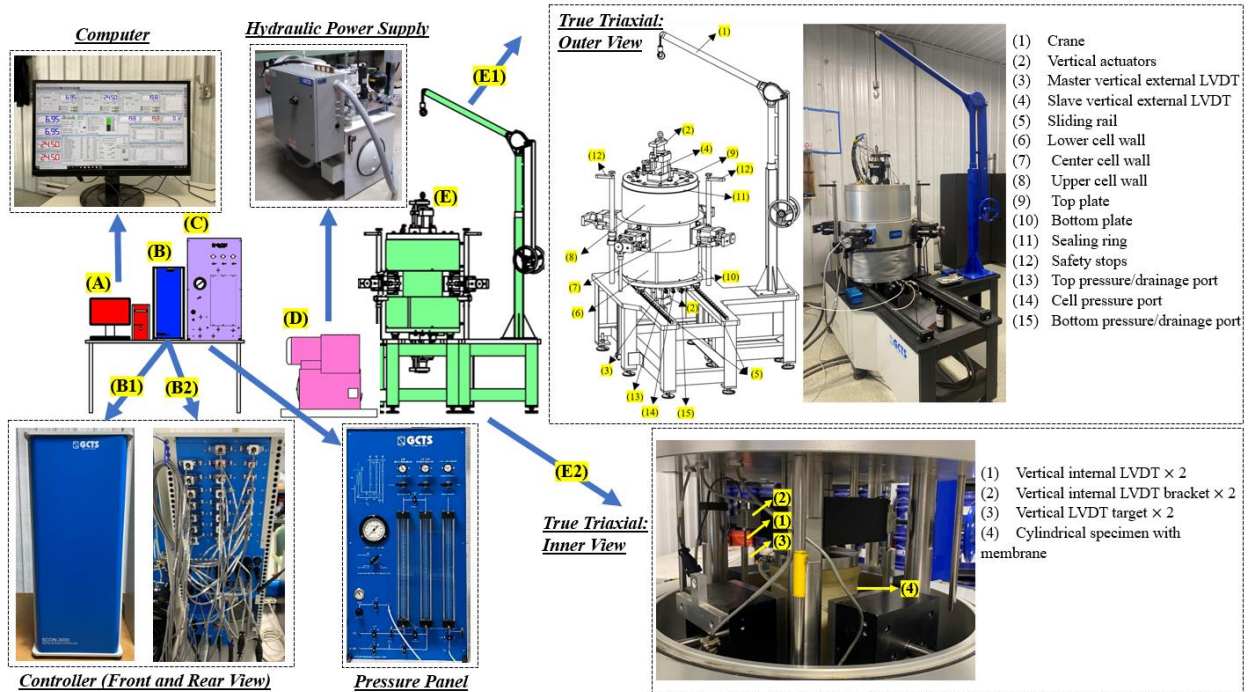
Figure 3. Components of SPAX-3000: (a) desktop computer, (b) digital servo controller and data acquisition system, (c) pressure control panel and volume changing device, (d) hydraulic power supply, and (e) cyclic true triaxial unit

Figure 4 illustrates the cylindrical specimen and stresses applied stresses during a test in terms of principal stresses where the vertical axis (z-axis) is the major principal stress (σ_1) and the horizontal axis is the minor principal stress (σ_3).
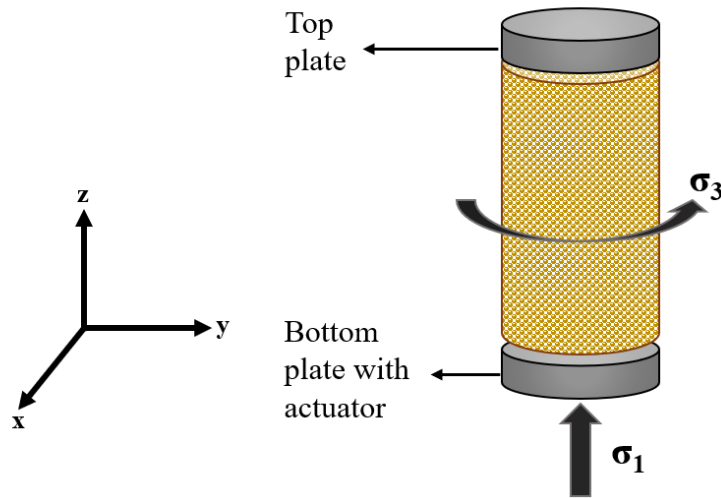
Figure 4. Principal stress configuration of cylindrical specimen

Figure 4 indicates that the σ_1 axis is oriented vertically, while the cyclic loading is specifically applied from the bottom due to the SPAX-3000's actuator configuration. In this configuration, only the bottom actuator is equipped with a load cell to apply cyclic stress. Nevertheless, it is important to note that the standard M_R testing conditions, as outlined in AASHTO T307 (2017), still apply regardless of the specific configuration.

The SPAX-3000 testing process involves three main stages: specimen preparation, specimen assembly, and M_R or/and PD testing. The materials introduced in detail in Chapter 2 were prepared to be tested for M_R testing following the specimen assembly.

Cylindrical specimens with 6 inches by 12 inches were prepared by vibratory compaction in a split compaction mold. Each specimen was compacted in six layers, with each layer consisting of the same material at the MDU and OMC. Prior to compaction, six separate batches of each material with similar gradations were prepared for each layer. The aim was to maintain uniformity in gradation within each layer to minimize any nonhomogeneity that could occur during specimen preparation. Figure 5 illustrates the batches of base material prepared for each layer prior to compaction.

Figure 5. Six separate batches of base material

Initially, a latex membrane was folded and inserted into the mold. To ensure a tight fit against the mold, a vacuum was applied, as depicted in Figure 6a. To prevent the clogging of porous stones by fine particles, a filter paper was positioned on the bottom platen. The first layer of the specimen was introduced into the mold and platen assembly, where it was compacted using vibratory compaction until reaching the desired thickness of approximately 2 inches per layer (Figure 6b). After compacting the first layer, the surface of the specimen was trimmed to ensure its integrity, and the subsequent layer was then placed and compacted accordingly. This process was repeated for each layer until a total height of 12 inches was attained. The compacted specimen was then transferred to the chamber for the subsequent assembly step. One significant concern during compaction, particularly for coarse-grained materials, was the risk of the latex membrane being punctured by sharp edges. To address this issue and mitigate its potential consequences, a second membrane (placed on the second membrane mold as depicted in Figure 6c) was utilized to create a confining space for the specimen within the chamber. This second membrane was introduced immediately after detaching the compaction mold. Before removing the mold, the vacuum port was redirected to the bottom platen to apply vacuum pressure during the placement of the second membrane. The folded membrane was then affixed to the bottom platen and sealed with O-rings (Figure 6d). Subsequently, filter paper and the top platen were positioned and sealed with O-rings as well (Figure 6e).

After transferring a specimen to the chamber, the vacuum lines of both the bottom and top platens were attached to the lower cell. Throughout the assembly process, the specimen remained under vacuum via a vacuum line connected to the top platen until the desired confining pressure was applied. To proceed with the assembly, the lower cell was slid backward (Figure 7a), and the middle cell wall was lowered. Next, four steel tie rods were used to connect the top plate to the bottom plate (Figure 7b). Using the crane assembly the upper cell wall and the top plate were positioned (Figure 7c). The upper cell wall was lifted and placed on the safety stops (Figure 7d)

24

to secure the top actuator to the top platen. Finally, two internal LVDTs were installed to measure the deformation of the specimen (Figure 7e). The assembly of the SPAX-3000 was finalized by lowering the upper cell wall and installing the sealing ring (Figure 7f).
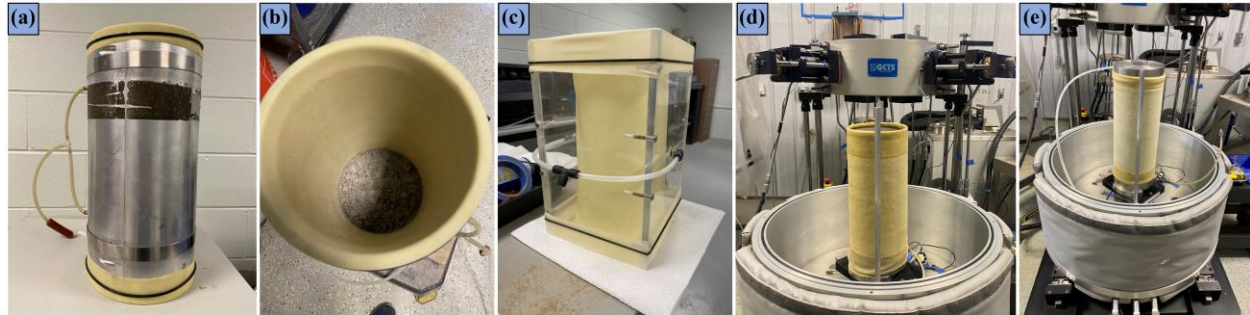
Figure 6. Cylindrical specimen preparation steps: (a) split mold and membrane, (b) first compaction layer, (c) second membrane with the second membrane mold, (d) compacted specimen placed into the chamber, (e) specimen ready for the assembly
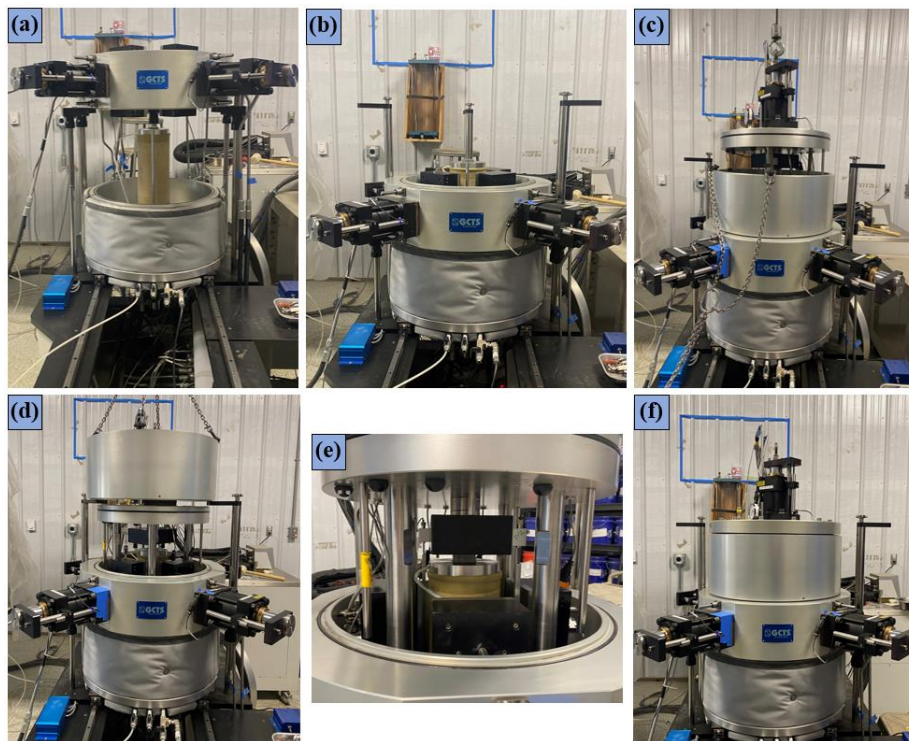
Figure 7. Assembly steps: (a) lower cell slid backward, (b) middle cell lowered, (c) top plate positioned, (d) upper cell placed on the safety spots, (e) internal LVDTs installed, (f) assembly completed

After completing the assembly of the specimen, the CATS software was employed to generate the required M_R testing sequences. These sequences were created based on the load sequences

outlined in AASHTO T307 (2017) for base/subbase and subgrade materials. The testing program for the materials is presented in Table 6.

Table 6. The load sequences for base/subbase and subgrade

Sequence No.	Base/Subbase		Subgrade	
	Confining Pressure, σ_c	Vertical Cyclic Stress, $\Delta\sigma$	Confining Pressure, σ_c	Vertical Cyclic Stress, $\Delta\sigma$
	psi	psi	psi	psi
0	15	15	6	4
1	3	3	6	2
2	3	6	6	4
3	3	9	6	6
4	5	5	6	8
5	5	10	6	10
6	5	15	4	2
7	10	10	4	4
8	10	20	4	6
9	10	30	4	8
10	15	10	4	10
11	15	15	2	2
12	15	30	2	4
13	20	15	2	6
14	20	20	2	8
15	20	40	2	10

Following the testing, the M_R of base, subbase, and subgrade materials were calculated for the average of deformations and stresses of the last five cycles of each sequence following Equation (1).

3.3 Results

Overall, the results revealed that the base materials exhibited the highest stiffness (10-54 ksi) while the lowest was observed for subgrade materials (4-12 ksi) as expected. This finding underscores the critical role played by the base material in providing structural support and stability. The observed stiffness can be attributed to the interlocking mechanism inherent in granular materials, which contributes significantly to the base material's overall stiffness. On the other hand, the subgrade materials exhibited the lowest stiffness, primarily due to their inherent lack of internal structural capacity. The subbase materials performed higher than the subgrade material due to their granular particle size (open-graded material) distribution (15-45 ksi).

However, despite their relatively better performance, the subbase materials suffered from a limitation of the absence of sufficient fine sand and fine-grained materials. This deficiency ultimately resulted in the subbase materials' stiffness being lower than that of the base materials. Regardless, of the material type and load sequences, all unbound materials demonstrated stress-dependent behavior for both confining and cyclic pressure. This fundamental characteristic has significant implications for the mechanical properties and performance of pavement foundation layers, making it essential to comprehend their stress-strain relationships thoroughly for effective design and engineering purposes. Furthermore, the findings from the study revealed that the stress dependency observed in unbound materials is nonlinear. In other words, the contribution of bulk stress ($\theta = \sigma_1 + 2\sigma_3$) to the overall stiffness varies depending on the level of applied stress. This nonlinearity implies that the stiffness of these materials does not change uniformly with increasing stress levels. Verification tests were conducted for all the materials.

In general, the base materials demonstrated similar ranges of stiffness. However, slight variations were observed based on the test results. Among the base materials, Weber Quarry exhibited the highest stiffness, ranging from 20 to 54 ksi, while Crocker Pit displayed a lower stiffness range of 10 to 36 ksi. Figure 8-13 illustrate the variations of stiffness with changing θ for Ames Mine, Bethany Falls Limestone, Crocker Pit, Oneota Formation Dolomite, Plano Quarry, and Weber Quarry, respectively. It is believed that despite having the same particle size distribution, the observed differences in material behavior can be attributed to factors like the material's origin (dolomite, limestone, crushed gravel) and particle angularity. However, establishing a direct link between these factors and their impact on performance necessitates further investigation. Additional research is required to thoroughly understand how these material characteristics influence mechanical behavior under various stress conditions. Despite their different origins, all the base materials exhibited stress-hardening behavior, characterized by an increase in stiffness with higher $\Delta\sigma$ and θ levels.
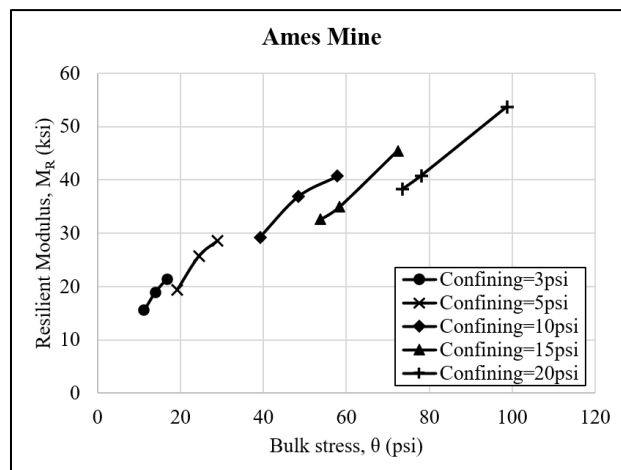
Figure 8. Resilient modulus (M_R) of Ames Mine varying with bulk stress (θ)
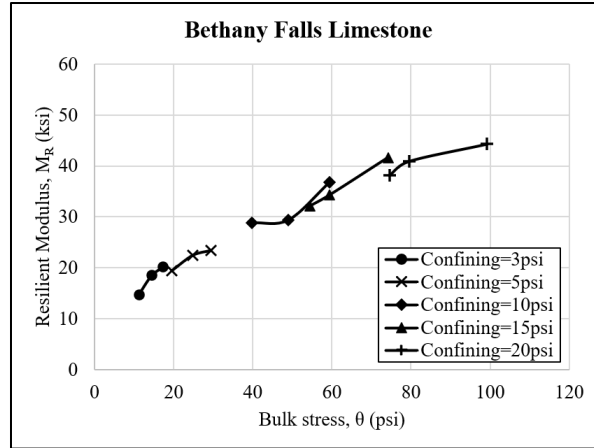
Figure 9. Resilient modulus (M$_R$) of Bethany Falls Limestone varying with bulk stress (θ)
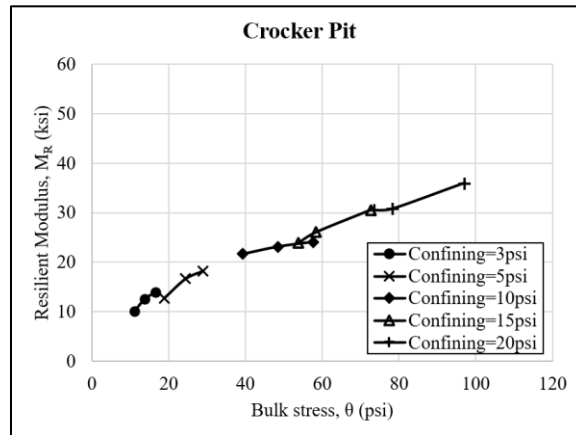
Figure 10. Resilient modulus (M$_R$) of Crocker Pit varying with bulk stress (θ)
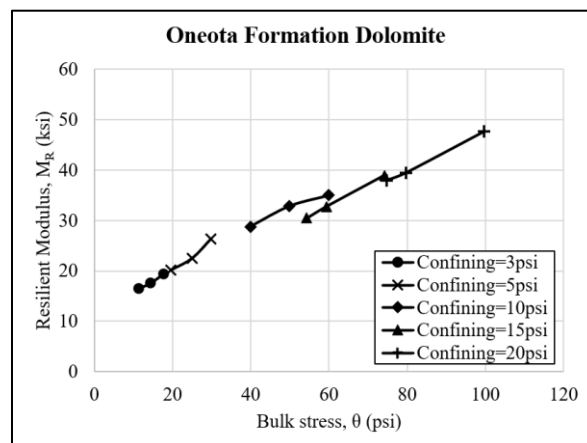
Figure 11. Resilient modulus (M$_R$) of Oneota Formation Dolomite varying with bulk stress (θ)
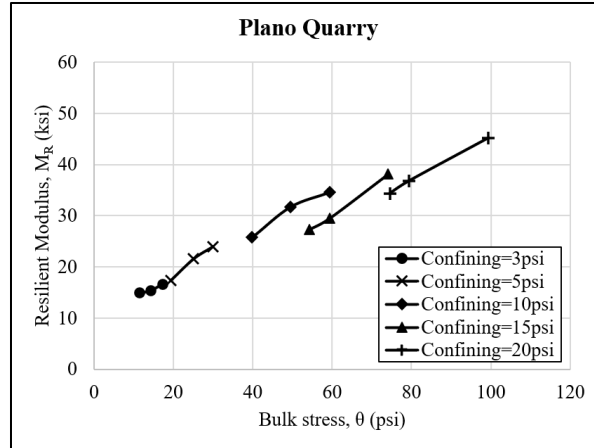
Figure 12. Resilient modulus (M$_R$) of Plano Quarry varying with bulk stress (θ)
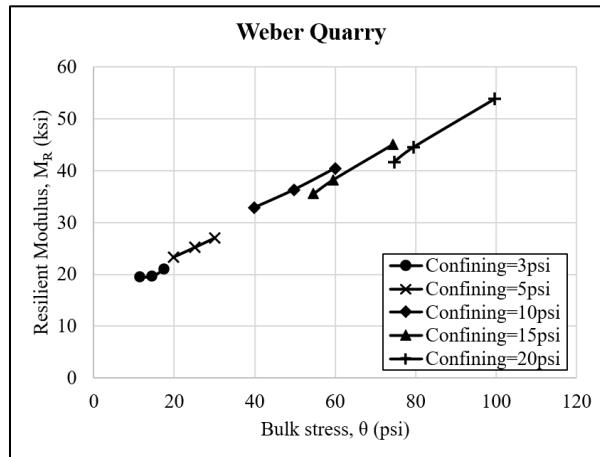
Figure 13. Resilient modulus (MR) of Oneota Weber Quarry varying with bulk stress (θ)

Stone City exhibited a better stress-strain performance among the subbase materials, having stiffness values ranging from 15 to 45 ksi. In contrast, Shambaugh Quarry demonstrated slightly lower stiffness, varying between 17 to 38 ksi. Figure 14-15 illustrate the variations of M$_R$ with θ for Shambaugh Quarry and Stone City Quarry, respectively. Irrespective of their origins, all subbase materials exhibited stress-hardening behavior, characterized by an increase in stiffness with increasing Δσ and θ levels.

29
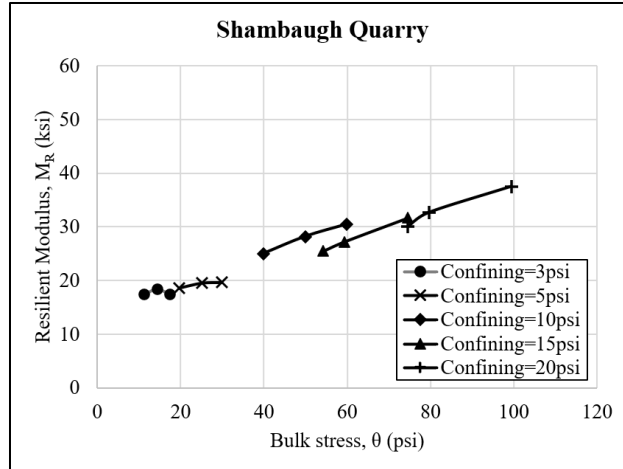
Figure 14. Resilient modulus (M$_R$) of Shambaugh Quarry varying with bulk stress (θ)
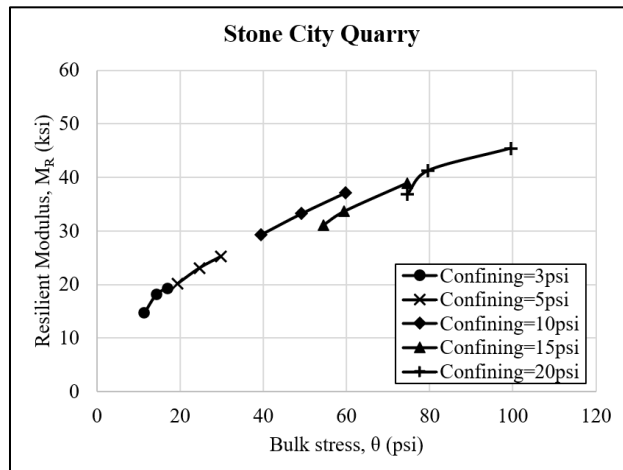
Figure 15. Resilient modulus (M$_R$) of Stone City Quarry varying with bulk stress (θ)

As anticipated, subgrade materials exhibited the lowest stiffness among all other materials, considering their role as pavement foundation layers experiencing minimal traffic loading. M$_R$ of CBIS ranged from 7 to 12 psi, while Plymouth County demonstrated lower M$_R$ values, ranging from 4 to 10 ksi (Figure 16-17). Despite both materials performing similarly under identical testing conditions, their stress-dependent behaviors were notably distinct.

CBIS displayed stress-hardening behavior, meaning its stiffness increased with higher Δσ levels. On the other hand, Plymouth County exhibited stress-softening behavior, indicating a degradation of stiffness with increasing Δσ. This behavior of stress-hardening or softening is believed to be independent of the applied stresses, with the particle size distribution playing a crucial role in determining these characteristics. The coarser structure of CBIS (soil classification: SM) resulted in granular material behavior due to its internal structure which enables the occurrence of frictional forces between each grain, which contributed to stress-hardening. Conversely, Plymouth County (soil classification: ML) lacked the contribution of

30

frictional forces from an internal granular structure, leading to stress-softening behavior owing to its fine-grained nature.
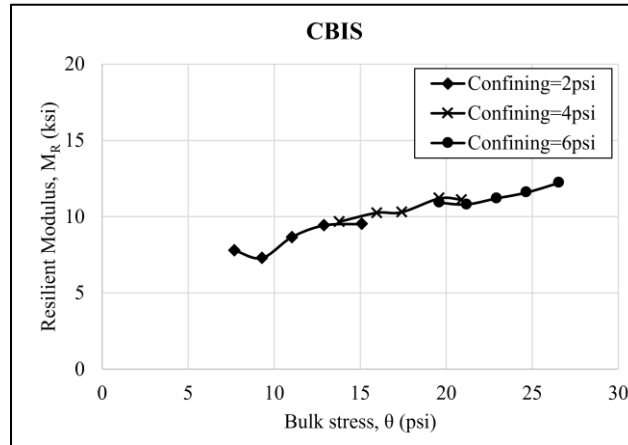
Figure 16. Resilient modulus (M$_R$) of Pottawattamie County CBIS varying with bulk stress (θ)
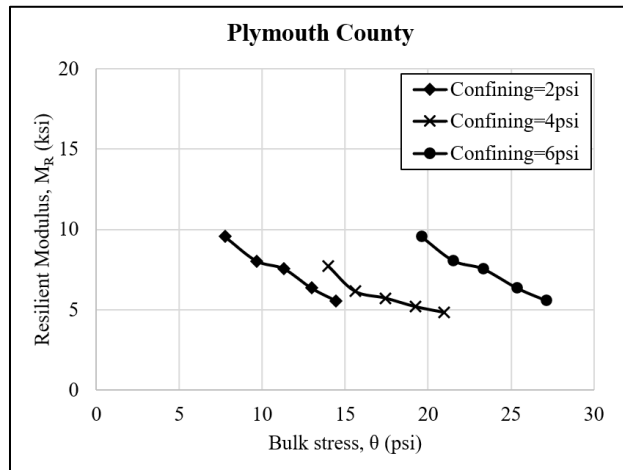
Figure 17. Resilient modulus (M$_R$) of Plymouth County varying with bulk stress (θ)

These results offer valuable insights into the complex behavior of different materials under various loading conditions. The interplay between particle size distribution, interlocking mechanisms, and the presence of fine-grained materials all play crucial roles in determining the overall stiffness and performance of the materials in the context of structural support. Understanding these factors will aid in making informed decisions during construction projects, ensuring the selection of appropriate materials for specific applications to enhance the overall integrity and longevity of infrastructures.

As can be seen from the results, the M_R testing generated fifteen data points for each test, capturing the stiffness behavior of the materials comprehensively. All of these data points are crucial in deriving the overall trend in stiffness behavior for low, medium, and high levels of traffic loading exposed by various vehicles. To describe this overall trend, which is known to be nonlinear for both base and subbase materials, a widely adopted model developed by Moossazadeh and Witczak (1981) is commonly utilized (Equation 3). This model establishes a connection between the M_R of materials and the θ.

$$M_R = k_1 \times \theta^{k_2} \tag{3}$$

where M_R is the resilient modulus, k_1 and k_2 are constants, θ is bulk stress.

Figure 18 presents the results of the Ames Mine material as a representative example, demonstrating the application of the bulk stress model. The figure showcases the model's fit to the data, displaying the model parameters and the coefficient of determination, which indicates the goodness of fit between the model and the observed data. This representation offers valuable insights into how the bulk stress model relates to the M_R behavior of the material, serving as a representative illustration for the rest of the results obtained.
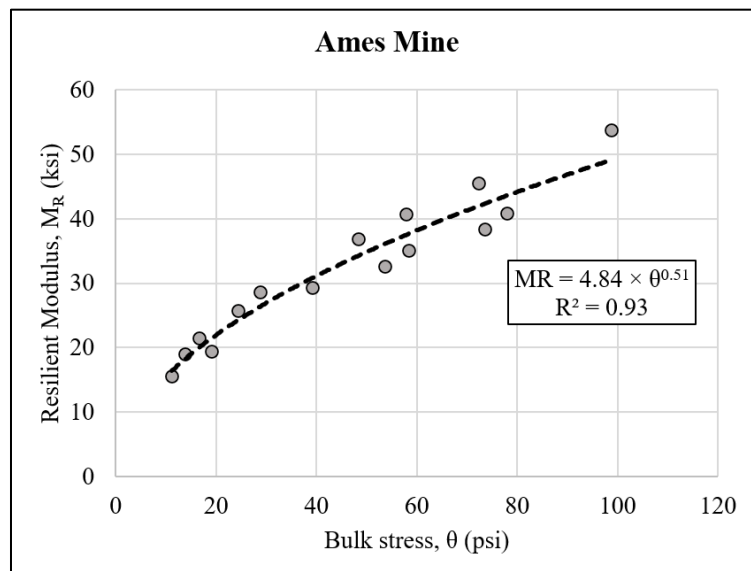
Figure 18. Bulk stress (θ) model fit for the resilient modulus (M_R) of Ames Mine

The model parameters of other materials along with the Ames Mine are given in Table 7.

Table 7. Model parameters and coefficient of determination for bulk stress model of base and subbase materials

Material	k_1	k_2	R^2
Ames Mine	4.84	0.51	0.93
Bethany Falls Limestone	4.63	0.49	0.98
Crocker Pit	2.75	0.55	0.99
Oneota Formation Dolomite	5.04	0.47	0.98
Plano Quarry	4.05	0.51	0.96
Weber Quarry	5.59	0.48	0.98
Shambaugh Quarry	6.49	0.36	0.94
Stone City Quarry	4.78	0.49	0.98

The observations revealed that the values of k_1 ranged from 2.75 to 6.49, while the values of k_2 ranged between 0.36 and 0.55. Additionally, the R^2 values were observed to fall within the range of 0.93 to 0.99.

In addition to the bulk stress model, the Summary MR (SMR) was determined for specific stress levels corresponding to the 6th sequence for base/subbase materials and the 13th sequence for subgrade materials. This approach follows the guidelines outlined in NCHRP 1-28A (Witczak 2002) and enables the reporting of a constant value. The selected stress sequences are considered the most representative of the traffic loading experienced by these respective layers. Figure 19 shows the SMR of the tested materials.
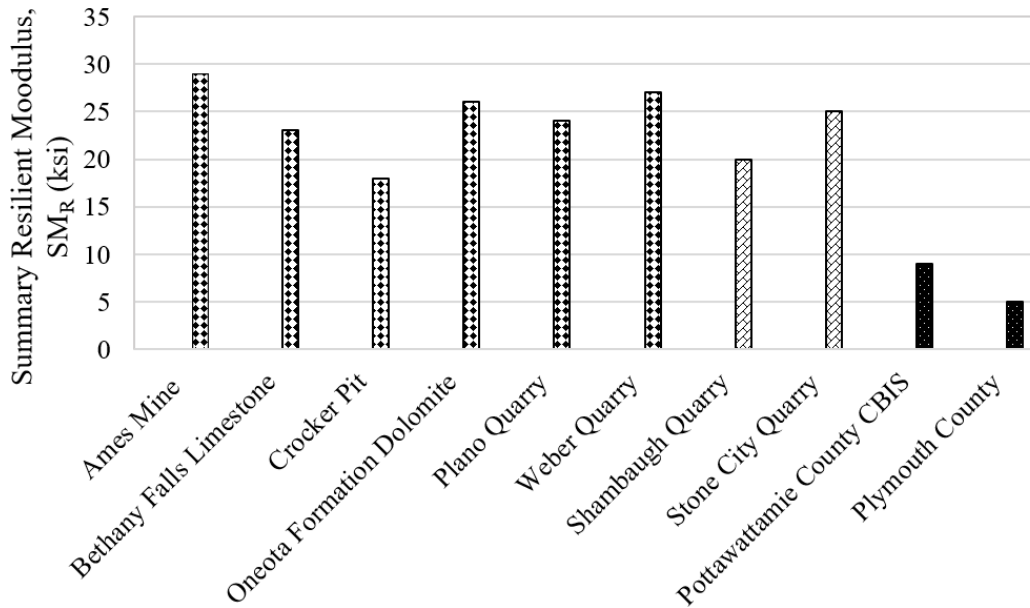
Figure 19. Summary resilient modulus (SM$_R$) of materials

SM$_R$ values of 29, 23, 18, 26, 24, 27, 20, 25, 9, and 5 ksi were recorded for Ames Mine, Bethany Falls Limestone, Crocker Pit, Oneota Formation Dolomite, Plano Quarry, Weber Quarry, Shambaugh Quarry, Stone City Quarry, Pottawattamie County CBIS, and Plymouth County, respectively. The findings from this study provide valuable insights into the complex behavior of various unbound materials under diverse loading conditions. The mechanical response of these materials is influenced by a combination of factors, including particle size distribution, material origin (e.g., dolomite, limestone, crushed gravel), and internal structural capacity. The interplay of these factors determines the overall stiffness and performance of the materials when subjected to different stress levels and loading patterns. In Chapter 3, the focus was primarily on investigating the mechanical behavior of the materials in the vertical direction through standard testing procedures. However, due to the inherent complexity of geomaterial behavior, it has become increasingly evident that more advanced investigations of stress-stiffness behavior are necessary to achieve a comprehensive characterization of these materials which is presented in Chapter 4.

CHAPTER 4 ADVANCED MECHANICAL CHARACTERIZATION OF GEOMATERIALS

In this chapter, advanced testing methods were employed to investigate the mechanical properties of unbound materials. Specifically, the SPAX-3000 testing equipment, which offers advanced features, was utilized. This chapter provides an in-depth introduction to the advanced capabilities and functionalities of the testing equipment introduced in Chapter 3 by highlighting how it enhances the testing process and enables a more comprehensive characterization of the material properties. By leveraging the advanced features of the SPAX-3000, a more detailed understanding of the mechanical behavior of the unbound materials can be obtained, contributing to improved engineering practices and better-informed decision-making in the field of material testing and characterization.

4.1 Materials

In this chapter, the same materials that were introduced and tested in Chapters 2 and 3, respectively were used.

4.2 Advanced features of SPAX-3000

The standard features of SPAX-3000 for standard M_R testing were introduced in Chapter 3 in detail. The modified version of the testing setup with the introduced advanced features (horizontal x-axis actuators, horizontal x-axis external LVDTs, horizontal x-axis internal LVDTs, horizontal y-axis actuators, horizontal y-axis external LVDT, horizontal y-axis internal LVDTs) are shown in Figure 20.

As shown in the Figure 20, the true triaxial component of the SPAX-3000 testing equipment incorporates supplementary dynamic load actuators, external and internal LVDTs, and LVDT targets to determine the stress-strain behavior of prismatic specimens with dimensions of 6 inches by 6 inches by 12 inches. The dynamic load actuators are located in each direction. The application of loads on a prismatic specimen, both in the vertical and horizontal directions, is achieved through a rigid aluminum platen that is connected to dynamic load actuators. The loading platens in each direction can be independently controlled, allowing for the alteration of principal stress directions during testing. In both horizontal directions, similar to the vertical, one pair of internal LVDTs was adopted in addition to the external ones. There are in total twelve LVDTs (six internal and six external) in the cyclic true triaxial cell, four for each axis (x-, y-, and z-axes). The LVDT setup for each axis in the SPAX-3000 follows a symmetrical configuration.

To optimize the testing process and minimize end platen friction, the SPAX-3000 incorporates a master-slave configuration through external LVDTs. In the setup, one of the LVDTs on each axis functions as the master LVDT and is connected to hydraulic loaders, while the opposing LVDT serves as the slave LVDT. The master LVDT is controlled through the CATS software, allowing

precise control over the applied deformation. Simultaneously, the slave LVDT is automatically programmed to mimic the deformation commanded to the master LVDT. By adopting this configuration, the specimen remains centered, ensuring uniform loading and minimizing the impact of end platen friction. This arrangement contributes to more accurate and reliable test results by reducing potential measurement errors caused by friction between the specimen and the end platens. Overall, the master-slave configuration enhances the testing process of the SPAX-3000, ensuring more precise control over deformation and improving the quality and reliability of the obtained data. These additions were crucial in achieving the full capacity and advanced capabilities of the testing equipment. This integration of advanced components enabled more comprehensive and detailed testing, enhancing the accuracy and reliability of the results obtained from the true triaxial testing conducted with the SPAX-3000.
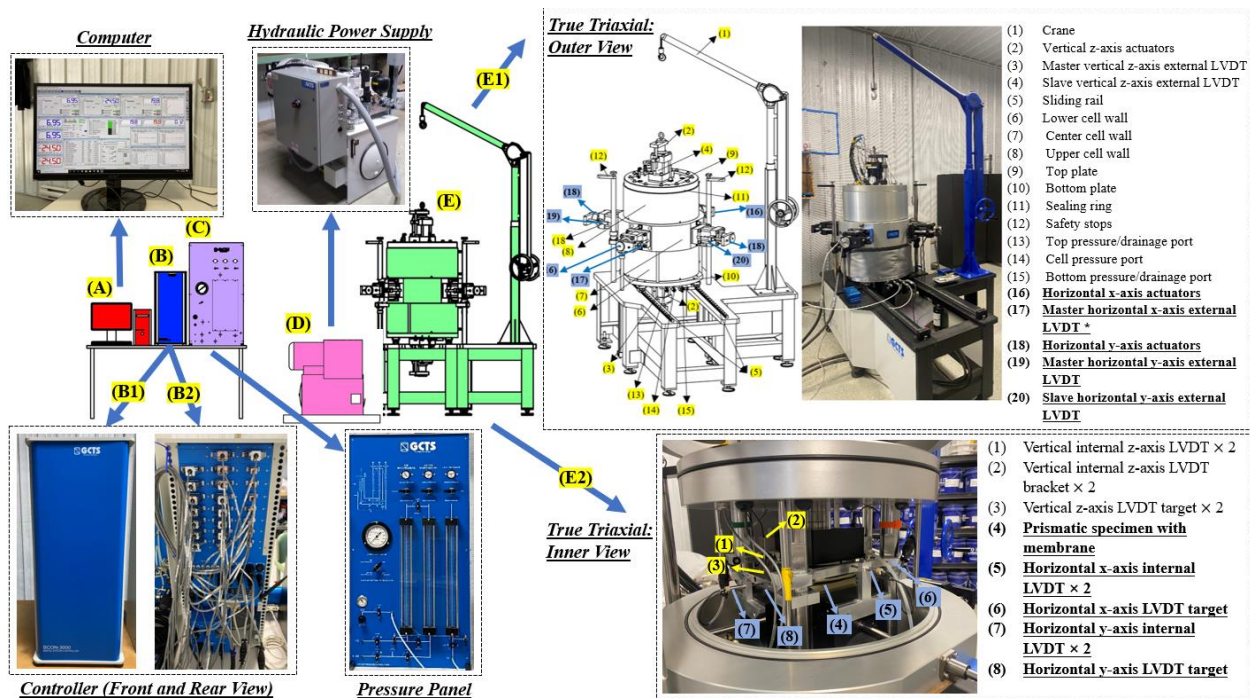
Figure 20. Advanced features of SPAX-3000 (a) desktop computer, (b) digital servo controller and data acquisition system, (c) pressure control panel and volume changing device, (d) hydraulic power supply, and (e) cyclic true triaxial unit with advanced features*

*Additional components are shown with blue highlighted numbers.

Advanced features of SPAX-3000 enable prismatic specimens to be experienced the simulation of the traffic loadings (cyclic stresses) under various boundary conditions which affects the stress-strain behavior. The boundary conditions (rigid-rigid-rigid, rigid-rigid-flexible, rigid-flexible-flexible) are used to simulate the boundary conditions materials experience in the field. Figure 21 shows the boundary conditions along with the principal stresses (σ_1, σ_2=intermediate principal stress, σ_3).

As illustrated in Figure 21 21, the SPAX-3000's independently moving actuators provide the flexibility to apply different configurations of principal stresses to the specimen depending on the boundary type.
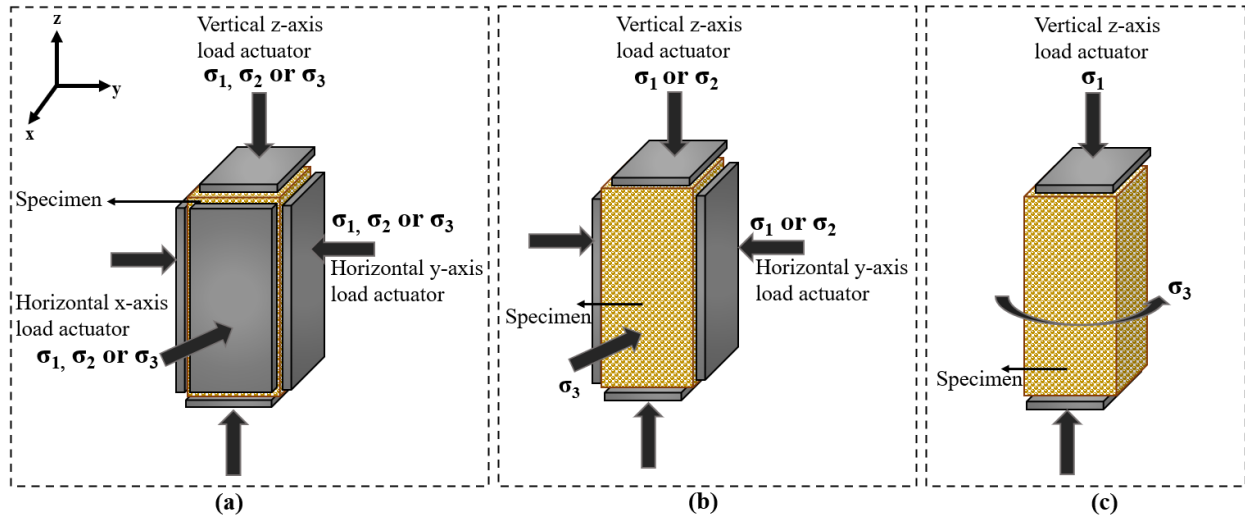
Figure 21. Boundary conditions of SPAX-3000: (a) rigid-rigid-rigid, (b) rigid-rigid-flexible and (c) rigid-flexible-flexible

Prismatic specimens with dimensions of $6 \times 6 \times 12$ inches were prepared through vibratory compaction using a split compaction mold. The compaction process involved six equal layers, each compacted at the MDU and the OMC specific to the respective materials. To ensure consistency and accuracy, six separate batches were prepared for each material and compaction layer, all featuring similar material gradations similar to cylindrical specimen preparation. This careful preparation aimed to maintain uniformity and minimize any potential nonhomogeneity during the specimen creation process. In the specimen preparation process, a latex membrane was carefully placed inside the mold, and vacuum pressure was applied to ensure a tight fit against the mold, as illustrated in Figure 22a. The mold, now containing the membrane, was then positioned on the bottom platen for compacting the specimen. This method was chosen to minimize any potential disturbance during the process. To prevent fine particles from clogging the porous stones, filter paper was laid on the bottom platen. The first layer of the specimen was added to the mold and platen assembly, and it was compacted using vibratory compaction until reaching the desired thickness of approximately 2 inches per layer (Figure 22b). After compacting the first layer, the surface of the specimen was carefully trimmed to maintain its integrity, and then the next layer was added and compacted (Figure 22c). This procedure was repeated for each layer until the specimen reached a total height of 12 inches. Upon completion of compaction, the compacted specimen was transferred to the chamber for the next assembly step. Notably, one major concern during the compaction of coarse-grained materials was the possibility of the sharp edges causing punctures in the membrane. To address this issue, a second membrane was used to provide additional confinement to the specimen within the chamber. The second membrane was promptly positioned after removing the compaction mold. Before mold removal, the vacuum port was switched to the bottom platen to apply vacuum pressure to the

specimen while placing the second membrane. The folded membrane was then securely attached to the bottom platen using O-rings (Figure 22d). Following the placement of the second membrane, filter paper was laid on top, and the top platen was positioned and sealed with O-rings (Figure 22e). These steps ensured proper containment and provided a controlled environment for accurate testing and assessment of the material's mechanical properties.
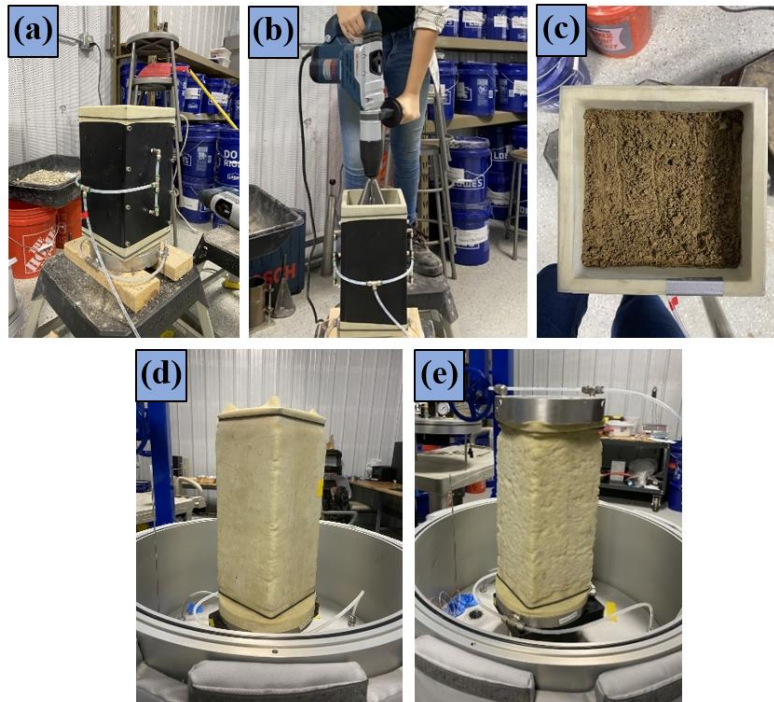
Figure 22. Prismatic specimen preparation steps: (a) mold with membrane, (b) compaction of the layer, (c) trimmed surface of the compacted specimen, (d) transferred compacted specimen, (e) specimen ready for the assembly

Upon transferring the specimen to the chamber, the bottom platen was attached to the bottom actuator, and both the bottom and top platen vacuum lines were connected to the lower cell. Throughout the assembly process, the specimen remained under vacuum via a vacuum line linked to the top platen until the confining pressure was applied. Following this, the lower cell was slid back (Figure 23a), and the middle cell wall was lowered. Four steel tie rods were then installed, connecting the top plate to the bottom plate. Utilizing a crane assembly, the upper cell wall and top plate were cautiously positioned (Figure 23b). To secure the top actuator to the top platen, the upper cell wall was lifted and placed on the safety stops (Figure 23c). Once the top actuator was fully attached to the top platen, the horizontal load cable was connected to the horizontal load actuator (Figure 23d). To ensure precise measurements, six LVDT brackets (two per direction) were installed to hold the internal LVDTs. These internal LVDTs were strategically positioned to capture the expected range of deformations in each direction (Figure 23e). The SPAX-3000 assembly process concluded with the lowering of the upper cell wall and the installation of the sealing ring (Figure 23f). By diligently following these steps, the SPAX-3000 was assembled, providing a reliable and controlled testing environment for advanced investigations into the material's mechanical behavior under varying stress conditions.

Figure 23. SPAX-3000 assembly process for prismatic specimen: (a) lower cell slid back, (b)placement of upper cell and top plate, (c) lifted upper cell, (d) load cell cable connection, (e)LVDT installation, (f) assembly completed

Following the specimen preparation and SPAX-3000 assembly, the cross-anisotropic stress-strain behavior of the unbound materials was investigated. Several different aspects were examined to gain a comprehensive understanding of the mechanical response of these materials under varying loading conditions.

4.3 Cross-anisotropy of Resilient Modulus

As mentioned in Chapter 1, geomaterials exhibit cross-anisotropic behavior, meaning their stress-strain characteristics are direction-dependent. To investigate the cross-anisotropy of Iowa soils and geomaterials, a series of cross-anisotropic M_R testing was conducted to determine M_R

in the vertical z-axis direction (M^z_R), horizontal x-axis (M^x_R) and horizontal y-axis (M^y_R). The equations are given below to calculate the M_R in each direction (Equations 4-6).

$$M^z_R = \frac{\Delta\sigma_z}{\varepsilon_z} \tag{4}$$

$$M^x_R = \frac{\Delta\sigma_x}{\varepsilon_x} \tag{5}$$

$$M^y_R = \frac{\Delta\sigma_y}{\varepsilon_y} \tag{6}$$

where $\Delta\sigma_z$ is the vertical cyclic stress, ε_z is the recoverable deformation in the z-axis, $\Delta\sigma_x$ is the horizontal cyclic stress and εx is the recoverable deformation in the x-axis direction, $\Delta\sigma_y$ is the horizontal cyclic stress and ε_y is the recoverable deformation in the y-axis direction.

Before conducting the unbound material testing, an isotropic urethane rubber sample measuring $6 \times 6 \times 12$ inches was manufactured and tested to validate the reliability and accuracy of the M_R results obtained using the SPAX-3000 equipment. Figure 24 displays the isotropic urethane rubber material used for verification testing.

Figure 24. Prismatic isotropic urethane rubber sample

The urethane rubber sample was subjected to testing as the base material in multiple directions, including M^z_R, M^x_R, and M^y_R. To achieve this, the CATS software was utilized to create the necessary M_R testing sequences. The load sequences specified in AASHTO T307 (2017) were employed for the vertical and both horizontal directions. The stress sequences for all three directions, for both the base/subbase and subgrade materials, can be found in Table 8 and 9, respectively.

Table 8. Testing sequences for base/subbase for three directions

Sequence No.	σ_c	Vertical M_R, M^z_R			Horizontal M_R, M^x_R			Horizontal M_R, M^y_R			Number of cycles
		$\Delta\sigma_z$	$\Delta\sigma_x$	$\Delta\sigma_y$	$\Delta\sigma_z$	$\Delta\sigma_x$	$\Delta\sigma_y$	$\Delta\sigma_z$	$\Delta\sigma_x$	$\Delta\sigma_y$	
	psi	psi	psi	psi	psi	psi	psi	psi	psi	psi	
0	15	15	0	0	0	15	0	0	0	15	500
1	3	3	0	0	0	3	0	0	0	3	100
2	3	6	0	0	0	6	0	0	0	6	100
3	3	9	0	0	0	9	0	0	0	9	100
4	5	5	0	0	0	5	0	0	0	5	100
5	5	10	0	0	0	10	0	0	0	10	100
6	5	15	0	0	0	15	0	0	0	15	100
7	10	10	0	0	0	10	0	0	0	10	100
8	10	20	0	0	0	20	0	0	0	20	100
9	10	30	0	0	0	30	0	0	0	30	100
10	15	10	0	0	0	10	0	0	0	10	100
11	15	15	0	0	0	15	0	0	0	15	100
12	15	30	0	0	0	30	0	0	0	30	100
13	20	15	0	0	0	15	0	0	0	15	100
14	20	20	0	0	0	20	0	0	0	20	100
15	20	40	0	0	0	40	0	0	0	40	100

σ_c = Confining pressure

$\Delta\sigma_z$ = Vertical z-axis cyclic stress

$\Delta\sigma_x$ = Horizontal x-axis cyclic stress

$\Delta\sigma_y$ = Horizontal y-axis cyclic stress

M^z_R = Vertical z-axis M_R

M^x_R = Horizontal x-axis M_R

M^y_R = Horizontal y-axis M_R

Table 9. Testing sequences for subgrade for three direction

Sequence No.	σ_c	Vertical M_R, M^z_R			Horizontal M_R, M^x_R			Horizontal M_R, M^y_R			Number of cycles
		$\Delta\sigma_z$	$\Delta\sigma_x$	$\Delta\sigma_y$	$\Delta\sigma_z$	$\Delta\sigma_x$	$\Delta\sigma_y$	$\Delta\sigma_z$	$\Delta\sigma_x$	$\Delta\sigma_y$	
	psi	psi	psi	psi	psi	psi	psi	psi	psi	psi	
0	6	4	0	0	0	4	0	0	0	4	500
1	6	2	0	0	0	2	0	0	0	2	100
2	6	4	0	0	0	4	0	0	0	4	100
3	6	6	0	0	0	6	0	0	0	6	100
4	6	8	0	0	0	8	0	0	0	8	100
5	6	10	0	0	0	10	0	0	0	10	100
6	4	2	0	0	0	2	0	0	0	2	100
7	4	4	0	0	0	4	0	0	0	4	100
8	4	6	0	0	0	6	0	0	0	6	100
9	4	8	0	0	0	8	0	0	0	8	100
10	4	10	0	0	0	10	0	0	0	10	100
11	2	2	0	0	0	2	0	0	0	2	100
12	2	4	0	0	0	4	0	0	0	4	100
13	2	6	0	0	0	6	0	0	0	6	100
14	2	8	0	0	0	8	0	0	0	8	100
15	2	10	0	0	0	10	0	0	0	10	100

σ_c = Confining pressure
$\Delta\sigma_z$ = Vertical z-axis cyclic stress
$\Delta\sigma_x$ = Horizontal x-axis cyclic stress
$\Delta\sigma_y$ = Horizontal y-axis cyclic stress
M^z_R = Vertical z-axis M_R
M^x_R = Horizontal x-axis M_R
M^y_R = Horizontal y-axis M_R

Figure 25 illustrates the variation of M_R with θ for each direction. The plot indicates that the measured M_R values were consistent (approximately 2 ksi) across all directions, which demonstrates the isotropic nature of the rubber specimen. This outcome was anticipated due to the manufacturing process involving the use of a uniform liquid form of urethane rubber to

produce the tested material. Moreover, the results indicated that the M_R of urethane rubber remained unaffected by the levels of applied stress, as the modulus remained nearly constant for θ. This observation aligns with findings from previous literature (Tutumluer and Seyhan 1999). Consequently, the verification tests confirmed that SPAX-3000 was capable of accurately measuring the M_R properties of materials under applied stresses in all three directions.
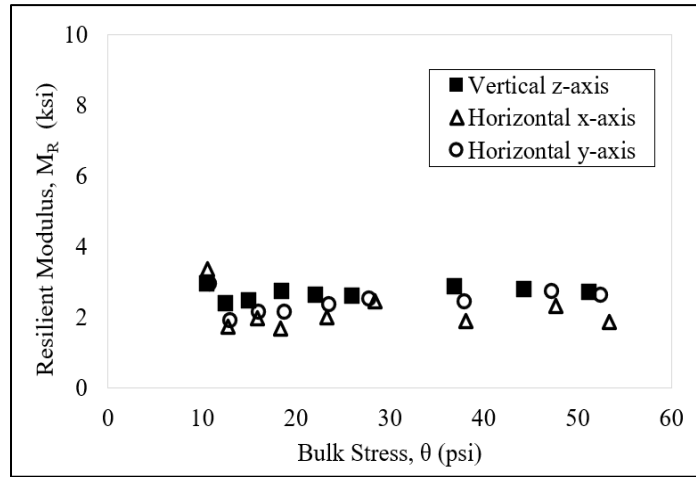
Figure 25. Resilient modulus of isotropic urethane rubber for all three directions

Following to verification of the testing sequences, two bases (Ames Mine and Crocker Pit), one subbase (Shambaugh Quarry), and one subgrade material (Plymouth County) were chosen to be tested under rigid-rigid-rigid boundary conditions (Figure 21a) for M_R. For each test, verification tests were performed and an average of these tests results was assumed as the final results. Testing sequences in Table 8 were followed for each direction.

Figure 26-28 display the results for Ames Mine, illustrating the variations of M^z_R, M^x_R, and M^y_R with varying θ, respectively.
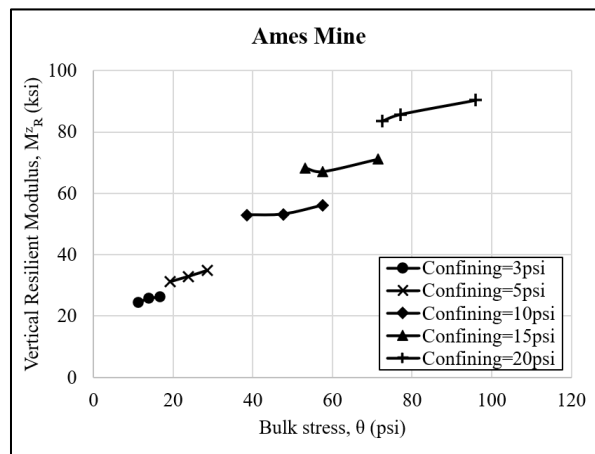
Figure 26. Vertical z-axis resilient modulus (M^z_R) of Ames Mine varying with bulk stress (θ)

43
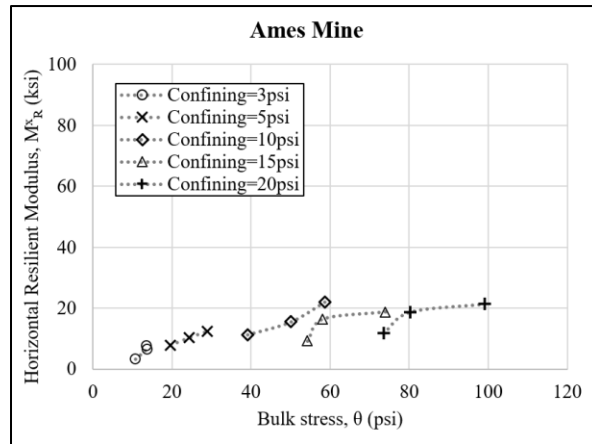
Figure 27.Horizontal x-axis resilient modulus (M^x_R) of Ames Mine varying with bulk stress (θ)
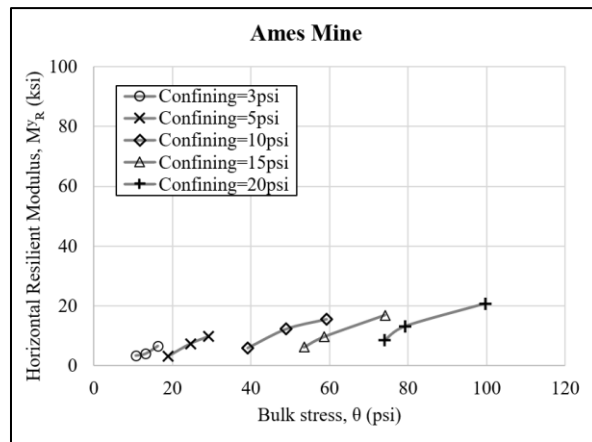
Figure 28. Horizontal y-axis resilient modulus (M^y_R) of Ames Mine varying with bulk stress (θ)

As can be seen from the figures, M_R exhibited nonlinear stress-dependent characteristics in each direction: vertical z-axis, horizontal x-axis, and horizontal y-axis. The vertical direction exhibited the highest M_R values (24-90 ksi), while the other two horizontal directions demonstrated similar M_R values, ranging between 3-22 ksi for the horizontal x-axis and 3-21 ksi for the horizontal y-axis. Additionally, a noticeable disparity between M^z_R and M^x_R, M^y_R under similar stress conditions highlighted the cross-anisotropic nature of the base materials, where stiffness characteristics are direction-dependent. Consistent with the results of cylindrical tests, the stiffness in the vertical direction was attributed to the interlocking mechanism of granular materials due to compaction and conditioning. Conversely, both horizontal directions lacked interlocking mechanisms since no compaction effort was undertaken in those orientations prior

44

to testing. Regardless of the direction, M_R increased with increasing $\Delta\sigma$ and θ which aligns with the stress-hardening behavior.

Figure 29-31 display the results for Crocker Pit, illustrating the variations of M^z_R, M^x_R, and M^y_R with varying θ, respectively.
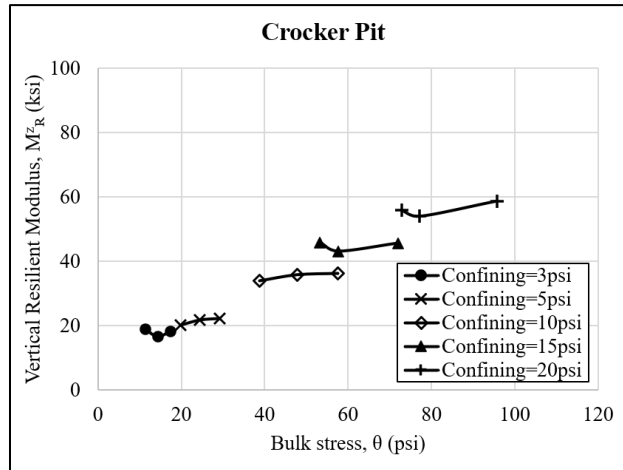
Figure 29. Vertical z-axis resilient modulus (M^z_R) of Crocker Pit varying with bulk stress (θ)
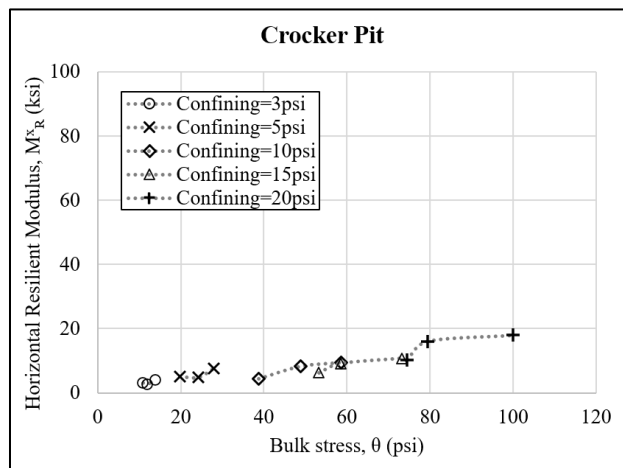
Figure 30. Horizontal x-axis resilient modulus (M^x_R) of Crocker Pit varying with bulk stress (θ)
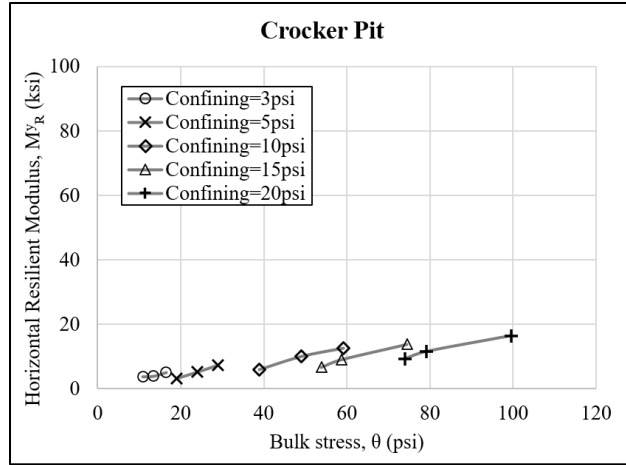
Figure 31. Horizontal y-axis resilient modulus (M^y_R) of Crocker Pit varying with bulk stress (θ)

As observed from the figures, the M$_R$ of Crocker Pit exhibited nonlinear stress-dependent characteristics in each direction: vertical z-axis, horizontal x-axis, and horizontal y-axis, similar to Ames Mine. The vertical direction demonstrated the highest M$_R$ values (17-59 ksi), while the other two horizontal directions displayed similar M$_R$ values, ranging between 3-18 ksi for the horizontal x-axis and 3-16 ksi for the horizontal y-axis. Moreover, a noticeable discrepancy between M^z_R and M^x_R, M^y_R under comparable stress conditions emphasized the cross-anisotropic nature of the base materials, where stiffness properties vary with direction. Consistent with the results of cylindrical tests, the stiffness in the vertical direction was attributed to the interlocking mechanism of granular materials resulting from compaction and conditioning. Conversely, both horizontal directions lacked interlocking mechanisms since no compaction efforts were conducted in those orientations prior to testing. Additionally, it was observed that Crocker Pit base material yielded lower M^z_R, M^x_R, and, M^y_R compared to the Ames Mine. This can be attributed to the angularity or the material origin where Ames Mine is high-quality limestone and Crocker Pit is medium-quality crushed gravel. Moreover, as can be seen in Figure 2, even by visual observation, it can be said that Ames Mine has more angular characteristics compared to the Crocker Pit. Regardless of the direction, M$_R$ increased with increasing Δσ and θ which aligns with the stress-hardening behavior.

Figure 32-34 show the results for Shambaugh Quarry, illustrating the variations of M^z_R, M^x_R, and M^y_R with varying θ, respectively.

46
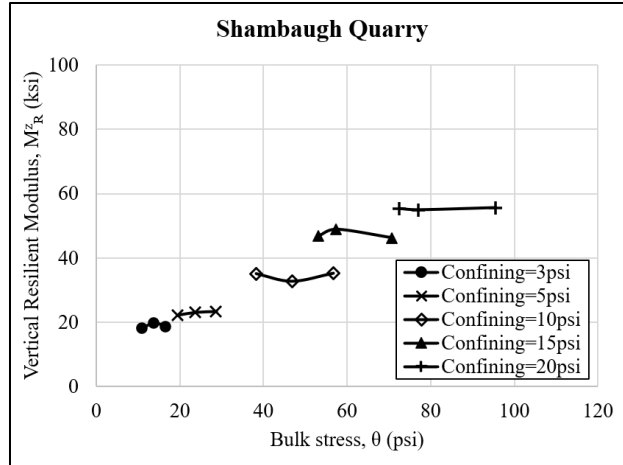
Figure 32. Vertical z-axis resilient modulus (M^z_R) of Shambaugh Quarry varying with bulk stress (θ)
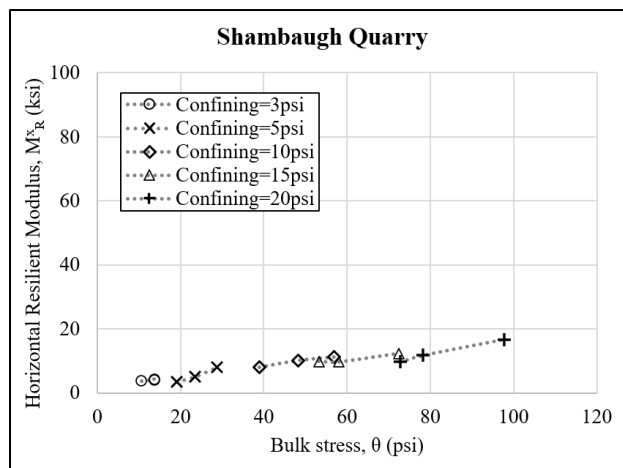
Figure 33. Horizontal x-axis resilient modulus (M^x_R) of Shambaugh Quarry varying with bulk stress (θ)

47
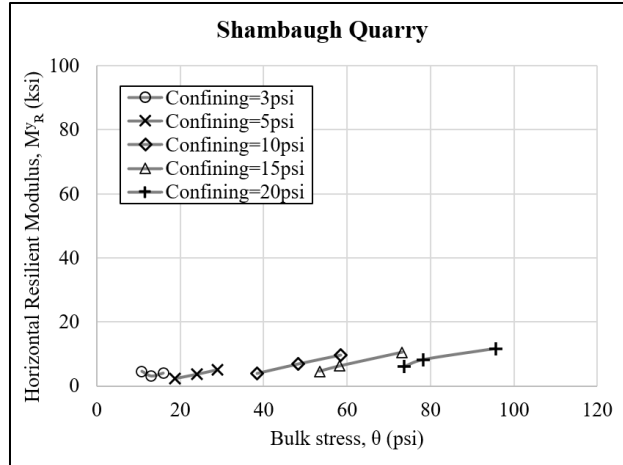
Figure 34. Horizontal y-axis resilient modulus (M^y_R) of Shambaugh Quarry varying with bulk stress (θ)

As evident from the figures, Shambaugh Quarry, similar to the base material, displayed nonlinear stress-dependent characteristics in each direction: vertical z-axis, horizontal x-axis, and horizontal y-axis. Consistent with the other results, the highest M_R values were observed for the vertical direction, ranging between 18-56 ksi, while M^x_R values were determined to be in the range of 4-17 ksi and M^y_R values ranged from 2-12 ksi. This indicates that cross-anisotropy was apparent not only for the base material but also for the subbase material, Shambaugh Quarry. Furthermore, similar to the base materials, the interlocking mechanism's effect was also evident in Shambaugh Quarry due to its granular structure. The interlocking mechanism provided additional interaction between particles, contributing to the overall stiffness of the material. Regardless of the direction, M_R increased with increasing $\Delta\sigma$ and θ which aligns with the stress-hardening behavior. However, stress-hardening behavior was observed to be more apparent in horizontal directions.

Overall, Shambaugh Quarry exhibited lower M^z_R, M^x_R, and M^y_R values compared to the other granular materials (base materials). This result can be attributed to the lack of fines within the geomaterial structure. Instead of fines, the voids within the structure were filled with air, which might have led to decreased stiffness during $\Delta\sigma$ application. Fines typically provide increased additional contact points between particles, leading to improved stiffness. The absence of fines in Shambaugh Quarry's composition likely contributed to the observed lower M_R values.

The subgrade material, Plymouth County, was also tested to determine cross-anisotropy following to testing sequences presented in Table 9. Figure 35-37 display the results for Plymouth County, illustrating the variations of M^z_R, M^x_R, and M^y_R with varying θ, respectively.

48
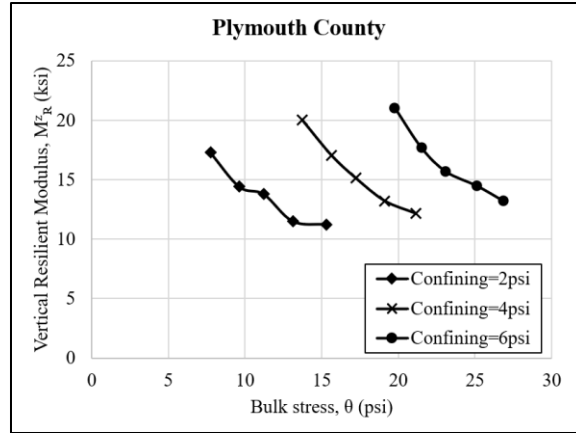
Figure 35. Vertical z-axis resilient modulus (M^z_R) of Plymouth County varying with bulk stress (θ)
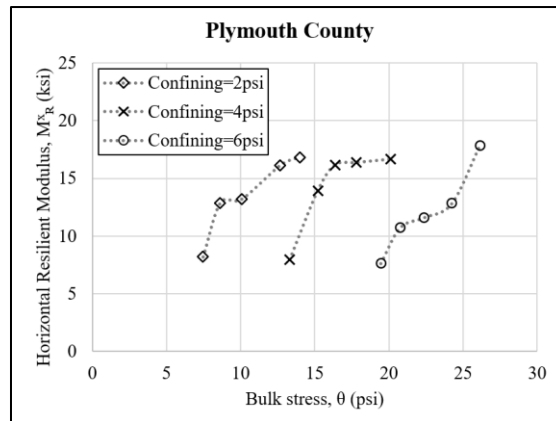
Figure 36. Horizontal x-axis resilient modulus (M^x_R) of Plymouth County varying with bulk stress (θ)
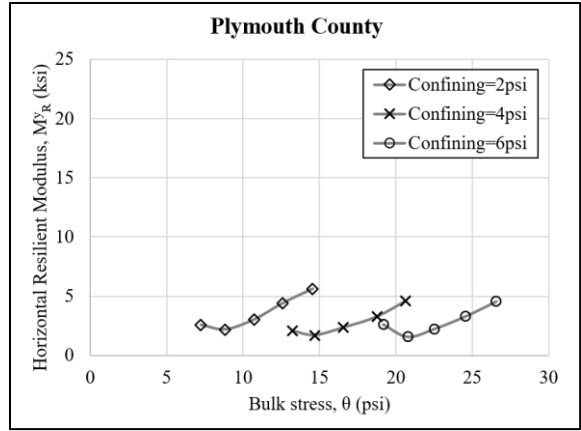
Figure 37. Horizontal y-axis resilient modulus (M^y_R) of Plymouth County varying with bulk stress (θ)

As evident from the results, the subgrade material exhibited distinct characteristics compared to the base and subbase materials. Firstly, it was observed that M^z_R displayed stress-softening behavior, which is in contrast to the stress-hardening behavior observed in the base/subbase materials. Additionally, both horizontal directions (M^x_R and M^y_R) showed stress-hardening behavior, but they exhibited different levels of stiffness characteristics. The horizontal x-direction had M_R values ranging between 8-17 ksi, while M^y_R values ranged from 2-6 ksi. These differences in stiffness are likely influenced by the stress history of the fine-grained materials. However, it is essential to emphasize that despite the varying stiffness levels, both horizontal directions still demonstrated stress-hardening behavior. Furthermore, M^z_R was recorded to be between 11-21 ksi for the subgrade material.

Overall, regardless of the direction, the subgrade exhibited the lowest M_R values compared to all the other materials tested in this section. This outcome was expected, considering the applied stress levels and the fact that subgrade layers are typically the weakest foundation layers due to their function within the pavement foundation layers.

Similar to the cylindrical test results, the commonly used M_R model by Moossazadeh and Witczak (1981) was used to determine the model parameter not just for vertical direction but also for horizontal directions. Table 10 shows the model parameters and coefficient of determination for each base/subbase material tested for each direction.

50

Table 10. Model parameters and coefficient of determination for bulk stress model of base and subbase materials

Material	Direction	k_1	k_2	R^2
	Vertical z-axis	4.24	0.67	0.96
Ames Mine	Horizontal x-axis	1.22	0.62	0.72
	Horizontal y-axis	0.68	0.68	0.68
	Vertical z-axis	3.05	0.65	0.94
Crocker Pit	Horizontal x-axis	0.53	0.71	0.83
	Horizontal y-axis	0.67	0.66	0.83
	Vertical z-axis	3.82	0.60	0.91
Shambaugh Quarry	Horizontal x-axis	0.69	0.67	0.91
	Horizontal y-axis	0.81	0.53	0.68

k_1, k_2 = model parameters
R^2 = coefficient of determination

In summary, the table reveals that the highest coefficients of determination (0.91-0.96) were consistently recorded for the vertical z-axis across all tested materials. However, for the horizontal directions, the model analysis indicated that conventional approaches, such as using the commonly used bulk stress model, provide lower R^2 (R^2 varying between 0.68-0.91). This discrepancy can be attributed to the fact that the developed models were primarily focused on representing the vertical directions. Consequently, the results suggest that further investigation is required to develop a more suitable model that accurately represents the stiffness characteristics in the horizontal direction.

In addition to the bulk stress model, the SM_R was determined for specific stress levels corresponding to the 6th sequence for base/subbase materials and the 13th sequence for subgrade materials for each direction (Figure 38).
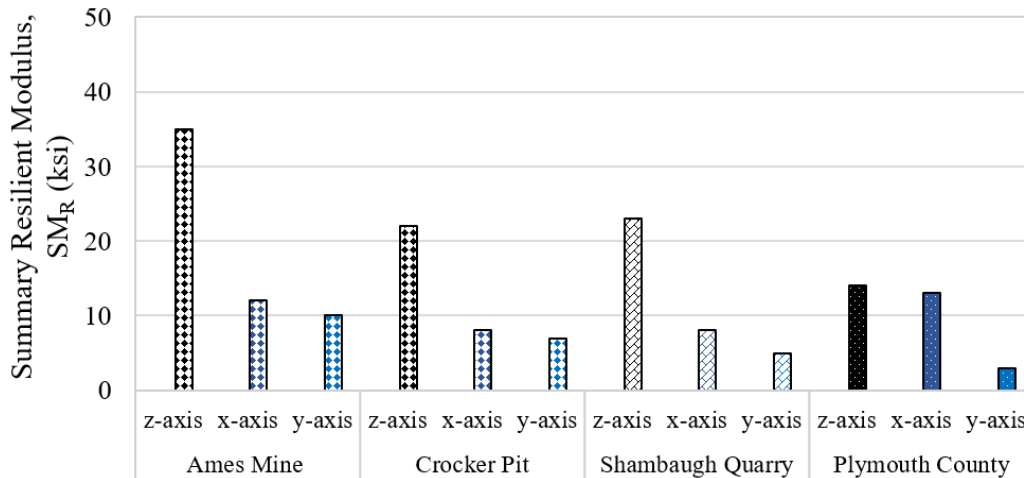
Figure 38. Summary resilient modulus (SM_R) of materials

For Ames Mine, SM_R values were determined as 35, 12, and 10 ksi for M^z_R, M^x_R, and M^y_R, respectively. For Crocker Pit, SM_R values were determined as 22, 8, and 7 ksi for M^z_R, M^x_R, and M^y_R, respectively. For Shambaugh Quarry, SM_R values were determined as 23, 8, and 5 ksi for M^z_R, M^x_R, and M^y_R, respectively. For Plymouth County, SM_R values were determined as 14, 13, and 3 ksi for M^z_R, M^x_R, and M^y_R, respectively.

Moreover, in addition to calculating the SM_R values, anisotropy ratios [anisotropy ratio$_{x-z}$ (AR_{x-z}) and anisotropy ratio$_{y-z}$ (AR_{y-z})] also computed for the tested materials, using Equations (7) and (8). These ratios offer crucial insights into the directional variations of the materials' mechanical properties. Analyzing the cross-anisotropy ratios provides a comprehensive understanding of how the stiffness characteristics vary between the vertical and horizontal directions. This additional analysis aids in assessing the materials' response under different loading conditions and optimizing their performance in engineering applications.

$$\text{Anisotropy ratio}_{x-z} = \frac{M^x_R}{M^z_R} \tag{7}$$

$$\text{Anisotropy ratio}_{y-z} = \frac{M^y_R}{M^z_R} \tag{8}$$

where M^z_R is the vertical z-axis resilient modulus, M^x_R horizontal x-axis resilient modulus, and, M^y_R horizontal y-axis resilient modulus.

AR_{x-z} and AR_{y-z} for Ames Mine, Crocker Pit, Shambaugh Quarry, and Plymouth County were given in Figure 39-42, respectively.
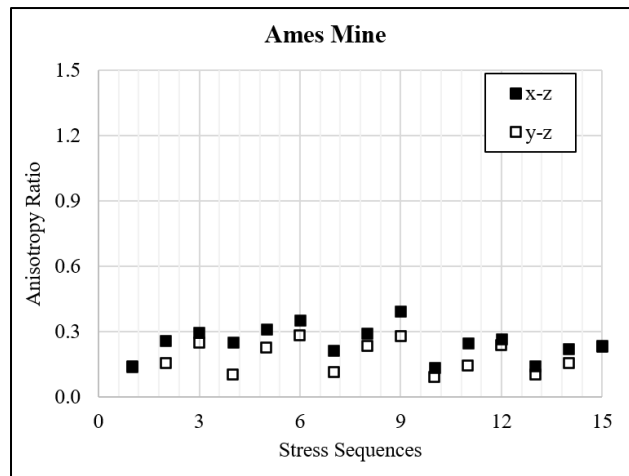
Figure 39. Anisotropy ratios for Ames Mine
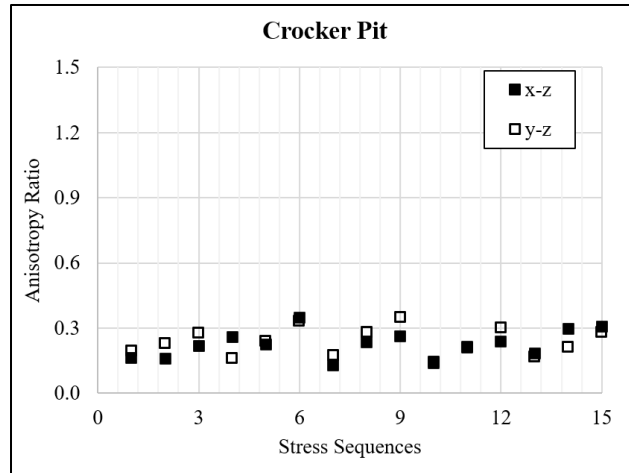
Figure 40. Anisotropy ratios for Crocker Pit
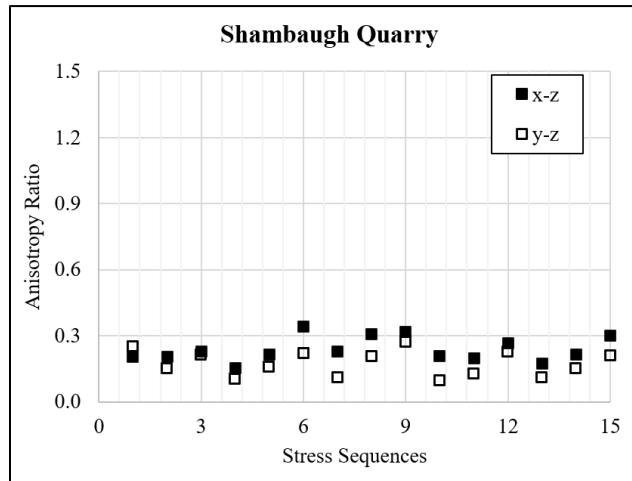
Figure 41. Anisotropy ratios for Shambaugh Quarry
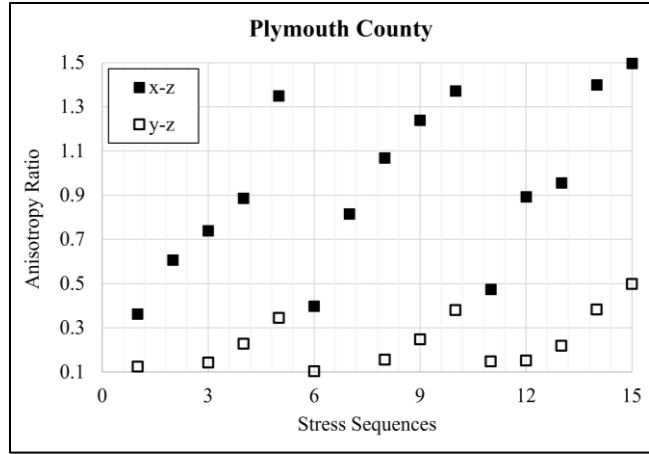
Figure 42. Anisotropy ratios for Plymouth County

Overall, all the materials showed cross-anisotropic behavior, where the stiffness was direction-dependent. As seen from Figure 39-42, regardless of the material type, the anisotropy ratios were observed to be stress-dependent, with the ratio increasing with increasing $\Delta\sigma$ for the same θ (sequences 1-3, 4-6, 7-9, 10-12, 13-15 for base/subbase and sequences 1-5, 6-10, and 11-15 for subgrade).

For Ames Mine, the anisotropy ratios (AR_{x-z} and AR_{y-z}) were observed to be between 0.13 to 0.39 and 0.09 to 0.28, respectively, indicating that M^z_R was 3 to 7 times higher than M^x_R and 4 to 11 times higher than M^y_R. Similarly, for Crocker Pit, the ratios were determined to be varying between 0.13-0.38 for AR_{x-z} (M^z_R 3 to 8 times higher than M^x_R) and 0.14-0.35 for AR_{y-z} (M^z_R 3 to 7 times higher than M^y_R). For Shambaugh Quarry, the anisotropy ratios were observed to be between 0.15 to 0.34 for $ARx-z$ (M^z_R 3 to 7 times higher than M^x_R) and 0.10-0.27 for AR_{y-z} (M^z_R 4 to 10 times higher than M^y_R).

Overall, for the base/subbase materials, it was shown that the horizontal stiffnesses in both directions (AR_{x-z} and AR_{y-z}) were just fractions of the vertical stiffness. This is due to the interlocking mechanism observed in granular materials in the vertical direction which is achieved with compaction and conditioning. However, for the subgrade material, Plymouth County, the anisotropy ratios (AR_{x-z} and AR_{y-z}) were also direction-dependent in addition to the stress-dependency. For AR_{x-z}, the ratios varied from 0.36 to 1.50, while for AR_{y-z}, the ratios ranged from 0.09 to 0.50. This result is believed to be influenced by the order of stress application, where the $\Delta\sigma$ was lastly applied to the horizontal x-axis direction. It is hypothesized that during the previous $\Delta\sigma$ applications (vertical z-axis and horizontal y-axis), the geomaterial became more compacted, leading to variations in the calculated M_R values.

Furthermore, the highest anisotropy ratios were recorded for the subgrade material, where the stress-softening in the vertical direction and stress-hardening in both horizontal directions contributed to the outcome. Understanding the effect of stress history on the mechanical characteristics of fine-grained materials requires further investigation. These findings highlight the importance of considering cross-anisotropy and direction-dependent behavior when

analyzing and designing pavement structures to accurately account for the variations in the mechanical material response.

4.4 Cross-anisotropy of Permanent Deformation

After completing M_R testing in the previous section, PD tests were carried out on the same specimens for each direction. The applied stress and the number of cycles are provided in Table 11. Notably, the chosen stresses correspond to the SM_R for both the base/subbase (Sequence 6) and subgrade (Sequence 13) materials.

Table 11. PD stress sequences for base/subbase and subgrade materials

Material Type	σ_c	Vertical z-axis PD			Horizontal x-axis PD			Horizontal y-axis PD			Number of cycles
		$\Delta\sigma_z$	$\Delta\sigma_x$	$\Delta\sigma_y$	$\Delta\sigma_z$	$\Delta\sigma_x$	$\Delta\sigma_y$	$\Delta\sigma_z$	$\Delta\sigma_x$	$\Delta\sigma_y$	
	psi	psi	psi	psi	psi	psi	psi	psi	psi	psi	
Base/subbase	5	15	0	0	0	15	0	0	0	15	10,000
Subgrade	2	6	0	0	0	6	0	0	0	6	10,000

σ_c = Confining pressure, PD = Permanent deformation, $\Delta\sigma_z$ = Vertical z-axis cyclic stress, $\Delta\sigma_x$ = Horizontal x-axis cyclic stress, $\Delta\sigma_y$ = Horizontal y-axis cyclic stress

The observed permanent strains (ratio of the permanent deformation to specimen height) for Ames Mine, Crocker Pit, Shambaugh Quarry, and Plymouth County are given in Figure 43-46, respectively.
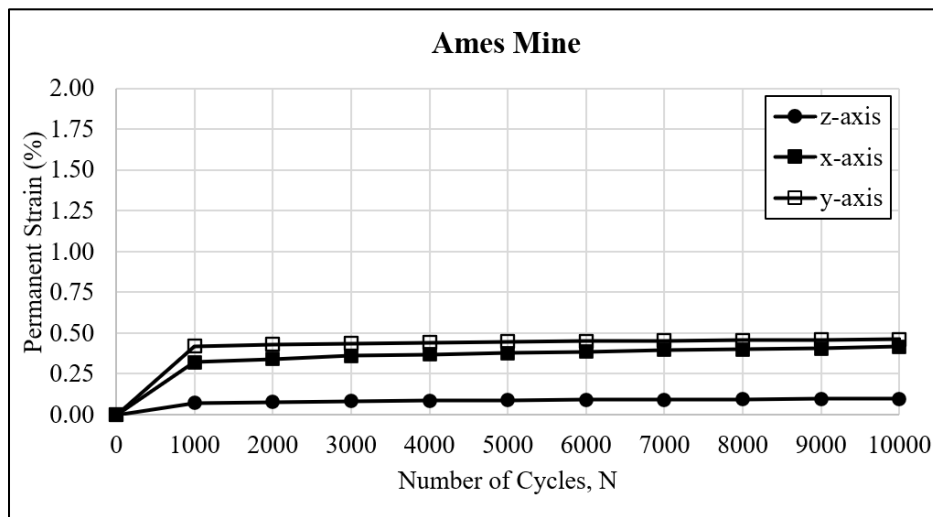
Figure 43. Permanent strains in the vertical z-axis, horizontal x-axis, and y-axis of Ames Mine
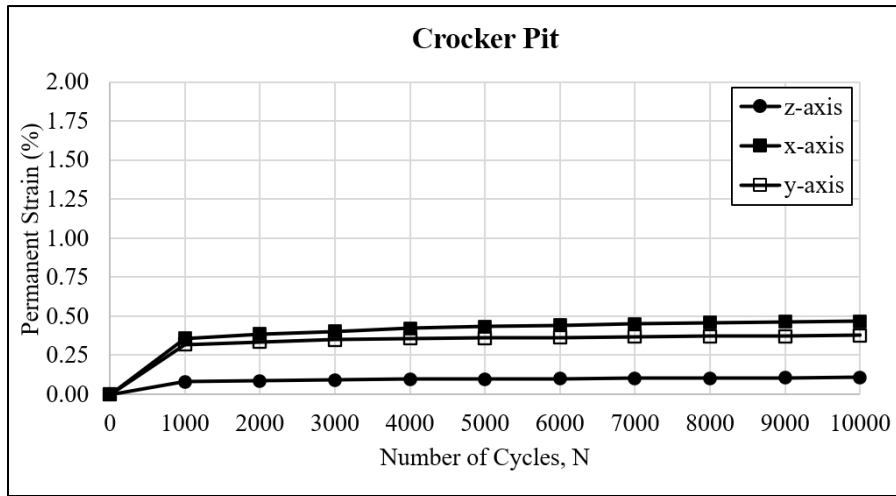
Figure 44. Permanent strains in the vertical z-axis, horizontal x-axis, and y-axis of Crocker Pit
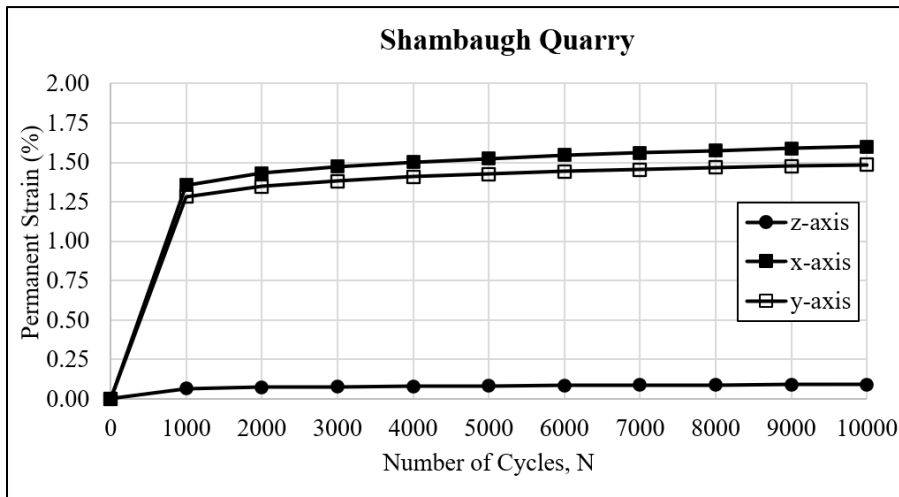
Figure 45. Permanent strains in the vertical z-axis, horizontal x-axis, and y-axis of Shambaugh Quarry
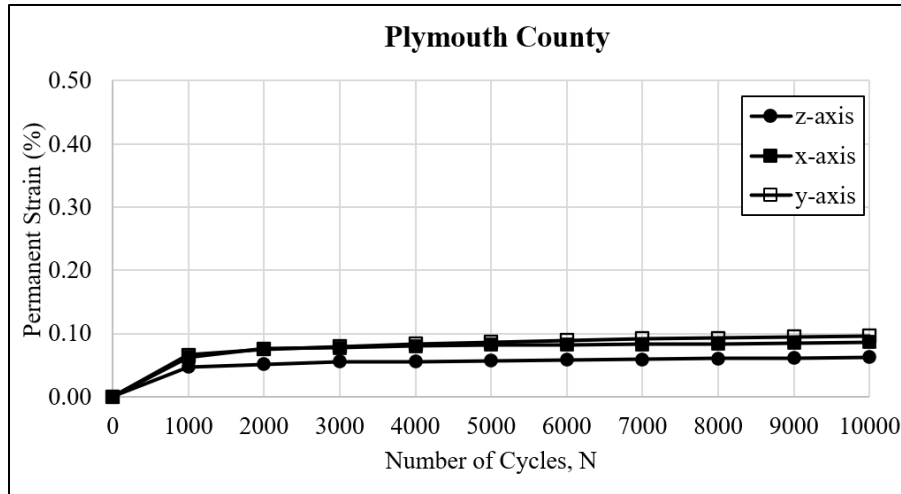
Figure 46. Permanent strains in the vertical z-axis, horizontal x-axis, and y-axis of Plymouth County

In summary, the study revealed that both the base and subbase materials, similar to M_R, exhibit highly cross-anisotropic behavior, with higher PD observed in the horizontal directions. Specifically, for Ames Mine, the vertical z-axis showed a permanent strain of 0.10%, while the horizontal x-axis and y-axis recorded higher values of 0.42% and 0.46%, respectively. Similarly, for Crocker Pit, the vertical z-axis showed a slightly higher PD of 0.11%, while the horizontal x-axis and y-axis deformed plastically at rates of 0.47% and 0.38%, respectively. Notably, the base materials demonstrated approximately 4 to 5 times higher deformation in both horizontal directions.

The subbase material exhibited a very similar permanent strain in the vertical x-axis when compared to the base materials, measuring at 0.09%. However, in both horizontal directions, the permanent strains were approximately 4 times higher than those observed in the base materials. Specifically, the horizontal x-axis and y-axis displayed plastic deformations of 1.60% and 1.49%, respectively. The significant plastic deformation observed in both horizontal directions can be attributed to the absence of fines content within the geomaterial structure. The lack of fines particles reduces the number of contact points in the vertical direction, leading to a higher tendency for plastic deformation in the horizontal plane. This observation provides concrete insight into the underlying factors contributing to the higher permanent strains in the horizontal directions. The findings highlight the importance of fines content within the geomaterial structure, suggesting that modifications aimed at increasing fines particles could potentially mitigate the excessive plastic deformation in the horizontal directions and improve the material's overall performance and stability. However, further research and analysis would be required to ascertain the most effective and practical methods to address this issue and enhance the subbase material's behavior under various stress and loading conditions.

In the case of Plymouth County, similar to the stiffness characteristics, the PD behavior of the materials also demonstrated low anisotropy, indicating comparable responses in both the vertical

and horizontal directions. Specifically, the vertical z-axis exhibited slightly lower permanent strains at 0.06%, while the horizontal x-axis and y-axis recorded values of 0.09% to 0.10%, respectively. An important observation to highlight is that the level of permanent strains in Plymouth County was overall lower than that observed in the base/subbase materials. This difference can be attributed to the applied stress levels used to induce permanent strains during the testing process. For the base and subbase materials, higher confining stress (5 psi) and $\Delta\sigma$ (15 psi) were applied, while the subgrade material experienced lower confining stress (2 psi) and $\Delta\sigma$ (6 psi). These varying stress levels played a significant role in influencing the observed permanent strains, resulting in lower values in Plymouth County.

In conclusion, the research revealed that all the tested geomaterials exhibited similar horizontal permanent strains in both horizontal directions. This consistent behavior confirms the presence of cross-anisotropy, where the materials' responses to stress differ between the vertical and horizontal orientations.

4.5 Stress-dependent Cross-anisotropy

In this chapter, directional and stress dependency of the stiffness characteristics of Ames Mine, Weber Quarry, and CBIS were investigated for the vertical z-axis and horizontal y-axis with rigid-rigid-flexible boundary conditions (Figure 21b) through M_R testing. In the previous chapter, it was proven that geomaterials have similar elastic and plastic deformations in both horizontal directions which aligns with the cross-anisotropic behavior. To this end, only one horizontal direction (horizontal y-axis) is investigated within the scope of this chapter. In addition, the subgrade material, CBIS, was tested also with subbase testing sequences to determine the effect of applied stress on the stiffness characteristics and cross-anisotropy. The same specimen preparation and assembly procedures were followed as in previous chapters. The stress levels (for base/subbase) in Table 8 were followed for Ames Mine, Weber Quarry, and CBIS. In addition, stress levels for subgrade (Table 9Table 8) were also followed for the CBIS material to investigate the effect of applied stresses (subbase versus subgrade) on hardening/softening and cross-anisotropy.

Figure 47 and 48 show the stiffness of Ames Mine with θ in vertical (z-axis) and horizontal (y-axis), respectively.

Figure 49 and 50 show the stiffness of Weber Quarry with θ in vertical (z-axis) and horizontal (y-axis), respectively.

Figure 51 and 52 show the stiffness of CBIS (subbase) with θ in vertical (z-axis) and horizontal (y-axis) as subbase, respectively.

Figure 53 and 54 show the stiffness of CBIS (subgrade) with θ in vertical (z-axis) and horizontal (y-axis) as subgrade, respectively.

Figure 55 shows the anisotropy ratios with varying applied cyclic stresses for all the tested materials.
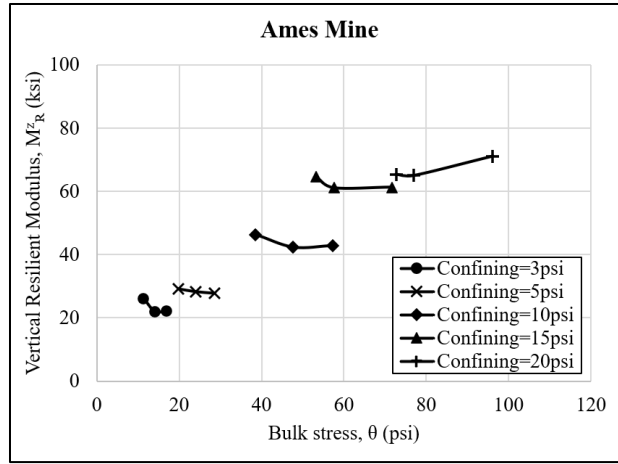
Figure 47. Vertical z-axis resilient modulus (MᶻR) versus bulk stress (θ) of Ames Mine
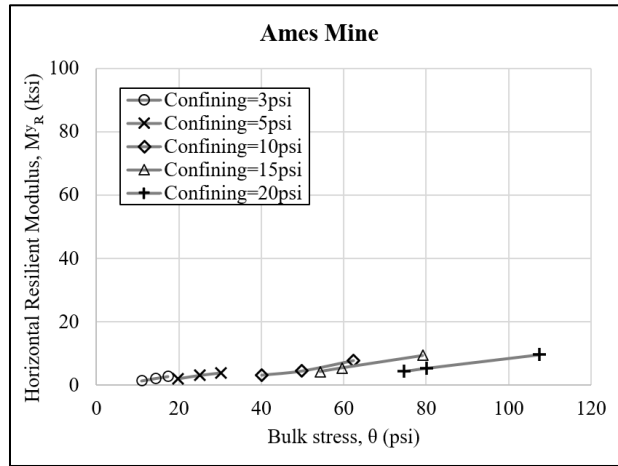
Figure 48. Horizontal y-axis resilient modulus (MʸR) versus bulk stress (θ) of Ames Mine
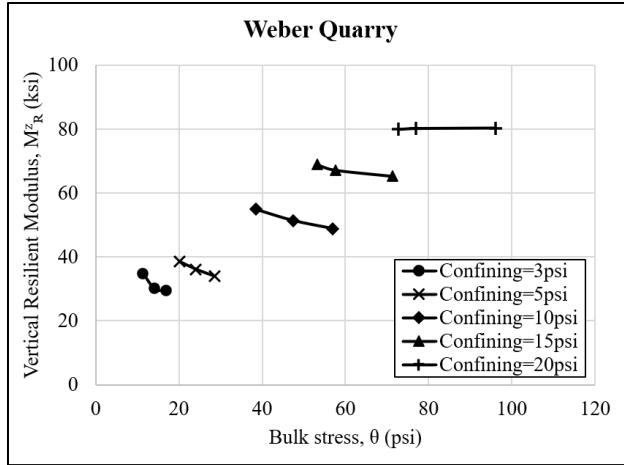
Figure 49. Vertical z-axis resilient modulus (M^z_R) versus bulk stress (θ) of Weber Quarry
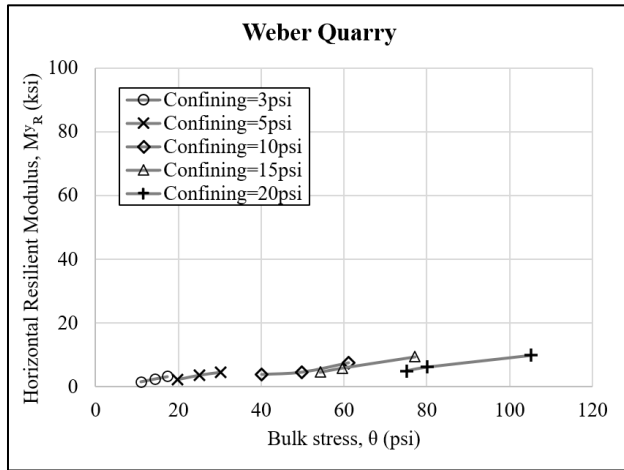
Figure 50. Horizontal y-axis resilient modulus (M^y_R) versus bulk stress (θ) of Weber Quarry
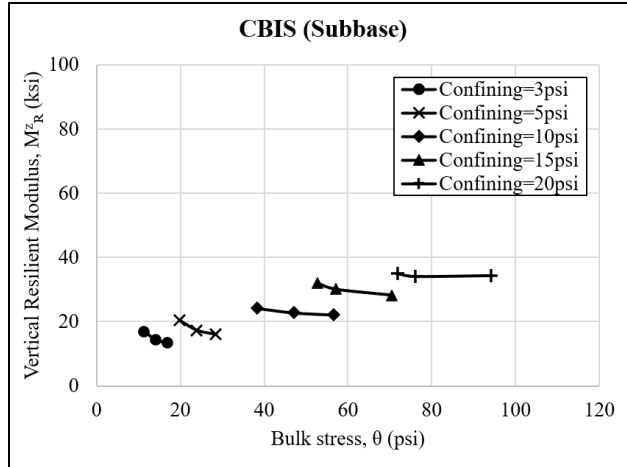
Figure 51. Vertical z-axis resilient modulus (M^z_R) versus bulk stress (θ) of CBIS (subbase)
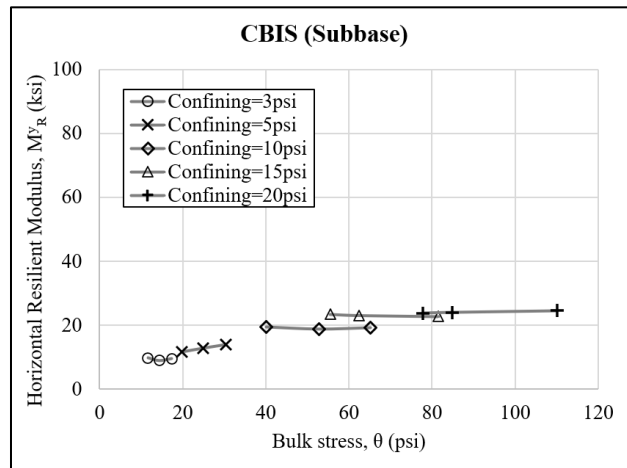
Figure 52. Horizontal y-axis resilient modulus (M^y_R) versus bulk stress (θ) of CBIS (subbase)
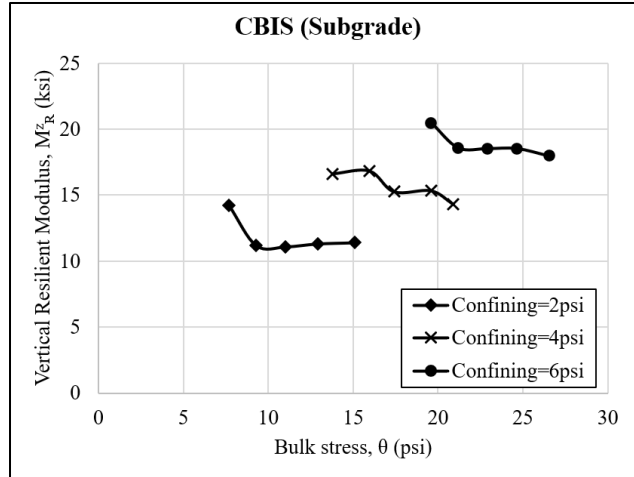
Figure 53. Vertical z-axis resilient modulus (M^z_R) versus bulk stress (θ) of CBIS (subgrade)
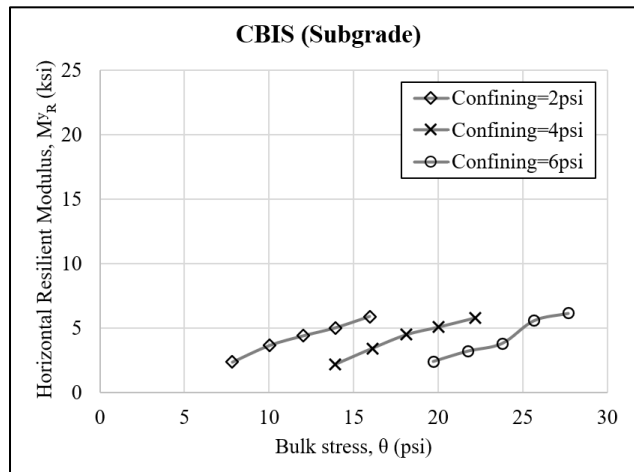
Figure 54. Horizontal y-axis resilient modulus (M^y_R) versus bulk stress (θ) of CBIS (subgrade)
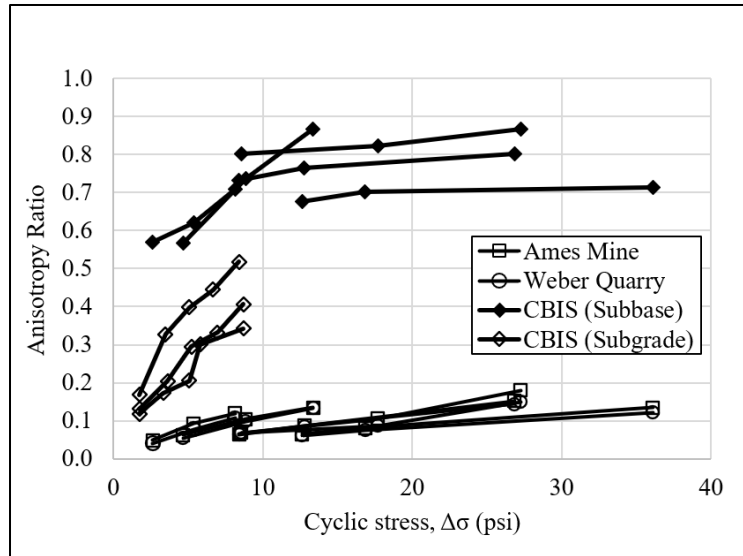
Figure 55. Anisotropy ratios of materials with cyclic stress (Δσ)

Overall, the study revealed that the stiffness of tested materials was stress-dependent in both vertical and horizontal directions. Irrespective of material type, gradation, and applied stress levels (CBIS material with subbase and subgrade stress levels), the stiffness characteristics exhibited cross-anisotropic behavior. Figure 47 illustrates that the stiffness of Ames Mine increased in both directions with increasing θ. However, for the same confining pressures (Sequences 1-3, 4-6, 7-9, 10-12, 13-15), an increase in Δσ led to a decrease in M^z_R. In the horizontal direction, the M^y_R exhibited a slight stress-hardening behavior, unlike M^z_R (Figure 48). This phenomenon can be attributed to the strengthened structural capacity of granular materials in the horizontal direction due to the application of cyclic stresses in the vertical direction. On the other hand, the case representing induces stress-hardening behavior, as the granular material had already become more compacted, yielding less elastic deformation during the M^z_R testing program. Similar trends were observed for the Weber Quarry in both the vertical and horizontal directions (Figure 49 and 50).

To investigate the effect of applied stresses on the directional and stress dependency of the stiffness, the sand used in this study was tested for both subbase and subgrade stress levels. Figure 51-54 show that both M^z_R and M^y_R were stress-dependent with different testing programs (subbase and subgrade). Similar to the result for dolomite and limestone materials, sand exhibited stress-softening behavior in the vertical direction during the subbase testing sequences (Figure 51) for the same confining pressure (Sequences 1-3, 4-6, 7-9, 10-12, 13-15). However, in the horizontal direction rather than the vertical direction, the sandy material exhibited stress-hardening behavior, particularly in the first six sequences, as a result of the increased compaction effect during testing where the wheel load was modeled as being on top of the tested material (Figure 52). The apparent disappearance of the stress-hardening effect for some sequences (Sequences 7-15) might be because of the limited contribution of compaction effort due to the previously applied Δσ in the vertical stiffness testing where the material also lacks interlocking and cohesion in the horizontal direction. Figure 53 shows that cyclic softening was observed for

63

M^z_R, especially after the application of the first $\Delta\sigma$ of the same confining pressures (Sequences 1, 6, and 11). This is due to the amount of the applied $\Delta\sigma$ in the testing sequences in which the granular surface road material is subjected to the lowest cyclic stresses in Sequences 1, 6, and 11 for the same confining pressures, compared to the following sequences that result in greater deformation. The following sequences (Sequences 2-5, 7-10, 12-15) contribute to the compaction of the soil structure that would have eliminated the softening effect. Conversely, in the horizontal direction, M^y_R increased with an increase in $\Delta\sigma$ due to further compaction during $\Delta\sigma$ application (Figure 54).

Figure 55 shows that both Ames Mine and Weber Quarry exhibited very similar cross-anisotropy characteristics (anisotropy ratios varying between 0.04 to 0.18), with M^z_R approximately 7 to 25 times higher than M^y_R for Weber Quarry and 6 to 21 times higher than for Ames Mine. For CBIS, an increase in $\Delta\sigma$ caused a decrease in anisotropy for subgrade stress levels as a result of significant stress-hardening in the horizontal direction. The anisotropy ratio for CBIS (subgrade) varied between 0.12 and 0.52 (M^z_R is approximately 2.0 to 8.5 times higher than M^y_R), and higher anisotropy ratios were particularly observed for Sequences 11-15 compared to the other sequences, explained by low confining pressure (2 psi) and its adverse effects on vertical stiffness. The lowest overall anisotropy was observed for sand material tested under subbase stress levels; the anisotropy ratio was determined to be between 0.57 and 0.87 (M^z_R is approximately 1.2 to 1.8 times higher than M^y_R). Both subgrade and subbase stresses resulted in similar anisotropy ratios for the same cyclic stresses, showing that cross-anisotropy was directly correlated to applied $\Delta\sigma$. Under subbase stress levels sand-material anisotropy decreased with an increase in $\Delta\sigma$ as a result of stress-softening in the vertical direction of the sand material, it can be seen that this effect was more significant for lower cyclic stresses.

Furthermore, this chapter also examines the influence of stress history on the Plano Quarry, CBIS, and Plymouth County geomaterials. To address this, two distinct methods were employed in the testing process, named Method A and Method B, based on the sequence of $\Delta\sigma$ application along the z- and y-axes. Method A involved subjecting the geomaterials to vertical $\Delta\sigma$ first, followed by horizontal $\Delta\sigma$. In contrast, Method B applied horizontal $\Delta\sigma$ initially, followed by vertical $\Delta\sigma$. The implementation of these methods is aimed to assess directional dependency and understand how the stress history impacts the cross-anisotropic behavior of the geomaterials. In addition, the effect of stress on stress-softening and stress-hardening behavior was investigated. For both investigations, stress levels in Table 8 and 9 were used.

Figure 56 and 57 show the relationship for both Methods A and B between M_R and θ in vertical and horizontal directions, respectively for Plano Quarry.
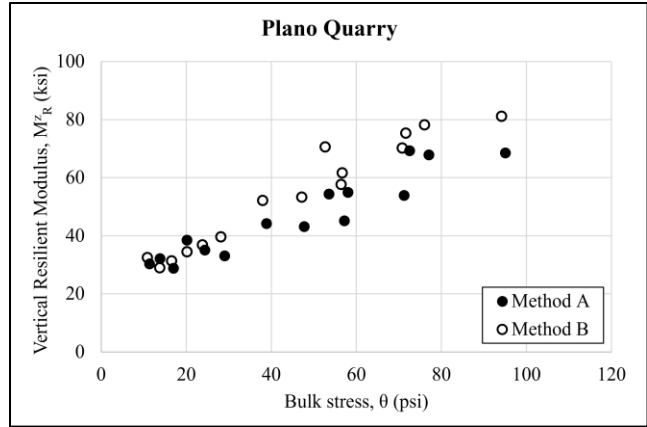
Figure 56. Vertical z-axis resilient modulus (M^z_R) versus bulk stress (θ) of Plano Quarry for both Methods A and B
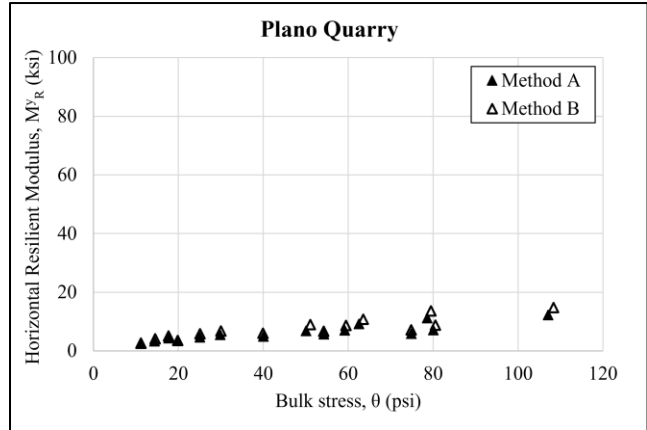
Figure 57. Horizontal y-axis resilient modulus (M^y_R) versus bulk stress (θ) of Plano Quarry for both Methods A and B

The findings indicated that the M_R values exhibited an increase in both directions as the θ was raised, demonstrating the stress-hardening behavior consistent with previous observations in base materials. Additionally, a notable difference was observed between M^z_R and M^y_R under similar stress conditions, indicating the cross-anisotropic nature of the base materials. The anisotropy ratios were determined to be in the range of 0.09 to 0.21 for Method A and 0.08 to 0.19 for Method B. The results further revealed that the stress history had a more pronounced effect on M^z_R at higher bulk stresses. For the base material, Method B (first horizontal pulsing then vertical pulsing) resulted in higher M^z_R values compared to Method A. This was attributed to an increase in stiffness in the vertical direction due to the contribution of applied horizontal cyclic stresses, leading to a more compact and densely packed structure within the specimen. In contrast, M^y_R values did not show significant variations with respect to stress histories.

Figure 58 and 59 show the relationship for both Methods A and B between M_R and θ in vertical and horizontal directions, respectively for CBIS.

65
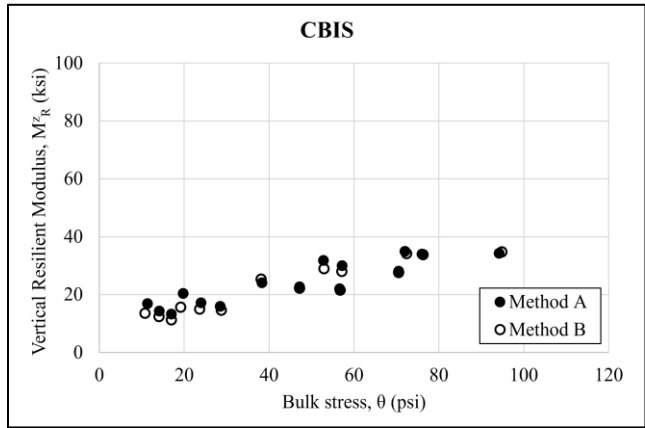
Figure 58. Vertical z-axis resilient modulus (M^z_R) versus bulk stress (θ) of CBIS for both Methods A and B
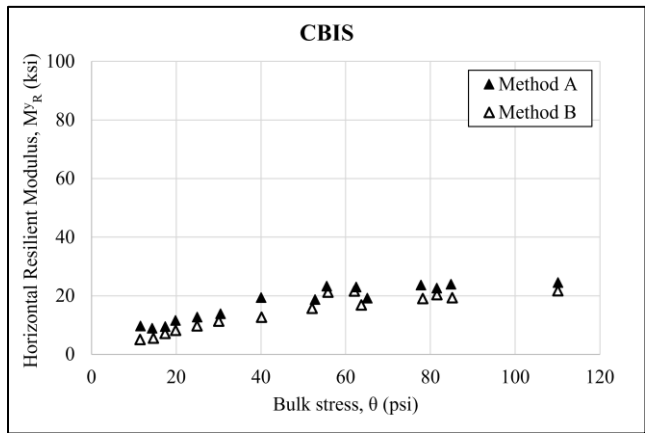
Figure 59. Horizontal y-axis resilient modulus (M^y_R) versus bulk stress (θ) of CBIS for both Methods A and B

Similar to the Plano Quarry findings, the M$_R$ values for CBIS increased in both directions as θ increased. The M$_R$ results also differed between the vertical and horizontal directions, indicating cross-anisotropy similar to that observed in base materials. The anisotropy ratios were within the ranges of 0.57 to 0.87 for Method A and 0.38 to 0.78 for Method B. In the vertical direction, both Method A and Method B exhibited a slight stress-softening behavior for CBIS under the same confining pressure levels but increasing cyclic stresses. This behavior was attributed to the cohesionless nature of sandy soils, where the interlocking mechanism found in coarser geomaterials did not exist. Conversely, stress-softening was not evident in the horizontal direction for different methods due to the geomaterial's weaker nature in that orientation, influenced by the specimen dimensions. Unlike the Plano Quarry results, varying stress histories had no significant effect on M^z_R values for CBIS. However, Δσ applied in the vertical direction (Method A) resulted in a more compact structure in the horizontal direction, leading to higher

66

M^y_R values. Specifically, M^y_R values were determined to be 1.1 to 1.9 times higher for Method A compared to Method B.

Figure 60 and 61 show the relationship for both Methods A and B between M_R and θ in vertical and horizontal directions, respectively for Plymouth County.
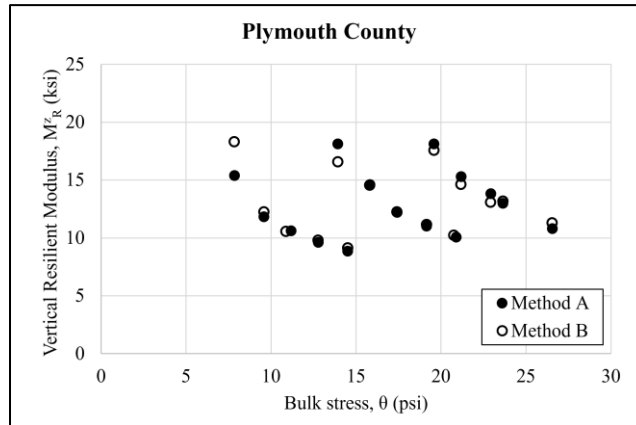
Figure 60. Vertical x-axis resilient modulus (M^z_R) versus bulk stress (θ) of Plymouth County for both Methods A and B
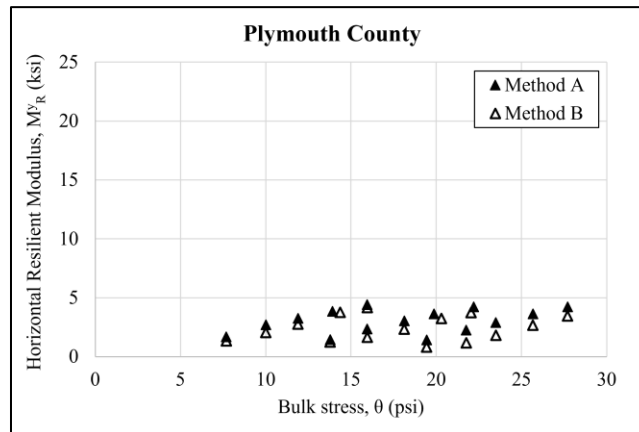
Figure 61. Horizontal y-axis resilient modulus (M^y_R) versus bulk stress (θ) of Plymouth County for both Methods A and B

The findings from Plymouth County revealed anisotropy ratios ranging from 0.08 to 0.50 for Method A and 0.05 to 0.46 for Method B, highlighting the cross-anisotropic nature of the materials. The subgrade exhibited higher anisotropy ratios compared to the base material due to the absence of an interlocking mechanism in fine-grained soils, resulting in increased vertical stiffness in granular materials. The subgrade material displayed a decreasing trend in M_R with an increase in $\Delta\sigma$, indicating stress-softening behavior in the vertical direction. It is believed that an increase in deviator stress could cause shear deformations in the vertical direction. M^y_R increased

with an increase in θ, exhibiting stress-hardening behavior contrary to the vertical direction. This observation could be explained by further compaction in the horizontal direction due to increased θ, potentially leading to higher M_R. Moreover, the different loading methods (Methods A and B) had minimal impact on the material's behavior in both the horizontal and vertical directions.

4.6 Cross-anisotropy under Moving Wheel Load

In this chapter, the effect of moving wheel load on the stiffness characteristics in both vertical (z-axis) and horizontal direction (y-axis) was investigated. Stress path sweep tests were conducted on the Ames Mine, Bethany Falls Limestone, Crocker Pit, Oneota Formation Dolomite, Plano Quarry, Weber Quarry, CBIS, and Plymouth County to model the approaching and receding wheel load. Stress path sweep tests allowed the application of representative stress states occurring in the field on the same specimen, preventing differences due to specimen variations such as dry density and moisture contents. The specimens were first tested at the stress path slope (m) of 3 (Equation 9), representing the wheel load on top of the geomaterial with σ_1 in the vertical direction. Following that, m values were gradually decreased to 1.7, 1.5, (-1.7), and (-3.0), where (-3.0) is associated with the wheel load away from the geomaterial (σ_1 in the horizontal direction). The values of 1.7, 1.5, and (-1.7) represent the cases that depict the transition from σ_1 in the vertical direction to the horizontal direction. By applying the testing program through different m values, the receding wheel load is modeled as referencing the geomaterial.

$$\text{Stress path slope (m)} = \frac{\Delta q}{\Delta p} \tag{9}$$

where Δq and Δp are deviatoric and mean stresses, respectively. Equations (10) and (11) show the mean and deviatoric stress for three-dimensional stress states.

$$\Delta q = \sqrt{\frac{(\Delta\sigma_1 - \Delta\sigma_2)^2 + (\Delta\sigma_1 - \Delta\sigma_3)^2 + (\Delta\sigma_2 - \Delta\sigma_3)^2}{2}} \tag{10}$$

$$\Delta p = \frac{\Delta\sigma_1 + \Delta\sigma_2 + \Delta\sigma_3}{3} \tag{11}$$

where $\Delta\sigma_1$, $\Delta\sigma_2$ and $\Delta\sigma_3$ are the changes in the major, intermediate, and minor principal stresses.

Table 12 and 13 show the applied stresses at each m following the equations above for base/subbase and subgrade, respectively.

Table 12. Testing program of stress path sweep test for base/subbase

Sequence No.	σ_c	Base/Subbase									
		m = 3.0		m = 1.7		m = 1.5		m = -1.7		m = -3.0	
		$\Delta\sigma_z$	$\Delta\sigma_y$	$\Delta\sigma_z$	$\Delta\sigma_y$	$\Delta\sigma_z$	$\Delta\sigma_y$	$\Delta\sigma_z$	$\Delta\sigma_y$	$\Delta\sigma_z$	$\Delta\sigma_y$
	psi	psi	psi	psi	psi	psi	psi	psi	psi	psi	psi
0	15	15	0	15	0	15	0	15	0	15	0
1	3	3	0	3	1.5	3	3	1.5	3	0	3
2	3	6	0	6	3	6	6	3	6	0	6
3	3	9	0	9	4.5	9	9	4.5	9	0	9
4	5	5	0	5	2.5	5	5	2.5	5	0	5
5	5	10	0	10	5	10	10	5	10	0	10
6	5	15	0	15	7.5	15	15	7.5	15	0	15
7	10	10	0	10	5	10	10	5	10	0	10
8	10	20	0	20	10	20	20	10	20	0	20
9	10	30	0	30	15	30	30	15	30	0	30
10	15	10	0	10	5	10	10	5	10	0	10
11	15	15	0	15	7.5	15	15	7.5	15	0	15
12	15	30	0	30	15	30	30	15	30	0	30
13	20	15	0	15	7.5	15	15	7.5	15	0	15
14	20	20	0	20	10	20	20	10	20	0	20
15	20	40	0	40	20	40	40	20	40	0	40

Table 13. Testing program of stress path sweep test for subgrade

Sequence No.	σ_c	m = 3.0		m = 1.7		m = 1.5		m = -1.7		m = -3.0	
		$\Delta\sigma_z$	$\Delta\sigma_y$	$\Delta\sigma_z$	$\Delta\sigma_y$	$\Delta\sigma_z$	$\Delta\sigma_y$	$\Delta\sigma_z$	$\Delta\sigma_y$	$\Delta\sigma_z$	$\Delta\sigma_y$
	psi	psi	psi	psi	psi	psi	psi	psi	psi	psi	psi
0	6	4	0	4	0	4	0	4	0	4	0
1	6	2	0	2	1	2	2	1	2	0	2
2	6	4	0	4	2	4	4	2	4	0	4
3	6	6	0	6	3	6	6	3	6	0	6
4	6	8	0	8	4	8	8	4	8	0	8
5	6	10	0	10	5	10	10	5	10	0	10
6	4	2	0	2	1	2	2	1	2	0	2
7	4	4	0	4	2	4	4	2	4	0	4
8	4	6	0	6	3	6	6	3	6	0	6
9	4	8	0	8	4	8	8	4	8	0	8
10	4	10	0	10	5	10	10	5	10	0	10
11	2	2	0	2	1	2	2	1	2	0	2
12	2	4	0	4	2	4	4	2	4	0	4
13	2	6	0	6	3	6	6	3	6	0	6
14	2	8	0	8	4	8	8	4	8	0	8
15	2	10	0	10	5	10	10	5	10	0	10

Figure 62 and 63 show the results for Ames Mine for M^z_R and M^y_R, respectively.
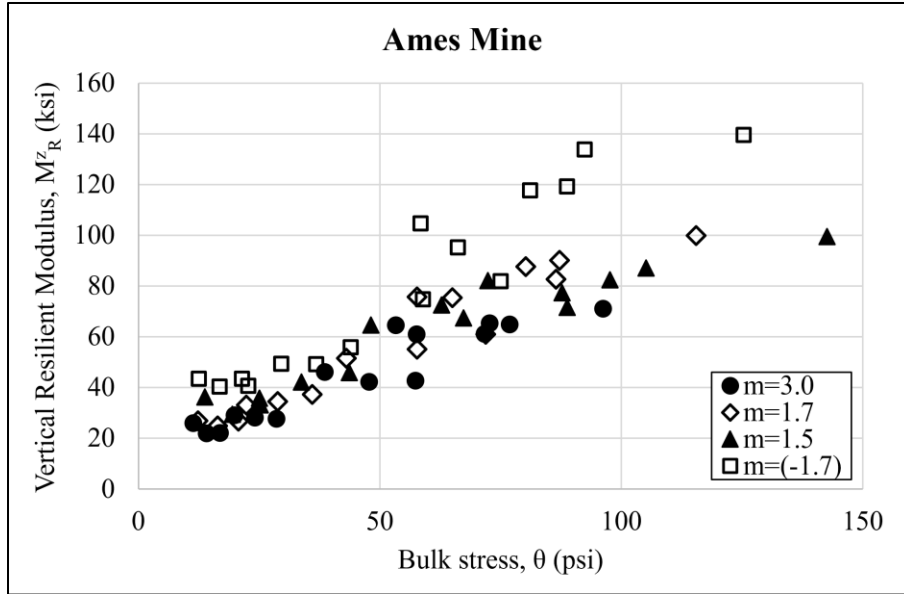
Figure 62. Vertical z-axis resilient modulus (M^z_R) change with bulk stress (θ) of Ames Mine at different stress path slopes (m)
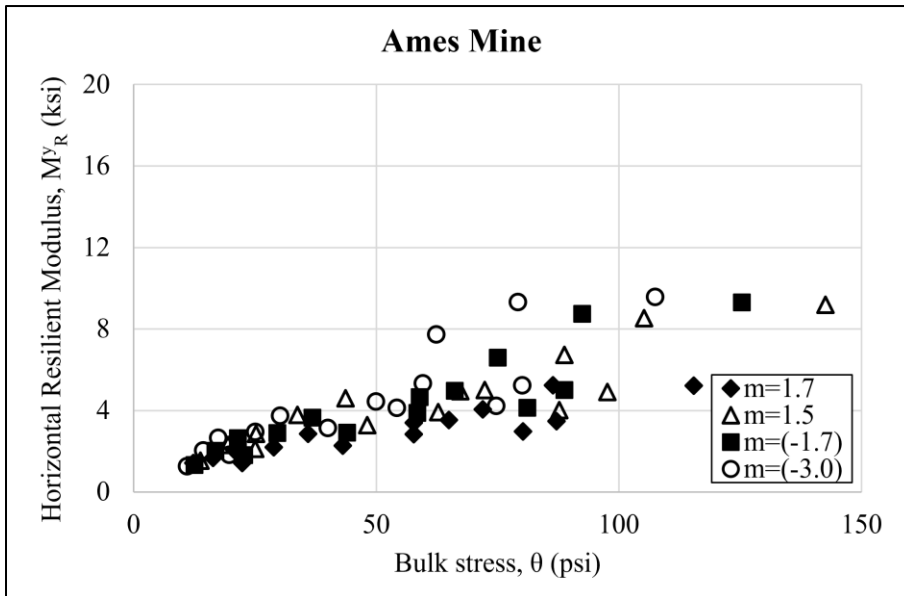
Figure 63. Horizontal y-axis resilient modulus (M^y_R) change with bulk stress (θ) of Ames Mine at different stress path slopes (m)

Figure 64 and 65 show the results for Bethany Falls Limestone for M^z_R and M^y_R, respectively.

71
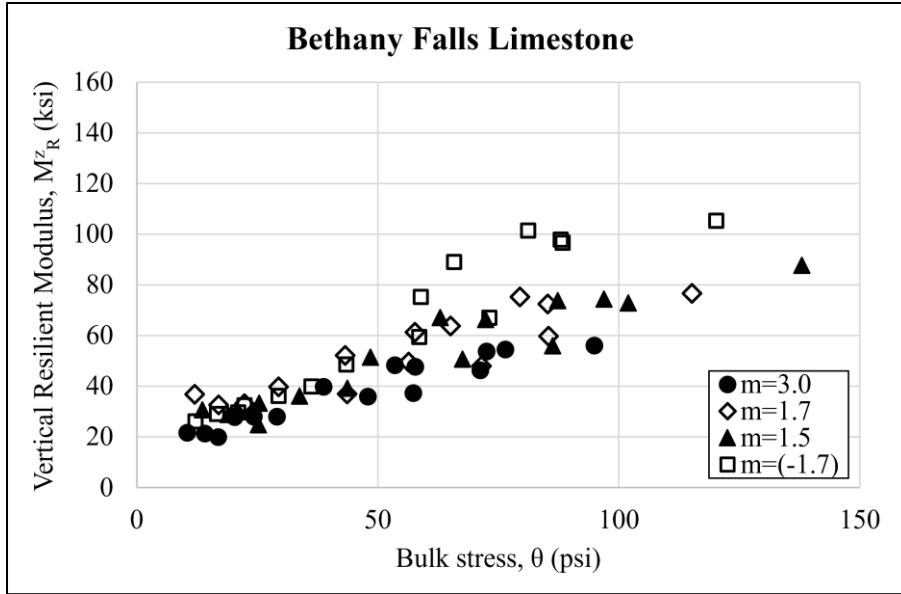
Figure 64. Vertical z-axis resilient modulus (M^z_R) change with bulk stress (θ) of Bethany Falls Limestone at different stress path slopes (m)
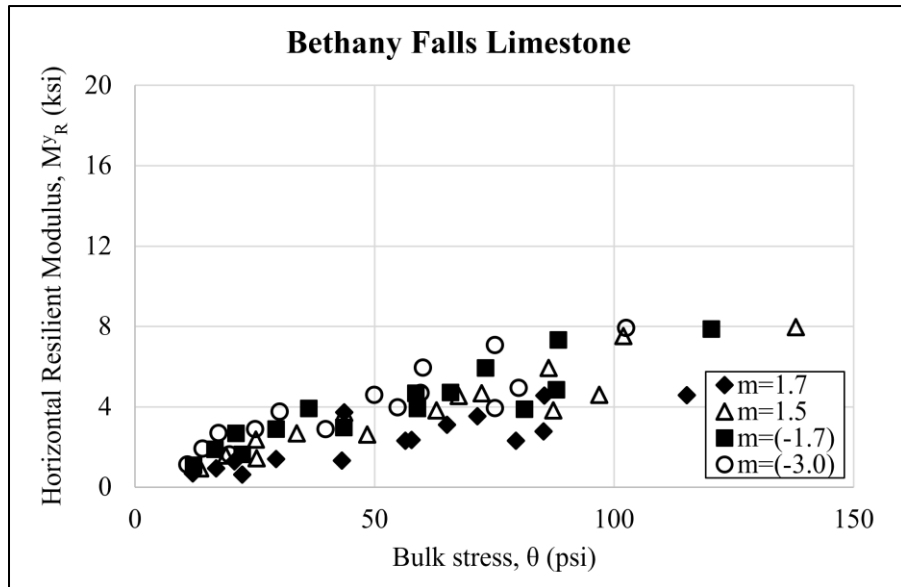
Figure 65. Horizontal y-axis resilient modulus (M^y_R) change with bulk stress (θ) of Bethany Falls Limestone at different stress path slopes (m)

Figure 66 and 67 show the results for Crocker Pit for M^z_R and M^y_R, respectively.

72
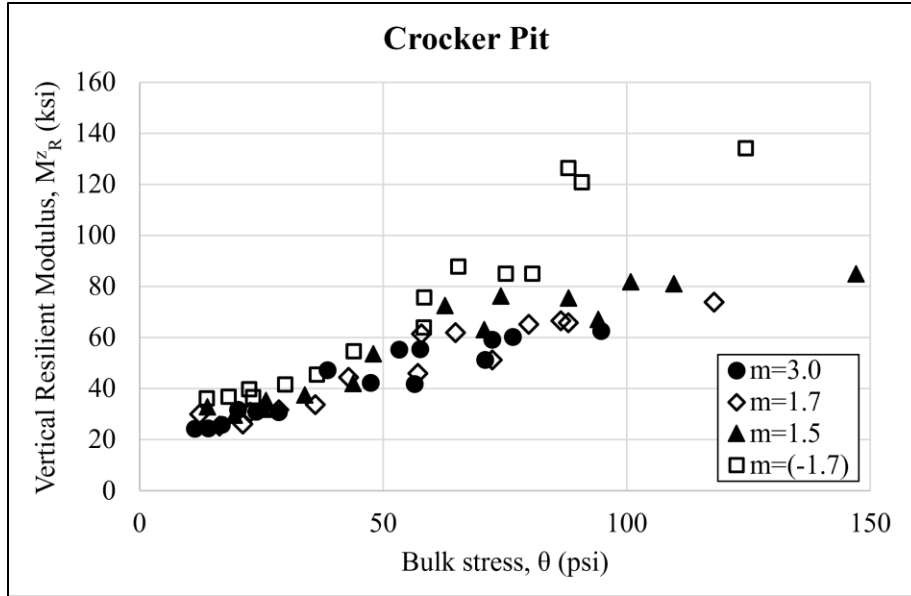
Figure 66. Vertical z-axis resilient modulus (M^z_R) change with bulk stress (θ) of Crocker Pit at different stress path slopes (m)
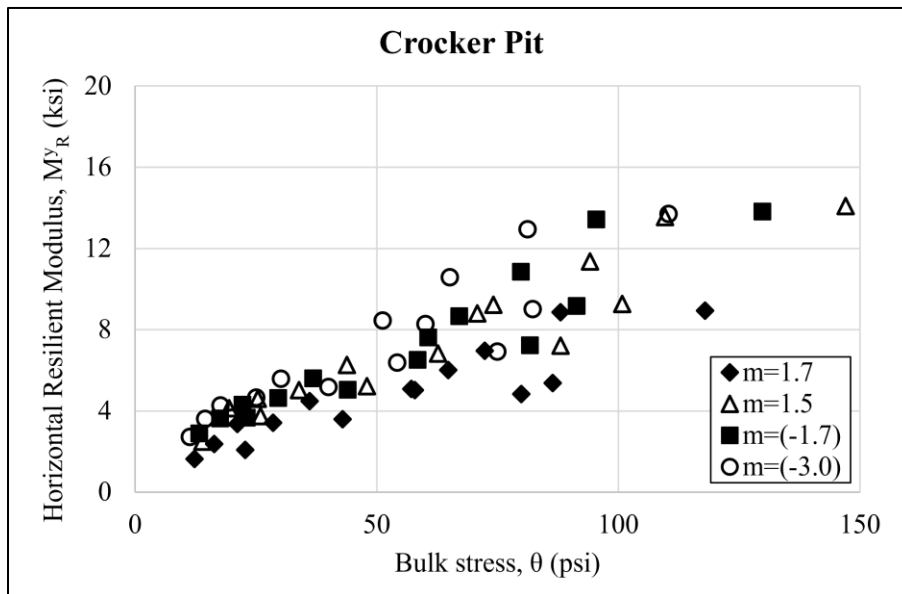
Figure 67. Horizontal y-axis resilient modulus (M^y_R) change with bulk stress (θ) of Crocker Pit at different stress path slopes (m)

Figure 68 and 69 show the results for Oneota Formation Dolomite for M^z_R and M^y_R, respectively.
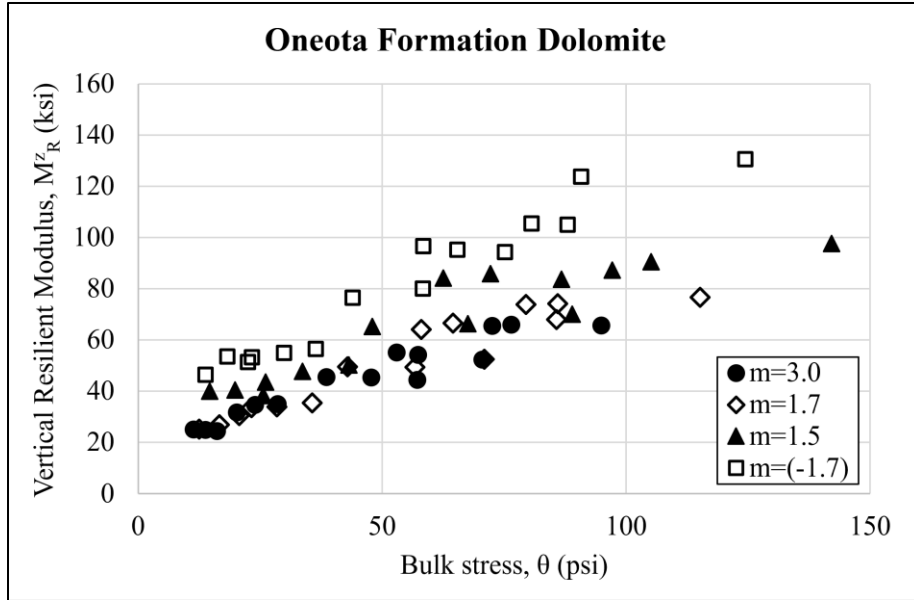
Figure 68. Vertical z-axis resilient modulus (M^z_R) change with bulk stress (θ) of Oneota Formation Dolomite at different stress path slopes (m)
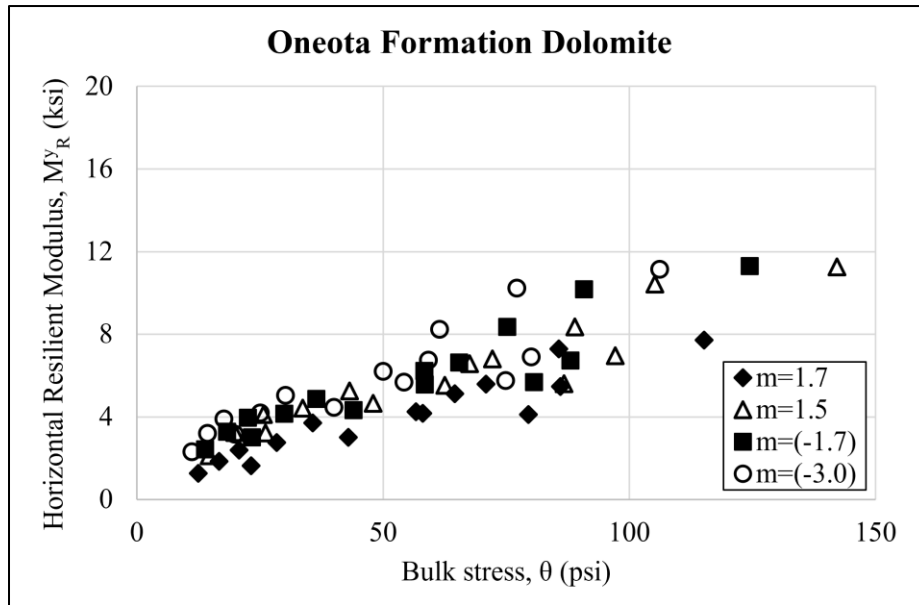
Figure 69 Horizontal y-axis resilient modulus (M^y_R) change with bulk stress (θ) of Oneota Formation Dolomite at different stress path slopes (m)

Figure 70 and 71 show the results for Plano Quarry for M^z_R and M^y_R, respectively.
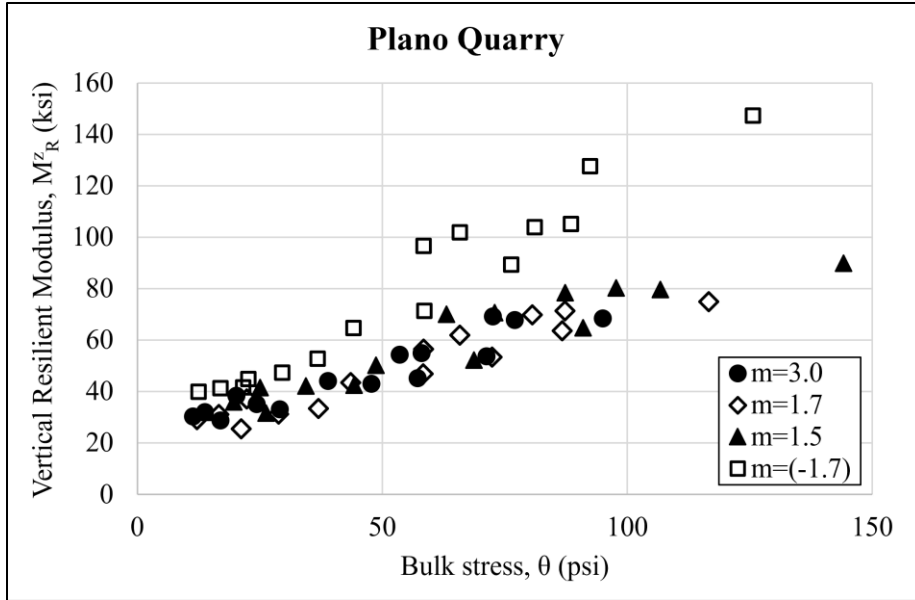
Figure 70. Vertical z-axis resilient modulus (M^z_R) change with bulk stress (θ) of Plano Quarry at different stress path slopes (m)
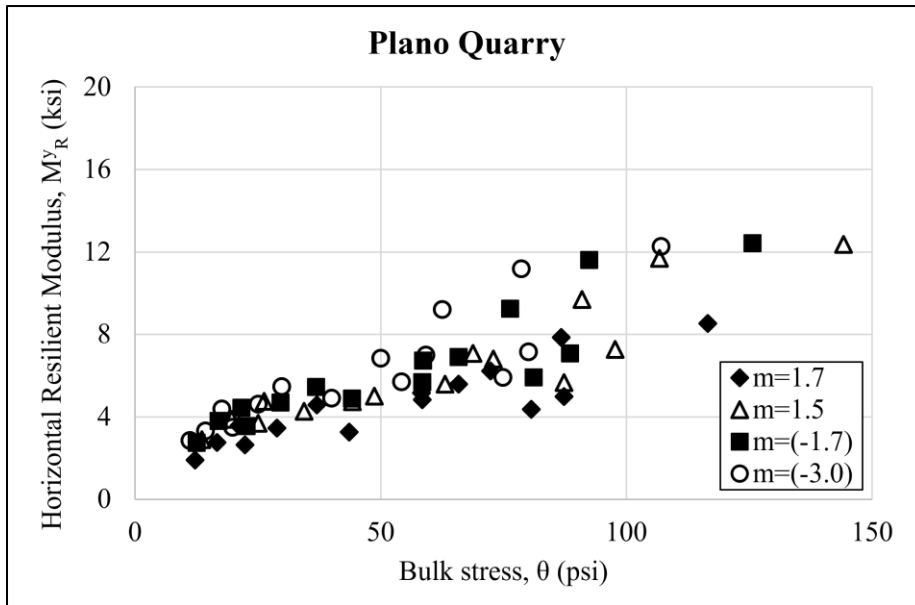
Figure 71. Horizontal y-axis resilient modulus (M^y_R) change with bulk stress (θ) of Plano Quarry at different stress path slopes (m)

Figure 72 and 73 show the results for Weber Quarry for M^z_R and M^y_R, respectively.
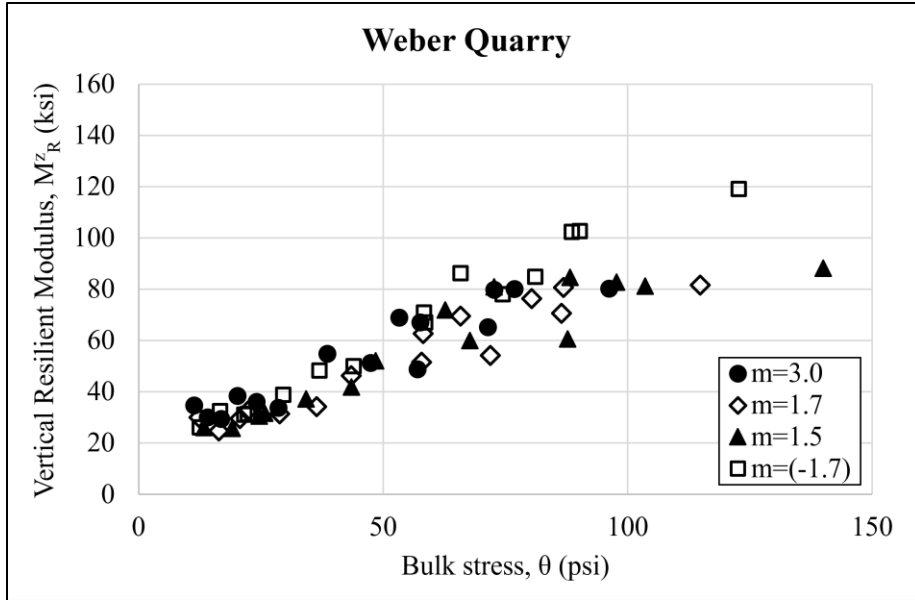
Figure 72. Vertical z-axis resilient modulus (M^z_R) change with bulk stress (θ) of Weber Quarry at different stress path slopes (m)
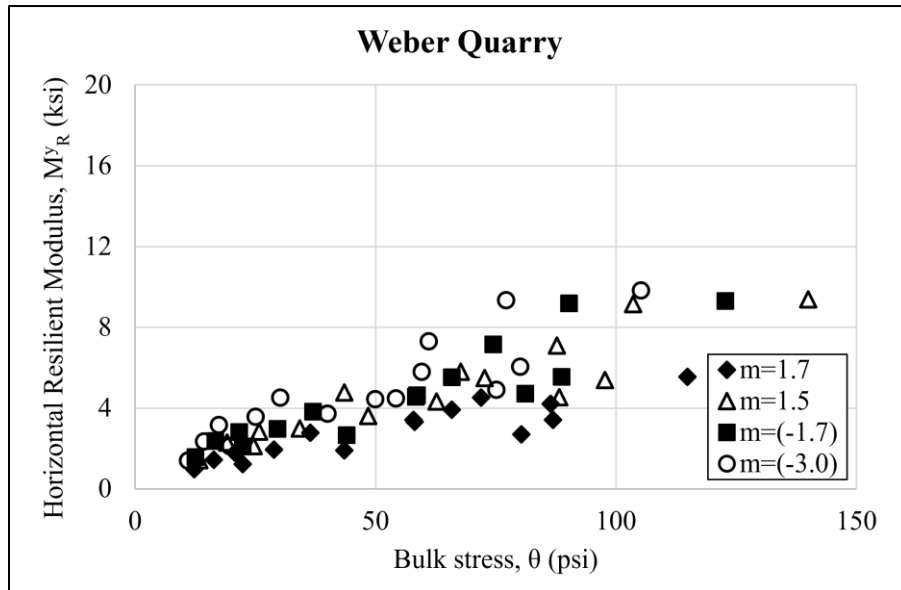
Figure 73. Horizontal y-axis resilient modulus (M^y_R) change with bulk stress (θ) of Weber Quarry at different stress path slopes (m)

Figure 74 and 75 show the results for CBIS for M^z_R and M^y_R, respectively.

76
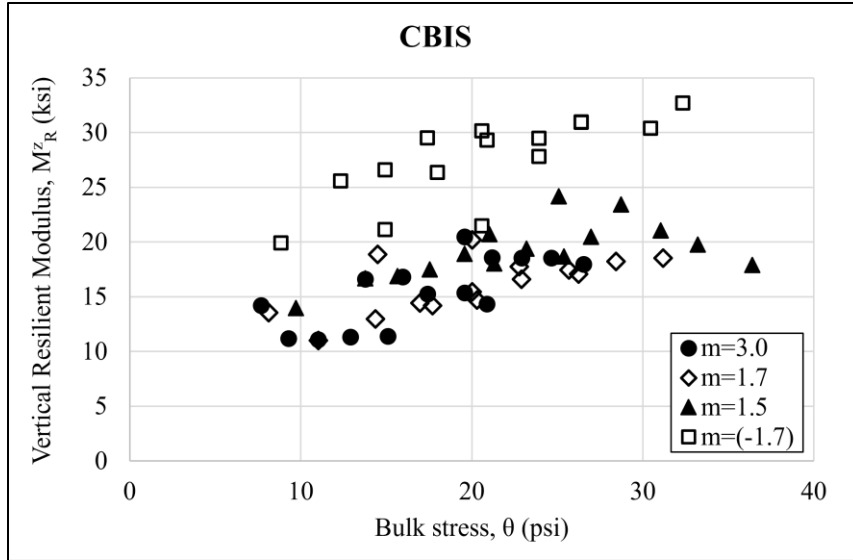
Figure 74. Vertical z-axis resilient modulus (M^z_R) change with bulk stress (θ) of CBIS at different stress path slopes (m)
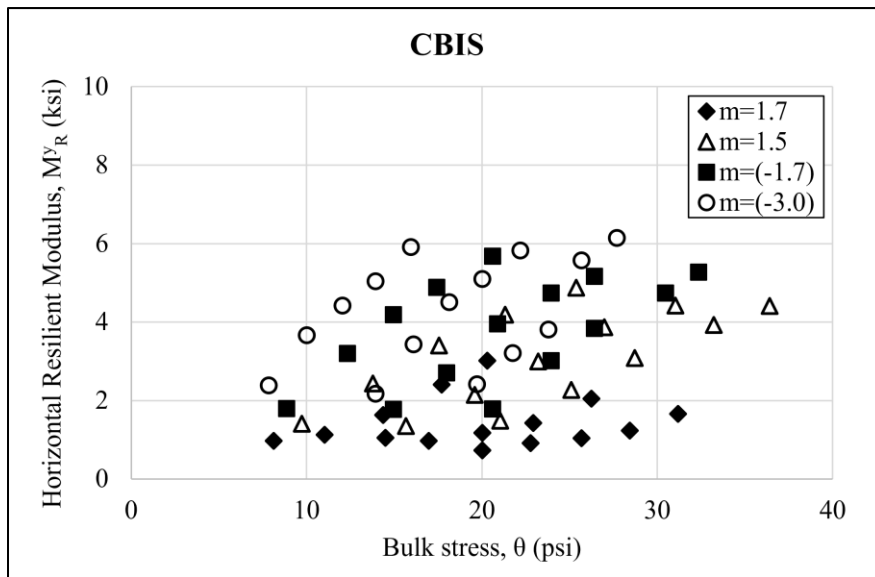
Figure 75. Horizontal y-axis resilient modulus (M^y_R) change with bulk stress (θ) of CBIS at different stress path slopes (m)

Figure 76 and 77 show the results for Plymouth County for M^z_R and M^y_R, respectively.
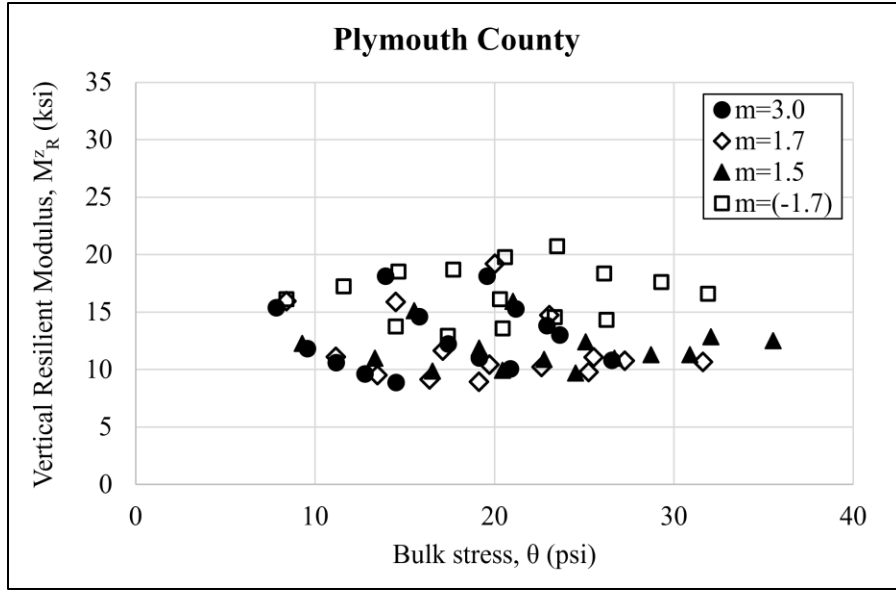
Figure 76. Vertical z-axis resilient modulus (M^z_R) change with bulk stress (θ) of Plymouth County at different stress path **slopes (m)**
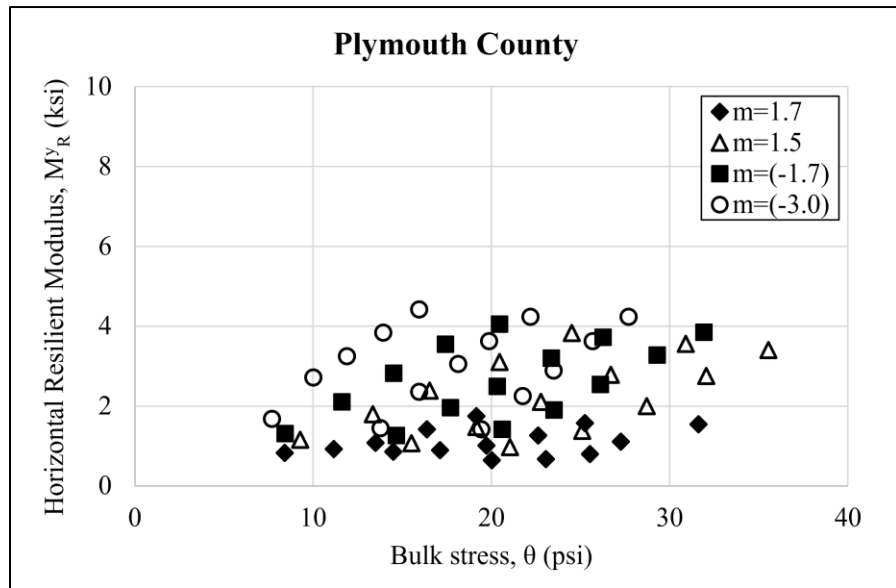
Figure 77. Horizontal y-axis resilient modulus (M^y_R) change with bulk stress (θ) of Plymouth County at different stress path slopes (m)

In summary, the results indicate that the M_R in each direction is dependent on the stress path as well as the stress level. Among the base materials (Ames Mine, Bethany Falls Limestone, Crocker Pit, Oneota Formation Dolomite, Plano Quarry, Weber Quarry), the highest M^z_R was observed for m=(-1.7), especially at higher confining stress levels. Conversely, the lowest M^z_R was recorded for m=3.0. These findings can be attributed to the applied stresses; m=(-1.7)

experienced higher lateral confining stresses due to the major principal stress being in the horizontal direction, while m=3.0 yielded the lowest M^z_R as it had the lowest lateral confining stresses and was exposed to $\Delta\sigma$ for the first time.

For M^y_R, the lowest values were observed for m=1.7, likely due to the horizontal direction being exposed to the first $\Delta\sigma$ application during that stress path slope. Subsequent stress path applications did not seem to increase M^y_R, likely because of the ultimate packing of the weak structure during the m=1.7 testing program. In general, both M^z_R and M^y_R exhibited stress-hardening behavior.

In comparison, the subgrade materials (CBIS and Plymouth County) displayed lower M^z_R and M^y_R values compared to the base materials. The highest M^z_R for both subgrade materials was observed at m=(-1.7), similar to the trend seen in the base materials. m=3.0 yielded slightly lower values compared to other m values [1.7, 1.5, (-1.7)]. For M^y_R, the highest values were observed at m=(-3.0), while the lowest values were seen at m=1.7, following the pattern observed in the base materials. Notably, with the exception of one case [CBIS m=(-1.7)], M^z_R for both subgrade materials exhibited stress-softening, whereas M^y_R showed stress-hardening behavior. The stress-hardening behavior in M^y_R can be explained by further compaction in the horizontal direction due to increased θ, potentially resulting in higher M_R. The atypical occurrence of stress-hardening behavior in M^z_R was attributed to the stiffened structure, which likely resulted from the applied stress history. Nonetheless, a more thorough and comprehensive analysis is required to gain a deeper understanding and address this observation properly.

CHAPTER 5 EVALUATION OF ACTUAL F-T PERFORMANCE OF GEOMATERIALS

5.1 Materials

In this chapter, the effect of F-T on the stiffness of base material (Ames Mine) with increasing fines content [5% (FC5), 10% (FC10), and 15% (FC15)] was investigated. Figure 78 shows the materials with increasing fines content.

Figure 78. Ames Mine with increasing fines contents: (a) 5%, (b) 10%, (c) 15%

The gradation of the materials used in this chapter was given in Table 14 along with the classification following to USCS and AASHTO.

Table 14. Gradation and classification of Ames Mine materials used for freeze-thaw (F-T) testing

Material	Gravel (%)	Sand (%)	Fines (%)	USCS	AASHTO
Fines Content 5%	64	31	5	GW	A-1-a
Fines Content 10%	59	31	10	GW-GM	A-1-a
Fines Content 15%	54	31	15	GM	A-1-a

Fines = silt and clay
USCS = Unified Soil Classification System
AASHTO = American Association of State Highway and Transportation Officials

According to the USCS, FC5 was categorized as GW, FC10 as GW-GM, and FC15 as GM. Following the AASHTO classification, all three, FC5, FC10, and FC15, were classified as A-1-a.

Table 15 shows the G_s and absorption capacity for the materials used in this chapter following ASTM C127 and C128.

Table 15. Specific gravity (G$_s$) and absorption of materials used for freeze-thaw (F-T) testing

Material	Oven-Dry (OD) G$_s$	Saturated - Surface-Dry (SSD) G$_s$	Apparent G$_s$	Absorption (%)
Fines Content 5%	2.61	2.65	2.72	1.03
Fines Content 10%	2.69	2.73	2.70	1.04
Fines Content 15%	2.69	2.73	2.70	1.03

The OD G$_s$ values were established as 2.61, 2.69, and 2.69 for FC5, FC10, and FC15, respectively. The G$_s$ values under surface-saturate- dry conditions were calculated as 2.65, 2.73, and 2.73 for FC5, FC10, and FC15, respectively. Additionally, the apparent G$_s$ values were derived as 2.72, 2.70, and 2.70 for FC5, FC10, and FC15, respectively. The absorption values were determined as 1.03%, 1.04%, and 1.035 for FC5, FC10, and FC15, respectively.

The vertical hydraulic conductivities (k) of the materials were determined using a specialized rigid-wall permeameter known as the 'bubble tube constant head permeameter'. This permeameter was specifically developed to measure the hydraulic conductivity of specimens with dimensions of 6 inches in diameter and 4.5 inches in length, which were compacted in three equal layers. The tests were conducted following the ASTM D2434-22 standard. The resulting hydraulic conductivity values for the constant head test, with a hydraulic gradient of 1.0, are shown in Table 16.

Table 16. Hydraulic conductivity (k) of the materials used for freeze-thaw (F-T) testing

Material	Hydraulic Conductivity, k (inches/sec)
Fines Content 5%	3.01×10^{-3}
Fines Content 10%	9.71×10^{-4}
Fines Content 15%	2.19×10^{-4}

The k values were determined as 3.01×10^{-3}, $9.71 \times 10^{-4,}$ and 2.19×10^{-4} for FC5, FC10, and FC15, respectively.

The MDU and OMC values for the base and subgrade materials were determined according to the ASTM D698-12 followed by the oversize correction following the guidelines of ASTM D4718. These corrections were applied to calculate the corrected MDU and OMC values for the materials, taking into account the presence of these oversize particles. Table 17 shows the uncorrected (actual) and corrected Proctor compaction test results for F-T testing.

Table 17. Uncorrected (actual) and corrected Proctor compaction test results for freeze-thaw (F-T) testing

Material	Proctor Compaction Results		Corrected Proctor Compaction Results	
	MDU (pcf)	OMC %	MDU (pcf)	OMC %
Fines Content 5%	131	6.50	146	3.50
Fines Content 10%	137	8.50	149	4.75
Fines Content 15%	141	7.50	150	4.30

Corrected MDU values were determined as 146, 149, and 150 pcf for FC5, FC10, and FC15. Corrected OMC values were determined as 3.50%, 4.75%, and 4.30% for FC5, FC10, and FC15.

A freezing-point depression test following ASTM D5918-13el was performed on Ames Mine to determine the temperature at which to freeze the specimen. The freezing-point depression test identifies the temperature at which the water in the material begins to freeze. Figure 79 shows the time history of the temperature during the test.
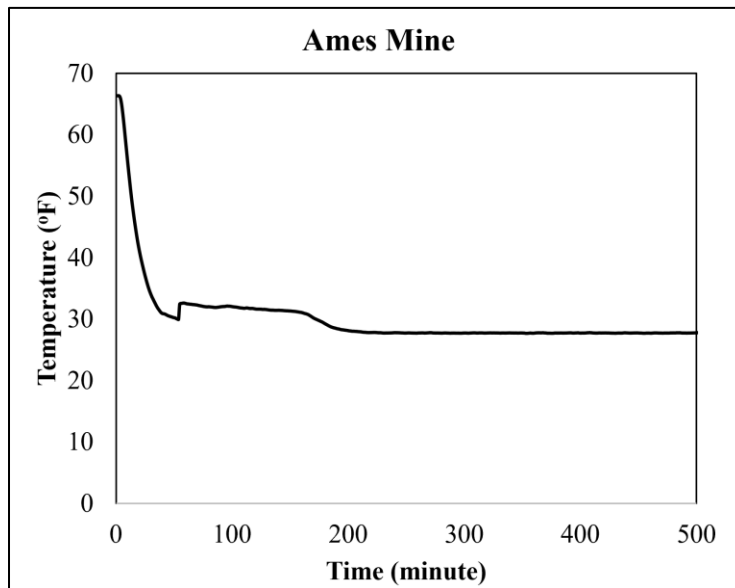
Figure 79. Freezing point depression test result of Ames Mine specimens

To ensure complete freezing of the sample, a temperature lower than the freezing-point depression temperature was selected, specifically. The specimen is exposed to 23 °F during the freezing.

After the freezing point depression test, a subsequent experiment was carried out to determine the time required for the specimen to freeze, and then thaw back to room temperature. For this purpose, a compacted specimen with a diameter of 6 inches and a height of 6 inches was prepared. Thermocouples were strategically placed at elevations of 1 inch and 3 inches to monitor the freezing and thawing processes. Figure 80 illustrates the observed durations of freezing and thawing at the Ames Mine location for both thermocouple elevations.
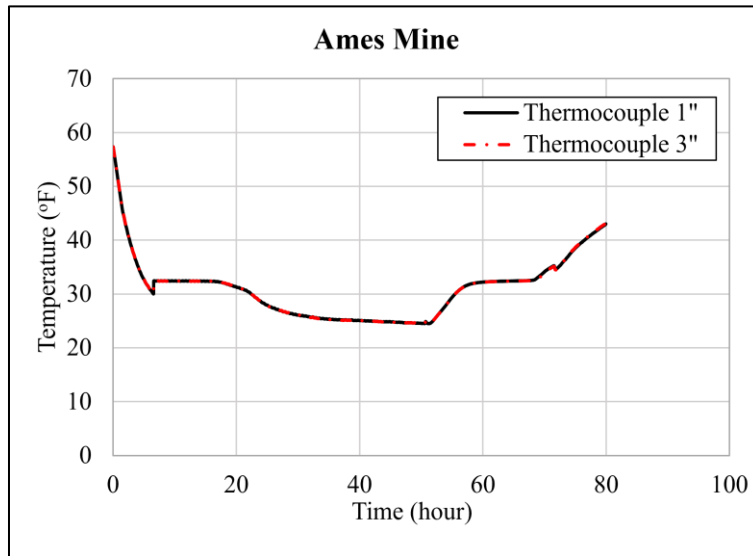
Figure 80. Freezing and thawing duration of specimen

As depicted in the figure, the freezing process lasted for approximately 22 hours, while thawing was completed in about 18 hours. To ensure complete freezing and thawing of the specimen, durations of 26 hours for freezing and 22 hours for thawing were chosen.

5.2 Methods

The cylindrical specimens for testing were prepared in accordance with the procedures outlined in Chapter 3. To conduct F-T testing and achieve a more comprehensive analysis, the SPAX-3000 was paired with an external freezing unit called JULABO (Figure 81a). This combination allowed for several advantages. Firstly, the SPAX-3000's unique feature of connecting to the external freezing unit enabled subjecting the specimens to F-T cycles while they remained within the triaxial chamber (Figure 81b). To simulate real-world stress conditions experienced during freezing and thawing in the field, the specimens were subjected to confining and surcharge loading. Furthermore, during the F-T process, measurements of heave and settlement were recorded to ensure a thorough assessment of the geomaterial behavior under conditions similar to those encountered in the field. The JULABO system circulates the Thermal C5 Polydimethylsiloxane coolant using hoses and embedded channels within the SPAX-3000 cell

walls. Consequently, the air temperature can be adjusted, either lowered or raised, based on the temperature of the coolant flowing through the SPAX-3000's walls.
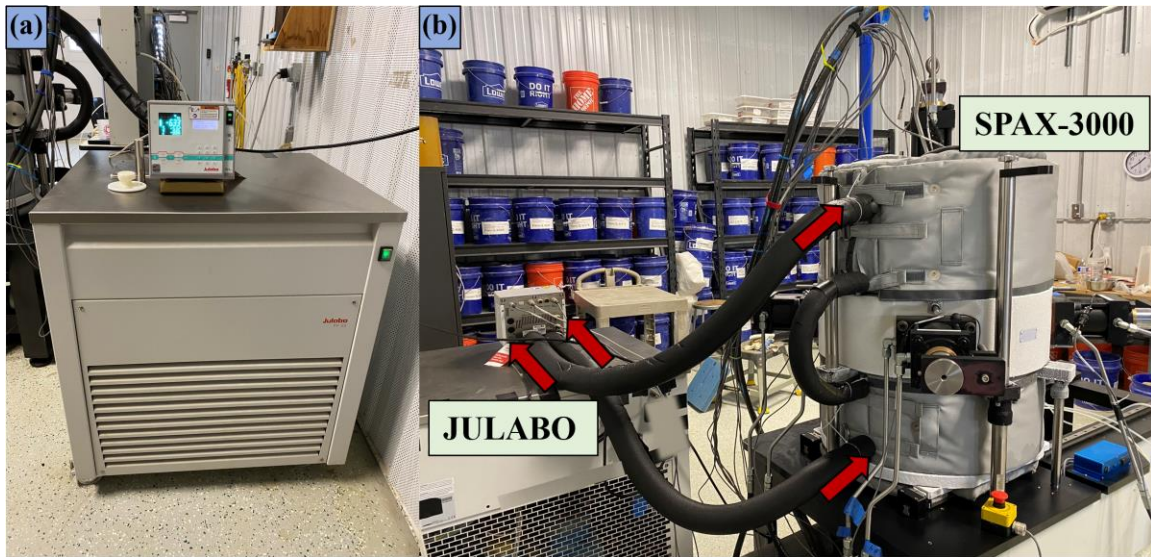
Figure 81. Freeze-thaw (F-T) setup; (a) JULABO, (b) JULABO connections (red arrows) to SPAX-3000

This capability streamlines F-T testing and addresses a significant concern in standard testing procedures. By conducting F-T cycles within the testing chamber itself, the potential sample disturbance that may occur in standard testing during transportation from a separate freezer is effectively minimized. This ensures a more accurate and reliable evaluation of stress-strain characteristics in the experiments.

Table 18 shows the applied testing program for all the materials tested within the scope of this chapter.

Table 18. Advanced freeze-thaw (F-T) testing program

Stage Number	State of Specimen	Resilient Modulus	Permanent Deformation	Internal Displacement Measurements
1	Optimum Moisture Content	✓	✓	✓
2	*Saturation*			
3	Saturated	✓	✓	✓
4	*Saturation*			
5	F-T cycle 1			✓
6	After F-T	✓	✓	✓
7	*Saturation*			
8	F-T cycles 2, 3, 4			✓
9	After F-T	✓	✓	✓
10	*Saturation*			
11	F-T cycles 5, 6, 7, 8			✓
12	After F-T	✓	✓	✓

Initially, the specimens were compacted at the optimum moisture content, and subsequent tests were conducted to assess M_R and PD (Stage 1). Once this initial testing was completed, the specimens underwent saturation to investigate their deformation characteristics in a fully saturated state (Stages 2-3). To prepare the specimens for the F-T period, another round of saturation was carried out (Stage 4). The first F-T cycle was then initiated and M_R and PD tests were performed again following that (Stages 5-6). Before subsequent F-T cycles (cycles 2, 3, and 4), saturation was applied again (Stage 7). After the completion of F-T cycles 2, 3, and 4, M_R and PD tests were conducted once more (Stages 8-9). Following this, a final saturation was performed, and the specimens were subjected to four additional continuous F-T cycles (cycles 5, 6, 7, and 8) (Stages 10-11). Finally, M_R and PD tests were conducted on the specimens after these cycles (Stage 12). During the testing program except for saturation stages (2,4,7,10) displacements (heave and settlements) were recorded for further analysis of the deformation under the F-T. During the F-T stages, the experiments were conducted in a closed system to simulate one of the most challenging scenarios that could be encountered in the field, taking into account the hydraulic conductivity of the materials under test. This closed system approach helps to replicate real-world conditions more accurately and allows for a comprehensive assessment of how the materials behave during freezing and thawing cycles, which can be crucial in understanding their performance and durability in practical applications. Table 6 and 11 were followed for M_R and PD testing, respectively.

Throughout the testing program, the materials underwent F-T cycles while being subjected to specific pressures to simulate realistic conditions. The specimens were kept under 0.45 psi of confining pressure and 0.90 psi of surcharge loading, which were carefully selected to represent a hypothetical flexible pavement cross-section. This cross-section consisted of a 6-inch Hot Mix

Asphalt (HMA) layer on top of a 6-inch base layer. The chosen confining pressure and surcharge loading were intended to replicate the overburden pressure that the geomaterials are likely to experience in real-world scenarios, particularly in the context of flexible pavement structures. By applying these pressures during the F-T testing, the behavior and performance of the materials under such conditions could be accurately evaluated.

5.3 Results

Following the F-T testing program the results, M_R, PDs and, heave and settlement during the F-T, for Ames Mine with varying fines content were calculated and presented within the scope of this chapter.

Figure 82-84 show the results of the M_R for three different fines content, namely 5%, 10%, and 15%. Throughout these figures, the M_R values are presented at various stages of interest. Firstly, MR-OPT represents the M_R at the optimum moisture content, indicating the material's stiffness under ideal moisture conditions. Secondly, MR-SAT displays the M_R at saturation, reflecting the material's stiffness when it reaches maximum moisture capacity. Additionally, the figures show MR1, MR4, and MR8, representing the material's stiffness after one F-T cycle, four F-T cycles, and eight F-T cycles, respectively. These multiple stages of F-T testing offer valuable insights into how the material's mechanical behavior and performance change under varying moisture contents and F-T conditions. Analyzing the M_R at different stages helps assess the material's overall durability and resilience, especially in the context of potential flexible pavement applications and its response to environmental challenges.
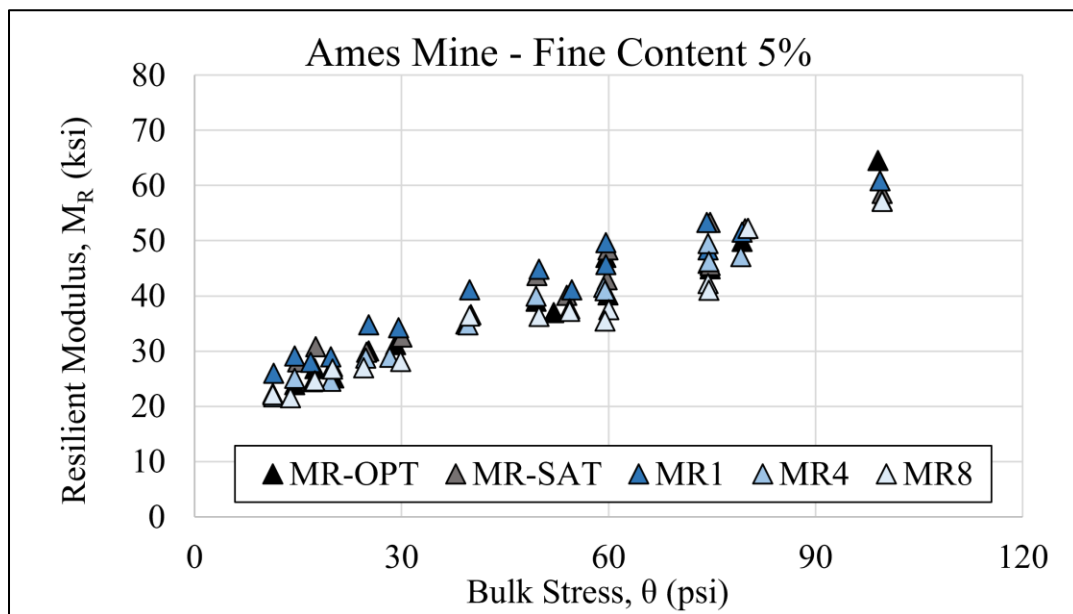
Figure 82. Resilient modulus (M_R) for freeze-thaw (F-T) testing of Ames Mine Fines Content 5% (FC5)
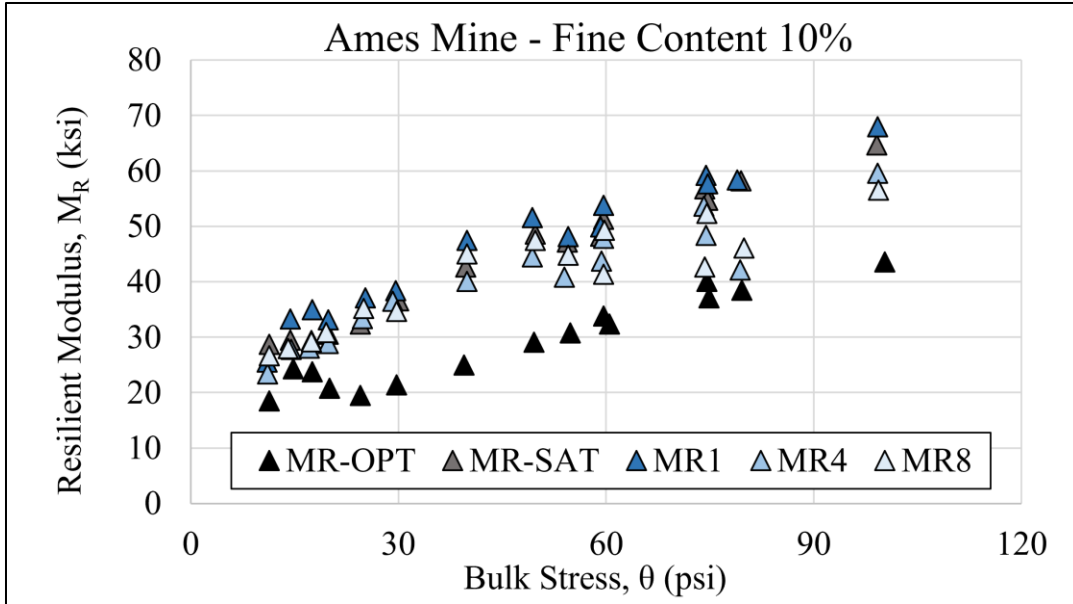
Figure 83. Resilient modulus (M$_R$) for freeze-thaw (F-T) testing of Ames Mine Fines Content 10% (FC10)
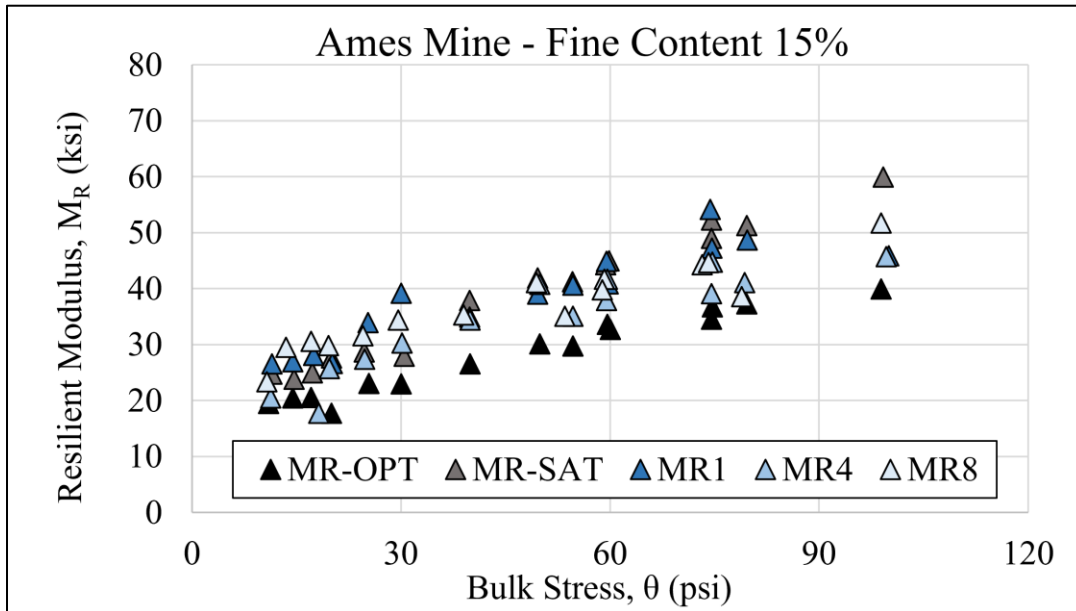
Figure 84. Resilient modulus (M$_R$) for freeze-thaw (F-T) testing of Ames Mine Fines Content 15% (FC15)

Overall, the results of the testing program revealed a consistent trend: an increase in fines content led to a decrease in the stiffness of the base materials at their optimum moisture content. Specifically, FC10, the M$_R$ values decreased by up to 35% compared to FC5. Similarly, for FC15, the M$_R$ values decreased by up to 38% compared to FC5. A notable observation from the

87

testing program was the consistent increase in stiffness at MR-SAT and MR1, regardless of the fines content, when the PD test was conducted immediately after the MR test at the optimum moisture content. This closely represented realistic field conditions, where geomaterials undergo constant PD during their pavement service life. This increase in stiffness was attributed to the packing effect within the material's structure under repeated loading, evident in the MR-SAT and MR1 test conditions. However, as the F-T cycles progressed (F-T4 and F-T8), the further F-T action caused a decrease in the observed M_R values. By the end of the testing program (F-T8), the M_R values decreased by 19%, 27%, and 25% for fines contents of 5%, 10%, and 15%, respectively, when compared to the stiffness observed in the saturated state (MR-SAT). These findings indicate that the fines content of the materials plays a significant role in their stiffness behavior, and the F-T cycles have an impact on the overall M_R, especially over the long term. Such insights are valuable for understanding the performance and durability of the materials, particularly in the context of engineering applications involving repeated loading and varying moisture conditions.

Table 19 presents the permanent strains observed during the testing stages for fines contents of 5%, 10%, and 15%. The table includes values for PD-OPT (PD at optimum moisture content) and PD-SAT (PD at saturation), as well as PD1, PD4, and PD8 corresponding to the PDs at F-T cycles F-T1, F-T4, and F-T8, respectively.

Table 19. Permanent strains at different testing stages for fines contents of 5%, 10%, and 15%

Fines Content (%)	5	10	15
PD-OPT	0.08%	0.23%	0.35%
PD-SAT	+0.04%	+0.03%	+0.03%
PD1	+0.01%	+0.03%	+0.01%
PD4	+0.02%	+0.01%	+0.03%
PD8	+0.01%	+0.01%	+0.02%
Total	**0.15%**	**0.30%**	**0.43%**

Overall, the results of the study indicated a clear trend: an increase in the fines content of the materials led to higher PDs. Specifically, FC10 exhibited a total PD that was 200% higher than the FC5 specimen. Similarly, FC15 showed a remarkable increase, with 300% more PD observed compared to the FC5 specimens. These findings highlight the significant influence of fines content on the material's PD behavior and emphasize the importance of considering fines content in engineering applications to ensure optimal performance and durability. The study revealed a consistent pattern irrespective of the fines content, wherein the highest PD was observed at the optimum moisture content. This result can be attributed to the fact that the material experienced the stresses leading to PD for the first time at this stage. Regardless of the fines content, all tested materials consistently exhibited an increase in PDs throughout the various stages of the testing program. This observation highlights the progressive nature of PD development in the materials under the applied testing conditions. Understanding such behavior is essential for engineering

applications, as it enables better assessment of the materials' long-term performance and aids in the development of appropriate pavement designs to mitigate the effects of PD (Table 5).

Throughout the F-T cycles, the specimens underwent repeated heave during freezing and settlement during thawing. Table 20 presents the recorded amounts of heave and settlement experienced by the specimens during the F-T cycles.

Table 20. Heave and settlement amounts of specimens during (freeze-thaw) F-T cycles

Fines Content (%)	5%		10%		15%	
Displacement (inches)	Heave	Settlement	Heave	Settlement	Heave	Settlement
Freeze 1	0.016		0.012		0.012	
Thaw 1		0.027		0.021		0.020
Freeze 2	0.024		0.012		0.011	
Thaw 2		0.030		0.019		0.015
Freeze 3	0.020		0.014		0.017	
Thaw 3		0.025		0.016		0.019
Freeze 4	0.018		0.014		0.016	
Thaw 4		0.023		0.020		0.019
Freeze 5	0.023		0.014		0.014	
Thaw 5		0.025		0.018		0.017
Freeze 6	0.021		0.013		0.016	
Thaw 6		0.022		0.015		0.023
Freeze 7	0.020		0.010		0.016	
Thaw 7		0.021		0.012		0.019
Freeze 8	0.019		0.010		0.014	
Thaw 8		0.020		0.010		0.016

In summary, the results indicated that FC5 underwent a total settlement of 0.070 inches, while FC10 and FC15 experienced settlements of 0.051 and 0.055 inches, respectively. On the other hand, FC5 exhibited heaving of 0.053 inches, while FC10 and FC15 had heaving of 0.036 and 0.042 inches, respectively. The results suggest that FC5 displayed higher heave and settlement compared to FC10 and FC15, which exhibited lower heave and settlement. This difference is likely attributed to the significant PDs experienced during the testing of FC10 and FC15, leading to a reduction in the overall deformation capacity. However, further analysis is necessary to fully comprehend the observed behavior.

CHAPTER 6 DISCUSSION

6.1. Standard Testing

In the scope of this chapter, the determination of stiffness and PD characteristics was carried out for base materials (Ames Mine, Bethany Falls Limestone, Crocker Pit, Oneota Formation Dolomite, Plano Quarry), subbase materials (Shambaugh Quarry, Stone City Quarry), and subgrade materials (CBIS and Plymouth County). In summary, the outcomes revealed a notable disparity in stiffness values across various materials, with base materials displaying the highest stiffness as anticipated. This observation highlights the fundamental role that base materials play in furnishing structural support and stability. The recorded stiffness can be ascribed to the presence of an interlocking mechanism inherent in granular materials, which substantially contributes to the overall stiffness of the base material. In contrast, subgrade materials exhibited the lowest stiffness primarily stemming from their inherent deficiency in internal structural capacity. Subbase materials, characterized by an open-graded particle distribution demonstrated superior performance compared to subgrade materials. However, despite this relatively improved performance, the subbase materials faced a limitation due to inadequate fine sand and fine-grained materials. This insufficiency ultimately resulted in the subbase materials' stiffness falling short of that exhibited by the base materials.

In summary, the base materials demonstrated relatively consistent ranges of stiffness, with slight variations discerned from the test outcomes. These variations in material behavior are believed to be from factors such as material origin (dolomite, limestone, crushed gravel), particle angularity, and particle size distribution, although a definitive link between these factors and performance awaits further investigation. A comprehensive analysis is required to evaluate how these material characteristics influence mechanical behavior under diverse stress conditions. Notably, all base materials exhibited stress-hardening behavior, marked by heightened stiffness as $\Delta\sigma$ and θ levels increased, despite their distinct origins.

Among the subbase materials, Stone City displayed higher stress-strain performance with stiffness values spanning 15 to 45 ksi. Conversely, Shambaugh Quarry exhibited slightly lower stiffness, ranging from 17 to 38 ksi. Notably, all subbase materials showcased stress-hardening behavior, showing increased stiffness as $\Delta\sigma$ and θ levels rose, regardless of their origin.

According to the results, the subgrade materials yielded the lowest M^z_R values. In addition, CBIS showed stress-hardening with increasing $\Delta\sigma$, while Plymouth County exhibited stress-softening, where stiffness decreased under higher $\Delta\sigma$. This behavior seems to be related to particle size distribution, with CBIS's coarser structure leading to stress-hardening due to internal frictional forces, while Plymouth County's fine-grained nature resulted in stress-softening due to the absence of such forces.

Furthermore, the stiffness trend was analyzed using a model devised by Moossazadeh and Witczak (1981). The outcomes present the model's parameters and the coefficient of determination, reflecting the agreement between the model and the actual data. This visualization provides a significant understanding of how the bulk stress model correlates with the material's M_R behavior, serving as an illustrative example for the subsequent findings. Alongside the bulk stress model, the SM_R was calculated for particular stress levels corresponding to the 6th sequence for base/subbase materials and the 13th sequence for subgrade materials. It was observed that the general trend of M_R was reflected in the SM_R approach.

6.2. Advanced Testing

The presented discussion revolves around the results obtained from testing the M_R and PD properties of different materials under varying stress conditions and in different directions.

6.2.1 Cross-anisotropy of Resilient Modulus

The focus of the study was to understand the anisotropic behavior of the materials and their stiffness characteristics in different directions. Four different materials were tested: two base materials (Ames Mine and Crocker Pit), one subbase material (Shambaugh Quarry), and one subgrade material (Plymouth County).

For the tested base and subbase materials, M_R exhibited nonlinear stress-dependent characteristics in different directions (z-, x-, and, y-axes). The vertical direction demonstrated (z-axis) the highest M_R values, while the two horizontal directions (x- and y-axes) showed similar M_R values but were lower than the vertical direction. The observed cross-anisotropic behavior highlighted that the stiffness of these materials was direction-dependent. The interlocking mechanism in granular materials due to compaction and conditioning contributed to the higher stiffness in the vertical direction. On the other hand, the lack of compaction efforts in horizontal directions resulted in lower stiffness. The differences in stiffness characteristics between Ames Mine and Crocker Pit can be attributed to the angularity and origin of the materials. Overall, the materials showed stress-hardening behavior as a result of the material gradation which enables the particle reorientation and particle interlocking as a result of the experienced deformation as the particles become more interlocked during deformation, the material's resistance to further deformation increases.

In general, Shambaugh Quarry displayed lower M^z_R, M^x_R, and M^y_R values in comparison to the other granular materials (base materials). This outcome can be attributed to the absence of fines within the geomaterial structure. Instead of fines, the voids within the structure were filled with air, which may have resulted in reduced stiffness during $\Delta\sigma$ application. Fines are known to create additional contact points between particles, thereby enhancing stiffness. The lack of fines in Shambaugh Quarry likely contributed to the observed lower M_R values.

The subgrade material displayed distinct characteristics compared to the base and subbase materials. Notably, the M^z_R exhibited stress-softening behavior, which is different from the stress-hardening behavior observed in the base/subbase materials. On the other hand, both horizontal directions (M^x_R and M^y_R) showed stress-hardening behavior, but they displayed varying levels of stiffness. The horizontal x-direction had M_R values ranging from 8 to 17 ksi, while M^y_R values ranged from 2 to 6 ksi. These differences in stiffness can be attributed to the stress history of the fine-grained materials. It is crucial to note that despite the varying stiffness levels, both horizontal directions still demonstrated stress-hardening behavior.

In summary, the subgrade material consistently displayed the lowest M_R values among all the materials tested in this section, irrespective of the direction. This result was anticipated, given the applied stress levels and the inherent nature of subgrade layers as the weakest foundation layers within pavement structures. The subgrade's role within the pavement foundation layers naturally leads to its lower stiffness characteristics compared to base and subbase materials, which are designed to provide greater support and load-bearing capacity.

The modeling efforts showed that the M_R model provided higher coefficients of determination (R^2) for the vertical z-axis (0.91-0.96) compared to the horizontal x and y-axes (0.68-0.91). This indicates that the model is more accurate in representing the stiffness characteristics in the vertical direction which is expected considering the fact that the model was developed for the vertical direction. SM_R was determined for all the tested materials, successfully reflecting the observed trends in the overall results, where the materials had higher M^z_R than M^x_R and M^y_R.

After calculating AR_{x-z} and AR_{y-z}, it was observed that for the base/subbase materials, the horizontal stiffnesses in both directions were significantly lower than the vertical stiffness, and these ratios varied with applied stress. The directional variance is attributed to the interlocking mechanism present in granular materials, primarily observed in the vertical direction due to compaction and conditioning. For the subgrade material, the anisotropy ratios (AR_{x-z} and AR_{y-z}) were not only influenced by the applied stress but also showed directional variations AR_{y-z} was lower than the AR_{x-z}. It is believed that this outcome was affected by the order of stress application, with the $\Delta\sigma$ being lastly applied to the horizontal x-axis direction. Additionally, it is believed that the previous $\Delta\sigma$ applications (vertical z-axis and horizontal y-axis) caused the geomaterial to become more compacted, leading to variations in the calculated M_R values in the y-axis and x-axis.

In summary, the study's findings are crucial for pavement engineering and design as they provide valuable insights into the behavior of different materials under varying stress conditions. The observed differences in stiffness characteristics between vertical and horizontal directions, along with the influence of fines on material stiffness, highlight the significance of considering anisotropic behavior in pavement analysis. The study's focus on subgrade materials and their stress-softening behavior in the vertical direction underscores the need for tailored design approaches for weaker foundation layers within pavement structures. The higher coefficients of determination obtained for the vertical direction using the M_R model underscore its efficacy in precisely capturing vertical stiffness. Nevertheless, the lower coefficients of determination

observed for the horizontal directions suggest that further refinements could enhance the model's ability to accurately represent horizontal stiffness. Overall, these findings contribute to improving pavement design methodologies, ensuring accurate performance predictions, and optimizing pavement structures for enhanced durability and longevity.

6.2.2 Cross-anisotropy of Permanent Deformation

The discussion of the scientific report highlights significant findings related to the PD behavior of base, subbase, and subgrade materials under different stress conditions. The study demonstrates that both the base and subbase materials exhibit highly cross-anisotropic behavior, with significantly higher PD observed in the horizontal directions compared to the vertical z-axis. The higher plastic deformation observed in the horizontal directions of the subbase material, compared to the base materials, can be attributed to the absence of fines content within the geomaterial structure. This lack of fines results in a reduced number of contact points, making the subbase material more susceptible to plastic deformation. As a consequence, the significant PD observed in the subbase material can be explained by the nearly absent fines content, highlighting the importance of fine particles in mitigating plastic deformation and maintaining material stability. This insight into the underlying factors influencing deformation behavior provides valuable information for improving material performance and stability. The discussion also emphasizes the importance of fines content within the geomaterial structure and suggests potential modifications to mitigate excessive plastic deformation in the horizontal directions. Furthermore, the study reveals that the subgrade material exhibited low anisotropy, with comparable responses in both the vertical and horizontal directions. The differences in permanent strains observed among the materials (lower deformation for the subgrade material than the base/subbase) are attributed to the different stress levels applied during the testing of the subgrade and base/subbase materials (Table 11).

The significant findings presented in this chapter offer valuable insights that can greatly contribute to the improvement of pavement analysis and overall service life. The research highlights the presence of cross-anisotropic behavior in the tested geomaterials, with higher PD observed in the horizontal directions. Understanding these deformation patterns is crucial for designing more resilient and durable pavements. The insights into the influence of fines content on material behavior can aid in developing strategies to mitigate excessive plastic deformation in the horizontal directions and enhance material performance. Moreover, recognizing the differences in permanent strains among the materials and their relationship to applied stress levels allows for better predictions of pavement behavior under various loading conditions. By considering anisotropic behavior in pavement design and analysis, engineers can optimize their approaches, leading to improved pavement performance and longer service life, ultimately benefiting transportation infrastructure.

6.2.3 Stress-dependent Cross-anisotropy

The study's findings reveal that the stiffness of tested materials is stress-dependent in both vertical and horizontal directions, displaying cross-anisotropic behavior regardless of material type, gradation, and applied stress levels. Ames Mine's stiffness increased in both directions with increasing θ, but an increase in Δσ led to a decrease in M^z_R for the same confining stress levels. M^y_R exhibited slightly stress-hardening behavior in the horizontal direction, attributed to the strengthened structural capacity of granular materials due to cyclic stresses in the vertical direction. Similar trends were observed for the Weber Quarry in both vertical and horizontal directions.

To investigate how applied stresses affect the stiffness characteristics concerning both direction and stress dependency, the sand utilized in this research underwent testing simulating both subbase and subgrade stress conditions. Similar to findings concerning dolomite and limestone materials, the sand exhibited a tendency towards stress-softening behavior along the vertical axis during subbase testing sequences under identical confining pressure conditions (Sequences 1-3, 4-6, 7-9, 10-12, 13-15). However, contrary to the vertical direction, the sandy material showcased stress-hardening tendencies, particularly within the initial six sequences in the horizontal direction. The apparent fading of stress-hardening effects within certain sequences (Sequences 7-15) might be attributed to the restricted contribution of compaction, a consequence of prior Δσ applied along the vertical axis (M_R), where the material lacked interlocking and cohesion in the horizontal direction. Cyclic softening was evident in M^z_R, particularly after the initial application of Δσ at equivalent confining pressures (Sequences 1, 6, and 11). This outcome was a result of the varying degrees of Δσ across testing sequences. Notably, the earliest sequences (1, 6, and 11) subjected the granular surface road material to lower Δσ compared to subsequent sequences, leading to more pronounced deformation. The subsequent sequences (2-5, 7-10, 12-15) contributed to soil structure compaction, effectively mitigating the softening effect. In contrast, M^y_R exhibited an increase with increasing Δσ levels. This phenomenon was due to the augmented compaction occurring in the horizontal direction during the application of Δσ.

Ames Mine and Weber Quarry exhibited similar cross-anisotropy characteristics with similar anisotropy ratios. For Weber Quarry, M^z_R was approximately 7 to 25 times greater than M^y_R, while in Ames Mine, this ratio was 6 to 21 times higher which aligns with the previous findings where the granular materials are stiffer in the vertical direction due to the interlocking mechanism and enhanced compaction as a result of stress-hardening behavior. for CBIS, augmenting Δσ levels led to decrease anisotropy in subgrade conditions due to marked stress-hardening horizontally where M^z_R was roughly 2.0 to 8.5 times higher than M^y_R. Significantly, both subgrade and subbase stresses yielded similar anisotropy ratios for equivalent Δσ levels, underscoring a direct correlation between cross-anisotropy and applied Δσ. It was observed that under subbase stress conditions, the anisotropy of sand material decreased with rising Δσ, a consequence of stress-softening occurring along the vertical direction of the sand material. Notably, this effect was more pronounced when lower Δσ levels were involved.

94

To address the effect of the stress history, two distinct methods were employed in the testing process, named Method A and Method B, based on the sequence of $\Delta\sigma$ application along the z- and y-axes for Plano Quarry, CBIS and Plymouth County. For Plano Quarry, the results highlighted that stress history had a more prominent impact on M^z_R at elevated bulk stresses. In the case of the base material, Method B (horizontal pulsing followed by vertical pulsing) yielded higher M^z_R values compared to Method A. This was attributed to increased vertical stiffness resulting from applied horizontal cyclic stresses, leading to a denser specimen structure. Conversely, M^y_R values showed relatively minor fluctuations in response to stress histories. In the vertical direction, both Method A and Method B displayed a mild stress-softening tendency for CBIS, using equivalent confining pressure levels but increasing cyclic stresses. This behavior was attributed to the absence of cohesive forces in sandy soils. In contrast, stress-softening was not apparent horizontally using different methods due to the weaker nature of the geomaterial in that orientation. In contrast to the Plano Quarry findings, different stress histories had negligible impact on M^z_R values in the case of CBIS. Nonetheless, the application of $\Delta\sigma$ vertically (Method A) led to a more densely packed structure horizontally, resulting in elevated M^y_R values. The subgrade material exhibited a decline in M_R as $\Delta\sigma$ escalated, signifying stress-softening in the vertical direction. M^y_R displayed a stress-hardening trend with higher θ, contrary to the vertical behavior. This discrepancy could be attributed to increased horizontal compaction due to elevated θ, potentially resulting in higher M_R. Furthermore, the distinct loading approaches (Methods A and B) had negligible influence on the material's response in both horizontal and vertical orientations.

The study's outcomes demonstrated that the stiffness of tested materials responds to stress changes in both vertical and horizontal directions, exhibiting cross-anisotropic behavior regardless of material type, gradation, and applied stress levels. The findings shed light on the intricate relationships between stress and directional behaviors, enhancing our understanding of material responses under varying stress conditions.

6.2.4 Cross-anisotropy under Moving Wheel Load

In this chapter, an investigation was carried out to explore the impact of a moving wheel load on the stiffness characteristics in both the vertical (z-axis) and horizontal (y-axis) directions. Stress path sweep experiments were carried out on Ames Mine, Bethany Falls Limestone, Crocker Pit, Oneota Formation Dolomite, Plano Quarry, Weber Quarry, CBIS, and Plymouth County to simulate the movement of the wheel load towards and away from the material. For the base materials, the highest M^z_R was observed for m=(-1.7), particularly under elevated confining stresses, while the lowest M^z_R was recorded for m=3.0. These findings can be attributed to the applied stresses; m=(-1.7) encountered higher lateral confining stresses due to the major principal stress orientation in the horizontal direction, and it was the last M^z_R test where previous stress applications had already induced hardening. On the other hand, m=3.0 exhibited the lowest M^z_R due to minimal lateral confining stresses and initial exposure to $\Delta\sigma$. The M^y_R values reached their lowest points at m=1.7, presumably because the horizontal direction experienced the initial $\Delta\sigma$ application along that stress path trajectory. There was no notable increase in M^y_R with subsequent stress path applications, possibly due to the full stiffening of the vulnerable structure during the m=1.7 testing phase. In a broader context, both M^z_R and M^y_R exhibited characteristics

of stress-hardening behavior for base materials. The highest M^z_R values for both subgrade materials were evident at m=(-1.7), consistent with the trend seen in the base materials. m=3.0 resulted in slightly lower values compared to other m values [1.7, 1.5, (-1.7)]. Regarding M^y_R, the greatest values emerged at m=(-3.0), while m=1.7 yielded the lowest values, aligning with the pattern observed in the base materials. Except for one instance [CBIS m=(-1.7)], M^z_R displayed stress-softening for both subgrade materials, while M^y_R exhibited stress-hardening behavior. M^y_R's stress-hardening trend could be attributed to increased horizontal compaction due to increased θ, potentially leading to higher M_R. The unusual occurrence of stress-hardening in M^z_R was linked to a strengthened structure resulting from the applied stress history. However, a more comprehensive analysis is required for a thorough understanding and proper addressing of this observation.

The exploration conducted in this chapter concerning the impact of a moving wheel load on stiffness characteristics in both vertical and horizontal directions has yielded significant discoveries. Through experiments emulating the motion of a wheel load towards and away from the material, pivotal insights have emerged, revealing the dynamic nature of material behavior in response to varying load positions. These findings not only hold important implications for pavement design but also underscore the advancement of material behavior, thus enhancing the overall design and analysis outcomes.

6.3. Freeze-thaw Testing

The F-T testing program conducted for Ames Mine provided valuable insights into the mechanical behavior and performance of base materials with varying fines contents under different moisture and F-T conditions. The results were presented in terms of M_R, PDs, and heave and settlement during the F-T cycles. The results consisted of M_R values for three different fines contents (5%, 10%, and 15%) at various stages, such as MR-OPT and MR-SAT as well as MR1, MR4, and MR8, representing the stiffness after one, four, and eight F-T cycles, respectively.

One significant trend observed in the results was that an increase in fines content led to a decrease in the material's stiffness at the optimum moisture content. For instance, the specimens with 10% and 15% fines content exhibited up to 35% and 38% lower M_R values, respectively, compared to those with 5% fines content. Interestingly, regardless of the fines content, an increase in stiffness was consistently observed at MR-SAT and MR1 since the PD tests were conducted immediately after the M_R tests following to test program (Table 18). This increase was attributed to the packing effect within the material's structure under a high number of repeated loading, which reflects realistic field conditions where geomaterials experience PD during pavement service life.

However, as the F-T cycles progressed (F-T4 and F-T8), a decrease in M_R values was observed. By the end of the testing program (F-T8), the M_R values decreased by 19%, 27%, and 25% for fines contents of 5%, 10%, and 15%, respectively, compared to MR-SAT. These findings

indicated that the fines content affected the material's stiffness behavior, and the F-T cycles had a considerable impact on the overall M_R, especially in the long term. These insights are crucial for understanding material durability and resilience, particularly in the context of pavement engineering applications that involve repeated loading and varying moisture conditions.

The investigation of PDs also yielded important results. The study showed that an increase in fines content led to higher PDs. For example, FC10 exhibited 200% more PD than FC5, while FC15 showed 300% more PD compared to the FC5 specimen. The highest PD was consistently observed at the optimum moisture content, suggesting that the material experienced stress leading to PD for the first time at this stage. Moreover, for all the materials, the F-T cycles cause a further increase in PDs. This understanding is essential for engineering applications, as it helps in the evaluation of long-term material performance and the development of suitable pavement designs to mitigate the effects of PD under F-T conditions.

During the F-T cycles, the specimens experienced repeated heaving during freezing and settlement during thawing. The recorded data for heave and settlement indicated that FC5 exhibited higher heave and settlement compared to FC10 and FC15, which showed lower heave and settlement. This disparity can be attributed to the significant PDs experienced by FC10 and FC15 during the PD testing, leading to reduced overall deformation capacity.

In conclusion, the F-T testing program provided comprehensive data on the behavior of base materials with varying fines contents under F-T conditions. The results demonstrated the influence of fines content on material stiffness, PDs, and deformation response to F-T cycles. These findings are invaluable for pavement applications involving flexible pavement design and can contribute to the development of durable and resilient infrastructure under varying environmental conditions. However, further analysis and ongoing research are required to fully understand the observed behavior and optimize the performance of base materials in practical engineering scenarios.

CHAPTER 7 CONCLUSIONS

Cross-anisotropy is a crucial factor to consider in engineering and construction projects, as it signifies that the geomaterials may behave differently when subjected to stress in multiple directions. Understanding and accounting for cross-anisotropy can help engineers design roadways that can better withstand the complex and varied stresses that will be experienced during the service life.

By acknowledging the cross-anisotropy behavior, engineers can develop more accurate and reliable models and predictions for the performance of the geomaterials in real-world applications. This knowledge contributes to better-informed decisions in infrastructure design, construction, and maintenance, ultimately leading to more robust and durable projects. However, it is essential to continue researching and investigating cross-anisotropy in geomaterials to gain a comprehensive understanding of its implications and to develop effective engineering practices that account for this behavior.

The key findings of the standard characterization of the stiffness characteristics are given below.

- Base materials exhibited the highest stiffness (10-54 ksi), while subgrade materials had the lowest stiffness (4-12 ksi).
- The interlocking mechanism in granular materials contributed significantly to base materials' stiffness. Subgrade materials had low stiffness due to their lack of internal structural capacity. Subbase materials had better stiffness (15-45 ksi) due to granular particle size distribution. Subbase materials suffered from unbalanced gradation characteristics.
- Unbound materials demonstrated stress-dependent behavior for confining and cyclic pressure. Stress dependency in base, subbase, and subgrade materials was nonlinear, impacting stiffness variations.
- Base and subbase materials yielded stress-hardening. CBIS exhibited stress-hardening, while Plymouth County showed stress-softening.
- Particle size distribution and internal structure affected stress-strain behavior.
- Moossazadeh and Witczak (1981) model related M_R to θ was used to determine model constants (k_1, k_2) and R^2. The observations revealed that the values of k_1 ranged from 2.75 to 6.49, while the values of k_2 ranged between 0.36 and 0.55. Additionally, the R^2 values were observed to fall within the range of 0.93 to 0.99.
- SM_R was determined for specific stress levels. SM_R values of 29, 23, 18, 26, 24, 27, 20, 25, 9, and 5 ksi were recorded for Ames Mine, Bethany Falls Limestone, Crocker Pit, Oneota Formation Dolomite, Plano Quarry, Weber Quarry, Shambaugh Quarry, Stone City Quarry, Pottawattamie County CBIS, and Plymouth County, respectively.

The key findings of advanced characterization of the stiffness and PD characteristics are given below.

- Ames Mine exhibited nonlinear stress-dependent characteristics in all directions: vertical z-axis, horizontal x-axis, and horizontal y-axis. The vertical direction displayed the highest M_R values (24-90 ksi), while the other two horizontal directions showed similar M_R values, ranging between 3-22 ksi for the horizontal x-axis and 3-21 ksi for the horizontal y-axis. Additionally, a noticeable difference between M^z_R and M^x_R, M^y_R under similar stress conditions highlighted the cross-anisotropic nature of the base materials, where stiffness characteristics vary with direction.
- Similar to Ames Mine, Crocker Pit displayed nonlinear stress-dependent characteristics in all directions: vertical z-axis, horizontal x-axis, and horizontal y-axis. The vertical direction had the highest M_R values (17-59 ksi), while the other two horizontal directions exhibited similar M_R values, ranging between 3-18 ksi for the horizontal x-axis and 3-16 ksi for the horizontal y-axis. Moreover, a noticeable difference between M^z_R and M^x_R, M^y_R under comparable stress conditions emphasized the cross-anisotropic nature of the base materials, where stiffness properties change with direction.
- Shambaugh Quarry, similar to the base material, exhibited nonlinear stress-dependent characteristics in all directions: vertical z-axis, horizontal x-axis, and horizontal y-axis. In line with other results, the highest M_R values were observed vertically, ranging between 18-56 ksi, while M^x_R values were between 4-17 ksi and M^y_R values ranged from 2-12 ksi. This indicates that cross-anisotropy was evident not only in the base material but also in the subbase material.
- Both base and subbase materials displayed stress-hardening behavior, meaning that stiffness increased with higher confining stress.
- Plymouth County showed distinct characteristics compared to the base and subbase materials. Notably, M^z_R exhibited stress-softening behavior, contrary to the stress-hardening behavior seen in the base/subbase materials. Moreover, both horizontal directions (M^x_R and M^y_R) exhibited stress-hardening behavior, with varying levels of stiffness characteristics. M^z_R measured between 11-21 ksi for the subgrade material. The horizontal x-direction had M_R values ranging between 8-17 ksi, while M^y_R values ranged from 2-6 ksi. The discrepancy between the M^x_R and M^y_R is believed to be the result of the applied stress history.
- The Moossazadeh and Witczak (1981) model was utilized to establish the relationship between stiffness and θ.
- SM_R values were determined for each direction of the tested materials. For Ames Mine, SM_R values were 35, 12, and 10 ksi for M^z_R, M^x_R, and M^y_R, respectively. For Crocker Pit, SM_R values were 22, 8, and 7 ksi for M^z_R, M^x_R, and My_R, respectively. Shambaugh Quarry had SM_R values of 23, 8, and 5 ksi for M^z_R, M^x_R, and M^y_R, respectively. In Plymouth County, SM_R values were 14, 13, and 3 ksi for M^z_R, M^x_R, and M^y_R, respectively.
- Anisotropy ratios were determined for each direction of the tested materials. In Ames Mine, anisotropy ratios (AR_{x-z} and AR_{y-z}) ranged from 0.13 to 0.39 and 0.09 to 0.28, respectively, indicating that M^z_R was 3 to 7 times higher than M^x_R and 4 to 11 times higher than M^y_R. Similarly, in Crocker Pit, ratios varied between 0.13-0.38 for AR_{x-z} (M^z_R 3 to 8 times higher than M^x_R) and 0.14-0.35 for AR_{y-z} (M^z_R 3 to 7 times higher than M^y_R).

Shambaugh Quarry's anisotropy ratios ranged from 0.15 to 0.34 for $AR_{x\text{-}z}$ (M^z_R 3 to 7 times higher than M^x_R) and 0.10-0.27 for $AR_{y\text{-}z}$ (M^z_R 4 to 10 times higher than M^y_R). In Plymouth County, the anisotropy ratios ($AR_{x\text{-}z}$ and $AR_{y\text{-}z}$) were also direction-dependent, in addition to stress-dependency. $AR_{x\text{-}z}$ ratios varied from 0.36 to 1.50, while $AR_{y\text{-}z}$ ratios ranged from 0.09 to 0.50.

- For Ames Mine, the vertical z-axis displayed a permanent strain of 0.10%, while the horizontal x-axis and y-axis had higher values of 0.42% and 0.46%, respectively. In Crocker Pit, the vertical z-axis exhibited a PD of 0.11%, while the horizontal x-axis and y-axis underwent plastic deformations at rates of 0.47% and 0.38%, respectively. The subbase material showed a very similar permanent strain in the vertical x-axis compared to the base materials, measuring at 0.09%. The horizontal x-axis and y-axis displayed plastic deformations of 1.60% and 1.49%, respectively. In the subgrade material, the vertical z-axis showed slightly lower permanent strains at 0.06%, while the horizontal x-axis and y-axis recorded values of 0.09% to 0.10%, respectively.

- Both Ames Mine and Weber Quarry exhibited similar cross-anisotropy characteristics (anisotropy ratios ranging between 0.04 to 0.18), with M^z_R approximately 7 to 25 times higher than M^y_R for Weber Quarry and 6 to 21 times higher than for Ames Mine. In the case of CBIS, increased $\Delta\sigma$ led to decreased anisotropy for subgrade stress levels due to significant stress-hardening in the horizontal direction. The anisotropy ratio for CBIS (subgrade) varied between 0.12 and 0.52 (M^z_R is approximately 2.0 to 8.5 times higher than M^y_R), and higher anisotropy ratios were particularly observed for Sequences 11-15 compared to other sequences. The lowest overall anisotropy was seen in sand material tested under subbase stress levels; the anisotropy ratio was between 0.57 and 0.87 (M^z_R is approximately 1.2 to 1.8 times higher than M^y_R).

- For Plano Quarry, anisotropy ratios were determined in the range of 0.09 to 0.21 for Method A and 0.08 to 0.19 for Method B. Anisotropy ratios for CBIS were in the ranges of 0.57 to 0.87 for Method A and 0.38 to 0.78 for Method B. Findings from Plymouth County indicated anisotropy ratios ranging from 0.08 to 0.50 for Method A and 0.05 to 0.46 for Method B, highlighting the cross-anisotropic nature of the materials.

- For the base materials (Ames Mine, Bethany Falls Limestone, Crocker Pit, Oneota Formation Dolomite, Plano Quarry, Weber Quarry), the greatest M^z_R value was noted at an m of -1.7, particularly when subjected to higher levels of confining stress. Conversely, the smallest M^z_R value occurred with an m of 3.0. As for M^y_R, the least values were observed with an m of 1.7. The subsequent application of stress paths did not appear to elevate M^y_R, likely due to the optimal packing of the structurally weak composition during the m=1.7 testing phase. Similar to the trend in the base materials, the highest M^z_R among subgrade materials was seen at m=-1.7. m=3.0 resulted in slightly diminished values in comparison to other m values [1.7, 1.5, -1.7]. In terms of M^y_R, the peak values occurred with m=-3.0, while the lowest values aligned with m=1.7, mirroring the pattern observed in the foundational materials.

The study's contributions lie in enhancing our understanding of the materials' response to F-T conditions, providing valuable data for roadway design and maintenance. The results can guide engineers in selecting appropriate materials and designing resilient roadways that can withstand environmental challenges and repeated loading over their service life.

The key findings of the effect of F-T on the stiffness and PD characteristics are given below.

- Overall, the results of the testing program revealed a consistent trend: an increase in fines content led to a decrease in the stiffness of the base materials at their optimum moisture content. Specifically, for FC10, the M_R values decreased by up to 35% compared to FC5. Similarly, for FC15, the M_R values decreased by up to 38% compared to FC5. A notable observation from the testing program was the consistent increase in stiffness at MR-SAT and MR1, regardless of the fines content. By the end of the testing program (F-T8), the M_R values decreased by 19%, 27%, and 25% for fines contents of 5%, 10%, and 15%, respectively.
- The results of the study indicated a clear trend: an increase in the fines content of the materials led to higher PDs. Specifically, FC10 exhibited a total PD that was 200% higher than the FC5 specimen. Similarly, FC15 showed a remarkable increase, with 300% more PD observed compared to the FC5 specimens.
- The results indicated that FC5 underwent settlements of 0.070 inches, while FC10 and FC15 experienced settlements of 0.051 and 0.055 inches, respectively. On the other hand, FC5 exhibited heaving of 0.053 inches, while FC10 and FC15 had heaving of 0.036 and 0.042 inches, respectively. The results suggest that FC5 displayed higher heave and settlement compared to FC10 and FC15, which exhibited lower heave and settlement.

CHAPTER 8 IMPLEMENTATION

The utilization of cross-anisotropic material properties in roadway analysis holds significant importance due to the insights gained from limited research studies. These investigations have demonstrated that incorporating cross-anisotropic properties can lead to more accurate predictions of material behavior under varying stress conditions. This is particularly crucial because these properties directly influence the distribution of tensile, shear, and compressive strains within the pavement structure. By accounting for the material's lower stiffness response in the horizontal direction, as highlighted in the studies (Adu-Osei et al. 2001, Masad et al. 2006, Wang and Al-Qadi 2013 and Luo et al. 2017), pavement analyses can better capture the complex interactions between loading and material behavior. This ultimately results in a more realistic representation of how the roadway will respond to real-world stresses, enabling engineers to make informed decisions during design and construction processes. Incorporating cross-anisotropic material properties enhances the accuracy and reliability of pavement analyses, ensuring the development of resilient and enduring transportation infrastructure.

The comprehensive understanding of cross-anisotropic material properties obtained from this research holds the potential to revolutionize the approach to pavement design and construction. Integrating these findings into practical applications requires a strategic approach, encompassing various methods, and acknowledging the associated advantages and challenges.

A comprehensive strategy for progress in roadway design involves the integration of cross-anisotropic material characteristics into both material characterization models embedded within pavement design software and structural models using finite element (FE) techniques. The inclusion of cross-anisotropic attributes strengthens material characterization models, enabling them to more effectively predict the behavior of geomaterials under a variety of stress conditions, thus enhancing the accuracy of predictions. Additionally, by leveraging FE methods, the incorporation of cross-anisotropic qualities into structural models heightens the precision of stress and strain predictions. This enhancement ultimately propels the development of more intricate pavement designs that account for the complexities of material behavior. The integration of cross-anisotropic material behavior can be achieved by implementing cross-anisotropic constitutive models, encompassing the exploration of horizontal stiffness within model properties. The report published by Lytton et al. (2019) advocates for the adoption of existing vertical M_R models for horizontal M_R as well, further emphasizing the potential for comprehensive cross-anisotropic incorporation.

The integration of cross-anisotropic material properties into roadway design applications offers multifaceted advantages. This includes heightened durability, as these properties enhance performance predictions, subsequently reducing maintenance needs and prolonging service life. Moreover, accurate predictions lead to cost savings through optimized design and construction practices, preventing unnecessary over-engineering while meeting performance goals. The inclusion of cross-anisotropic characteristics also results in enhanced pavement resilience, equipping structures to effectively withstand dynamic stress, temperature variations, and F-T cycles. This adaptability ensures prolonged pavement longevity amidst diverse environmental

conditions. Furthermore, comprehension of cross-anisotropic behavior facilitates tailored solutions, aligning pavement design precisely with the material's actual response and overall performance.

There are several challenges associated with implementing cross-anisotropic material properties in pavement applications. These include the necessity for technical expertise in both material behavior and advanced analysis techniques, along with the challenge of disseminating this knowledge effectively within the roadway industry. Furthermore, the adoption of these properties may require specialized equipment and software, posing accessibility concerns for certain projects. The transition from conventional pavement design approaches to incorporating cross-anisotropic behavior could introduce a learning curve, necessitating sufficient training and education during this phase. Additionally, validating the effectiveness of the implemented approach through real-world performance data is essential, despite the potentially time-consuming process of gathering and analyzing field data. Lastly, the inherent variability of geomaterials presents a challenge in accurately representing all scenarios, even as the research offers valuable insights into cross-anisotropic properties.

In conclusion, implementing the results of cross-anisotropy findings is a transformative step toward more accurate and resilient roadway/pavement design and construction. By employing various methods while capitalizing on the advantages and addressing challenges, the transportation industry can unlock the full potential of this research, leading to safer, longer-lasting, and more sustainable pavement systems.

CHAPTER 9 RECOMMENDATIONS

Performing laboratory tests for the field design and application requires a thorough characterization of the materials. As a result of the variable nature of the geomaterials, it is crucial yet challenging to have access to a database for the properties and characteristics of these materials. Therefore, it is one of the key goals to maximize the number of geomaterials tests and the testing conditions such as the stress combinations that these materials may be subjected to in the field.

Overall, cross-anisotropy is one of the most advanced topics investigated within the scope of the material behavior for several reasons such as the complexity of the analysis using the cross-anisotropic material properties and the equipment needed to investigate those properties.

Building upon the insights gained from the analyses performed, several recommendations are proposed to ensure a comprehensive and accurate understanding of these materials:

- **Comprehensive Laboratory Testing:** Accurately understanding the intricate behavior of geomaterials within granular road surface and pavement foundation layers and accommodating potential soil improvement techniques, such as geosynthetics and chemical stabilization, necessitates a comprehensive array of laboratory tests. These tests should encompass diverse loading conditions and stress combinations mirroring real field scenarios while factoring in the impacts of soil enhancement methods. Incorporating geosynthetics within test setups offers insights into their effectiveness by evaluating load distribution, stress dissipation, and overall stability enhancements. Similarly, chemical stabilization agents should be considered. Varying their type and concentration can demonstrate their interplay with cross-anisotropic material properties. This knowledge is vital for predicting long-term pavement performance under mechanical and chemical influences. This comprehensive approach bridges the gap between material characterization and practical roadway construction, ensuring the development of resilient and sustainable transportation infrastructure. In addition, the inclusion of F-T testing using an advanced technique further enriches the comprehensive laboratory testing approach. By subjecting geomaterial specimens to controlled F-T cycles without disturbing them prior to testing, a deeper understanding of how cross-anisotropic material properties respond to temperature variations can be gained. This innovative approach enhances the accuracy of material responses under diverse field conditions, contributing valuable insights to the database of material behaviors.
- **Diverse Geomaterial Sampling:** The variable nature of geomaterials necessitates a diverse sampling approach. It is recommended to collect samples from various locations within the project site to account for potential spatial variability in material properties. This approach will contribute to a more robust dataset and mitigate the risk of relying on overly simplified assumptions about material behavior.
- **Database Development:** Recognizing the challenge posed by the scarcity of accessible databases for cross-anisotropic material properties, a strong emphasis should be placed on

data sharing and database development. Collaborative efforts between research institutions, government agencies, and industry stakeholders can facilitate the creation of comprehensive databases that encompass a wide range of geomaterials and loading scenarios. Such databases will serve as invaluable resources for engineers and researchers working on pavement design and construction. The incorporation of advanced F-T testing techniques adds a valuable dimension to the creation of comprehensive material property databases. By including F-T responses alongside traditional mechanical tests, a holistic dataset that captures the interplay between cross-anisotropic behavior and temperature fluctuations can be established. Collaborative efforts to share such enhanced databases will greatly benefit engineers and researchers working on pavement design and construction in diverse environments.

- **Advancements in Analysis Techniques:** Acknowledging the complexity of analyzing cross-anisotropic material properties, researchers and practitioners should continue to explore and develop advanced analysis techniques. Incorporating computational modeling, machine learning, and data-driven approaches can aid in extracting meaningful insights from intricate material responses. Investing in research that refines these techniques will contribute to more efficient and accurate material characterization.
- **Integration of Field and Laboratory Data:** While laboratory tests provide controlled environments for material characterization, field data can offer valuable insights into real-world conditions. It is recommended to integrate field observations and measurements into the material characterization process. By correlating laboratory findings with actual field performance, a more accurate representation of material behavior can be achieved.
- **Collaborative Research Initiatives:** The investigation of cross-anisotropic material behavior requires specialized equipment and expertise. Collaborative research initiatives between academic institutions, research centers, and industry partners can pool resources and knowledge to advance the understanding of these properties. Such collaborations can lead to breakthroughs in both methodology and practical application.

In conclusion, the determination of the impact of F-T on the geomaterials through advanced techniques and cross-anisotropic material properties for the geomaterials represent a challenging yet essential pursuit. By implementing the recommended strategies of comprehensive testing, diverse sampling, database development, analysis technique advancement, integration of field and laboratory data, and collaborative research, the transportation industry can achieve a more accurate and holistic understanding of material behavior. These endeavors will ultimately contribute to the design and construction of safer, more resilient, and longer-lasting pavement systems.

REFERENCES

AASHTO M 145, 1991 Edition, 1991 - Standard Specification for Classification of Soils and Soil–Aggregate Mixtures for Highway Construction Purposes

Adu-Osei, A., Little, D.N. and Lytton, R.L., 2001. Cross-anisotropic characterization of unbound granular materials. Transportation Research Record, 1757(1), pp.82-91.

Airey, D.W. and Wood, D.M., 1988. Cambridge True Triaxial Apparatus. In Advanced triaxial testing of soil and rock (pp. 796-805). American Society for Testing Materials (ASTM).

Akbas, M., Iyisan, R., Dayioglu, A.Y. and Hatipoglu, M., 2021. Stiffness properties of recycled concrete aggregates as unbound base and subbase materials under freeze and thaw cycles. Arabian Journal for Science and Engineering, 46(11), pp.10569-10584.

American Association of State Highway and Transportation Officials. 2017. Standard Method of Test for Determining the Resilient Modulus of Soils and Aggregate Materials. AASHTO T 307-99. Washington, DC: American Association of State and Highway Transportation Officials

AnhDan, L. and Koseki, J., 2005. Small strain behaviour of dense granular soils by true triaxial tests. Soils and foundations, 45(3), pp.21-38.

ARA, Inc., ERES Consultants Division., 2004. Guide for Mechanistic-Empirical Design of New and Rehabilitated Pavement Structures. NCHRP 1-37 A Final Report, Transportation Research Board, National Research Council, Washington, DC.

ASTM Committee D-18 on Soil and Rock, 2017. Standard Practice for Classification of Soils for Engineering Purposes (Unified Soil Classification System) 1. ASTM international.

ASTM D2434-22; Standard Test Methods for Measurement of Hydraulic Conductivity of Coarse-Grained Soils. ASTM international: West Conshohocken, PA, USA, 2022.

ASTM D5918-13el, 2013, Standard Test Methods for Frost Heave and Thaw Weakening Susceptibility of Soils, ASTM International, West Conshohocken, PA, www.astm.org

ASTM D7382-08, 2008. Standard test methods for determination of maximum dry unit weight and water content range for effective compaction of granular soils using a vibrating hammer.

ASTM International. Standard Practice for Correction of UnitWeight andWater Content for Soils Containing Oversize Particles. ASTM D4718/D4718M-15. West Conshohocken, PA: ASTM International, approved December 15. 2015. https://doi.org/10.1520/D4718_D4718M-15

ASTM International. Standard Test Method for Relative Density (Specific Gravity) and Absorption of Coarse Aggregate. ASTM C127-15. West Conshohocken, PA: ASTM International, approved January 1, 2015. https://doi.org/10.1520/C0127-15

ASTM International. Standard Test Methods for Laboratory Compaction Characteristics of Soil Using Standard Effort (12,400 ftlbf/ft3 (600 kN-m/m3)). ASTM D698-12(2021). West Conshohocken, PA: ASTM International, approved July 1, 2021. https://doi.org/10.1520/D0698-12R21

ASTM International. Standard Test Methods for Liquid Limit, Plastic Limit, and Plasticity Index of Soils. ASTM D4318-17e1. West Conshohocken, PA: ASTM International, approved June 1, 2017. https://doi.org/10.1520/D4318-17E01

ASTM International. Standard Test Methods for Particle-Size Distribution (Gradation) of Soils Using Sieve Analysis. ASTM D6913/D6913M-17. West Conshohocken, PA: ASTM International, approved April 15, 2017. https://doi.org/10.1520/D6913_D6913M-17

ASTM International. Standard Test Methods for Specific Gravity of Soil Solids by Water Pycnometer. ASTM D854-14. West Conshohocken, PA: ASTM International, approved May 1, 2014. https://doi.org/10.1520/D0854-14

ASTM, 2007. Standard specification for materials for soil-aggregate subbase, base, and surface courses. West Conshohocken, PA: American Society for Testing and Materials.

ASTM, 2012. ASTM C128-12, Standard Test Method for Density, Relative Density (Specific Gravity), and Absorption of Fine Aggregate.

ASTM, D., 2017. Standard test method for particle-size distribution (gradation) of fine-grained soils using the sedimentation (hydrometer) analysis. In ASTM (Vol. 7928, pp. 1-25).

Aydin, C., Hatipoglu, M., Cetin, B. and Ceylan, H., 2021. Determination of the Resilient Modulus under Anisotropic Stress Conditions. In IFCEE 2021 (pp. 381-389).

Aydin, C., Hatipoglu, M., Cetin, B. and Ceylan, H., 2023a. A Cyclic True Triaxial with Rigid-Rigid-Flexible Boundary for Determination of Cross-Anisotropic Nature of Geomaterials. Geotechnical Testing Journal, 46(1), pp.1-19.

Aydin, C., Sinan Coban, H., Hatipoglu, M., Cetin, B. and Ceylan, H., 2023b, March. Effect of Cyclic True-Triaxial Boundary Types on Stress-Strain Behavior of Unbound Material. In Geo-Congress 2023 (pp. 397-407).

Barden, L., 1963. Stresses and displacements in a cross-anisotropic soil. Geotechnique, 13(3), pp.198-210.

Bell, J.M., 1965. Stress-strain characteristics of cohesionless granular materials subjected to statically applied homogenous loads in an open system (Doctoral dissertation, California Institute of Technology).

Bilodeau, J.P., Doré, G. and Poupart, J., 2012. Permanent deformation of various unbound aggregates submitted to seasonal frost conditions. In Cold Regions Engineering 2012: Sustainable Infrastructure Development in a Changing Cold Environment (pp. 155-164).

Brown, S.F., 1996. Soil mechanics in pavement engineering. Géotechnique, 46(3), pp.383-426.

Cerni, G., Cardone, F., Virgili, A. and Camilli, S., 2012. Characterisation of permanent deformation behaviour of unbound granular materials under repeated triaxial loading. Construction and Building Materials, 28(1), pp.79-87.

Chai, J.C. and Miura, N., 2002. Traffic-load-induced permanent deformation of road on soft subsoil. Journal of geotechnical and geoenvironmental engineering, 128(11), pp.907-916.

Chai, J.C. and Miura, N., 2002. Traffic-load-induced permanent deformation of road on soft subsoil. Journal of geotechnical and geoenvironmental engineering, 128(11), pp.907-916.

Choi, C., Arduino, P. and Harney, M., 2007. Development of a true triaxial apparatus for sands and gravels. Geotechnical Testing Journal, 31(1), pp.32-44.

Christopher, B.R., Schwartz, C.W., Boudreaux, R. and Berg, R.R., 2006. Geotechnical aspects of pavements (No. FHWA-NHI-05-037). United States. Federal Highway Administration.

Domitrović, J., Rukavina, T. and Lenart, S., 2019. Effect of freeze-thaw cycles on the resilient moduli and permanent deformation of RAP/natural aggregate unbound base mixtures. Transportation Geotechnics, 18, pp.83-91.

Domitrović, J., Rukavina, T. and Lenart, S., 2019. Effect of freeze-thaw cycles on the resilient moduli and permanent deformation of RAP/natural aggregate unbound base mixtures. Transportation Geotechnics, 18, pp.83-91.

Gao, Z., Zhao, J. and Yao, Y., 2010. A generalized anisotropic failure criterion for geomaterials. International Journal of Solids and Structures, 47(22-23), pp.3166-3185.

Graham, J. and Houlsby, G.T., 1983. Anisotropic elasticity of a natural clay. Géotechnique, 33(2), pp.165-180.

Green, G.E. and Bishop, A.W., 1969. A note on the drained strength of sand under generalized strain conditions. Geotechnique, 19(1), pp.144-149.

Hambly, E.C., 1969. A new true triaxial apparatus. Geotechnique, 19(2), pp.307-309.

Ibsen, L.B. and Prasstrup, U., 2002. The Danish rigid boundary true triaxial apparatus for soil testing. Geotechnical testing journal, 25(3), pp.254-265.

Jing, P., Nowamooz, H. and Chazallon, C., 2017. Effect of anisotropy on the resilient behaviour of a granular material in low traffic pavement. Materials, 10(12), p.1382.

Kim, S.H., Little, D.N., Masad, E. and Lytton, R.L., 2005. Estimation of level of anisotropy in unbound granular layers considering aggregate physical properties. The International Journal of Pavement Engineering, 6(4), pp.217-227.

Kjellman, W., 1936. Report on an Apparatus for Consummate Investigation of the Mechanical Properties of Soils, 1st ICSMFE.

Ko, H.Y. and Scott, R.F., 1967. A new soil testing apparatus. Geotechnique, 17(1), pp.40-57.

Konrad, J.M. and Lemieux, N., 2005. Influence of fines on frost heave characteristics of a well-graded base-course material. Canadian geotechnical journal, 42(2), pp.515-527.

Lade, P.V. and Abelev, A.V., 2005. Characterization of cross-anisotropic soil deposits from isotropic compression tests. Soils and foundations, 45(5), pp.89-102.

Lade, P.V. and Duncan, J.M., 1973. Cubical triaxial tests on cohesionless soil. Journal of the Soil Mechanics and Foundations Division, 99(10), pp.793-812.

Lekarp, F., Isacsson, U. and Dawson, A., 2000. State of the art. I: Resilient response of unbound aggregates. Journal of transportation engineering, 126(1), pp.66-75.

Lenart, S., Koseki, J., Miyashita, Y. and Sato, T., 2014. Large-scale triaxial tests of dense gravel material at low confining pressures. Soils and Foundations, 54(1), pp.45-55.

Li, L., Liu, J., Zhang, X. and Saboundjian, S., 2011. Resilient modulus characterization of Alaska granular base materials. Transportation research record, 2232(1), pp.44-54.

Li, L., Liu, J., Zhang, X., Li, P. and Saboundjian, S., 2019. Characterizing Permanent Deformation of Alaskan Granular Base–Course Materials. Journal of Materials in Civil Engineering, 31(11), p.04019267.

Li, L., Saboundjian, S., Liu, J. and Zhang, X., 2013. Permanent deformation behavior of alaskan granular base materials. In ISCORD 2013: Planning for Sustainable Cold Regions (pp. 428-435).

Li, M., Yin, G., Xu, J., Li, W., Song, Z. and Jiang, C., 2016. A novel true triaxial apparatus to study the geomechanical and fluid flow aspects of energy exploitations in geological formations. Rock Mechanics and Rock Engineering, 49, pp.4647-4659.

Liu, H.B., Sun, S., Wei, H.B. and Li, W.J., 2022. Effect of freeze-thaw cycles on static properties of cement stabilised subgrade silty soil. International Journal of Pavement Engineering, 23(11), pp.3770-3782.

Liu, Y., Stolle, D., Guo, P. and Emery, J., 2014. Stress-path dependency of resilient behaviour of granular materials. International Journal of Pavement Engineering, 15(7), pp.614-622.

Luo, X., Gu, F., Zhang, Y., Lytton, R.L. and Zollinger, D., 2017. Mechanistic-empirical models for better consideration of subgrade and unbound layers influence on pavement performance. Transportation Geotechnics, 13, pp.52-68.

Lytton, R.L., Luo, X., Saha, S., Chen, Y., Deng, Y., Gu, F. and Ling, M., 2019. Proposed enhancements to pavement ME design: improved consideration of the influence of subgrade and unbound layers on pavement performance (No. NCHRP Project 01-53).

Mandeville, D. and Penumadu, D., 2004. True triaxial testing system for clay with proportional-integral-differential (PID) control. Geotechnical Testing Journal, 27(2), pp.134-144.

Masad, S., Little, D. and Masad, E., 2006. Analysis of flexible pavement response and performance using isotropic and anisotropic material properties. Journal of Transportation Engineering, 132(4), pp.342-349.

Melo, L.D. and Cabral, B.P., 2012. Inherent anisotropy in pavement subgrades. In GeoCongress 2012: State of the Art and Practice in Geotechnical Engineering (pp. 1056-1065).

Menkiti, O.C., 1995. Behaviour of clay and clayey-sand, with particular reference to principal stress rotation (Doctoral dissertation, Imperial College London (University of London)).

Mishra, D., Tutumluer, E. and Butt, A.A., 2010. Quantifying effects of particle shape and type and amount of fines on unbound aggregate performance through controlled gradation. Transportation Research Record, 2167(1), pp.61-71.

Moossazadeh, J. and Witczak, M.W., 1981. Prediction of subgrade moduli for soil that exhibits nonlinear behavior. Transportation Research Record, (810).

Puppala, A.J., Mohammad, L.N. and Allen, A., 1999. Permanent deformation characterization of subgrade soils from RLT test. Journal of Materials in Civil Engineering, 11(4), pp.274-282.

Puppala, A.J., Mohammad, L.N. and Allen, A., 1999. Permanent deformation characterization of subgrade soils from RLT test. Journal of Materials in Civil Engineering, 11(4), pp.274-282.

Puppala, A.J., Saride, S. and Chomtid, S., 2009. Experimental and modeling studies of permanent strains of subgrade soils. Journal of geotechnical and geoenvironmental engineering, 135(10), pp.1379-1389.

Puppala, A.J., Saride, S. and Chomtid, S., 2009. Experimental and modeling studies of permanent strains of subgrade soils. Journal of geotechnical and geoenvironmental engineering, 135(10), pp.1379-1389.

Qi, J., Ma, W. and Song, C., 2008. Influence of freeze–thaw on engineering properties of a silty soil. Cold regions science and technology, 53(3), pp.397-404.

Recommended Standard Method for Routine Resilient Modulus Testing of Unbound Granular Base/Subbase Materials and Subgrade Soils. NCHRP Protocol 1-28A. TRB, National Research Council, Washington, D.C., 2002

Reddy, K.R., Saxena, S.K. and Budiman, J.S., 1992. Development of a true triaxial testing apparatus. ASTM International.

Rosa, M.G., Cetin, B., Edil, T.B. and Benson, C.H., 2017. Freeze–thaw performance of fly ash–stabilized materials and recycled pavement materials. Journal of Materials in Civil Engineering, 29(6), p.04017015.

Saberian, M. and Li, J., 2021. Effect of freeze–thaw cycles on the resilient moduli and unconfined compressive strength of rubberized recycled concrete aggregate as pavement base/subbase. Transportation Geotechnics, 27, p.100477.

Saberian, M., Li, J. and Setunge, S., 2019. Evaluation of permanent deformation of a new pavement base and subbase containing unbound granular materials, crumb rubber and crushed glass. Journal of Cleaner Production, 230, pp.38-45.

Saberian, M., Li, J., Nguyen, B. and Wang, G., 2018. Permanent deformation behaviour of pavement base and subbase containing recycle concrete aggregate, coarse and fine crumb rubber. Construction and Building Materials, 178, pp.51-58.

Seyhan, U. and Tutumluer, E., 2002. Anisotropic modular ratios as unbound aggregate performance indicators. Journal of materials in civil engineering, 14(5), pp.409-416.

Seyhan, U., Tutumluer, E. and Yesilyurt, H., 2005. Anisotropic aggregate base inputs for mechanistic pavement analysis considering effects of moving wheel loads. Journal of materials in civil engineering, 17(5), pp.505-512.

Shao, S., Wang, Q. and Luo, A., 2017. True triaxial apparatus with rigid-flexible-flexible boundary and remolded loess testing. Journal of Testing and Evaluation, 45(3), pp.808-817.

Shapiro, S. and Yamamuro, J.A., 2003. Effects of silt on three-dimensional stress–strain behavior of loose sand. Journal of geotechnical and geoenvironmental engineering, 129(1), pp.1-11.

Sidess, A., Uzan, J. and Nigem, P., 2021. Fundamental characterisation of the anisotropic resilient behaviour of unbound granular materials. International Journal of Pavement Engineering, 22(3), pp.283-293.

Silvestri, V., Yong, R.N. and Mohamed, A.M.O., 1988. A true triaxial testing cell. In Advanced Triaxial Testing of Soil and Rock. ASTM International.

Simonsen, E., Janoo, V.C. and Isacsson, U., 2002. Resilient properties of unbound road materials during seasonal frost conditions. Journal of Cold Regions Engineering, 16(1), pp.28-50.

Sture, S. and Desai, C.S., 1979. Fluid cushion truly triaxial or multiaxial testing device. Geotechnical Testing Journal, 2(1), pp.20-33.

Tutumluer, E. and Seyhan, U., 1999. Laboratory determination of anisotropic aggregate resilient moduli using an innovative test device. Transportation Research Record, 1687(1), pp.13-21.

Tutumluer, E., 2009. State of the art: Anisotropic characterization of unbound aggregate layers in flexible pavements. Pavements and materials: Modeling, testing, and performance, pp.1-16.

Uzan, J., 2004. Permanent deformation in flexible pavements. Journal of transportation engineering, 130(1), pp.6-13.

Voznesensky, E.A., Funikova, V.V. and Babenko, V.A., 2013. Deformability properties of model granular soils under true triaxial compression conditions. Moscow University Geology Bulletin, 68, pp.253-259.

Wang, H. and Al-Qadi, I.L., 2013. Importance of nonlinear anisotropic modeling of granular base for predicting maximum viscoelastic pavement responses under moving vehicular loading. Journal of engineering mechanics, 139(1), pp.29-38.

Wang, W., Qin, Y., Lei, M. and Zhi, X., 2018. Effect of repeated freeze-thaw cycles on the resilient modulus for fine-grained subgrade soils with low plasticity index. Road Materials and Pavement Design, 19(4), pp.898-911.

Werkmeister, S., Dawson, A.R. and Wellner, F., 2001. Permanent deformation behavior of granular materials and the shakedown concept. Transportation Research Record, 1757(1), pp.75-81.

Xie, W.B., Zhang, Q., Chen, J.J., Ye, G.L. and Zhang, F., 2022. A New True Triaxial Apparatus for Finite Deformation with a Novel Rigid–Flexible Loading Device. Geotechnical Testing Journal, 45(4), pp.707-724.

Yamada, Y. and Ishihara, K., 1979. Anisotropic deformation characteristics of sand under three dimensional stress conditions. Soils and Foundations, 19(2), pp.79-94.

Ye, G.L., Sheng, J.R., Ye, B. and Wang, J.H., 2012. Automated true triaxial apparatus and its application to over-consolidated clay. ASTM International.

Yin, J.H., Cheng, C.M., Kumruzzaman, M. and Zhou, W.H., 2010. New mixed boundary, true triaxial loading device for testing three-dimensional stress–strain–strength behaviour of geomaterials. Canadian Geotechnical Journal, 47(1), pp.1-15.

Zapata-Medina, D.G., Cortes-Garcia, L.D., Finno, R.J. and Arboleda-Monsalve, L.G., 2020. Stiffness and strength anisotropy of overconsolidated Bootlegger Cove clays. Canadian Geotechnical Journal, 57(11), pp.1652-1663.

Zheng, F., Wang, Y., Shao, S. and Shao, S., 2021. A new suction-controlled true triaxial apparatus for unsaturated soil testing. Geotechnical Testing Journal, 44(4), pp.833-850.